SYNTHESIS AND APPLICATION OF SERS ACTIVE GOLD NANOSTAR PROBES TO MONITOR VIRAL EVOLUTION

By

KHOLUD DARDIR

A dissertation submitted to the

School of Graduate Studies

Rutgers, The State University of New Jersey

In partial fulfillment of the requirements

For the degree of

Doctor of Philosophy

Graduate program in Chemistry and Chemical Biology

Written under the direction of

Laura Fabris

And approved by

_____

_____

_____

_____

New Brunswick, New Jersey

May 2019

ABSTRACT OF THE DISSERTATION

Synthesis and Application of SERS Active Gold Nanostar Probes to Monitor Viral Evolution

By KHOLUD DARDIR

Dissertation Director:

Laura Fabris

Gold nanoparticles have become increasingly popular due to their unique physical and optical properties. Their nanoscale dimensions place them in the ideal size range to study and manipulate biological systems. The shape and plasmonic properties of these particles contribute to significant signal enhancement in spectroscopic techniques, which is extremely relevant toward the analysis of biological samples. Furthermore, the gold surface allows for accurate surface conjugation, which holds tremendous potential for various biomedical applications, including drug delivery and biosensing. Researchers have made significant progress in the advancement of gold nanoparticles for applications in medicine; however, with respect to the eradication of viral diseases, the study of viral replication and mutation has not been approached with methods that leverage gold nanoparticle-based tools. Nonetheless, gold nanoparticles hold tremendous potential in this respect, especially for tracking viral mutations and understanding complex mechanisms of viral evolution. In this thesis, gold nanostars were utilized to monitor intracellularly viral mutations at the

single cell level. The synthesis of gold nanostars and their functionalization with various coatings and ligands for optimized cellular uptake was the first step to creating the proper tool for intracellular applications, in particular for the purpose of tracking viral RNA mutations intracellularly and provide mechanistic insight into viral evolution.

We demonstrated that gold nanostars, functionalized with a surface enhanced Raman spectroscopy (SERS) beacon, can create a sensitive tool for high resolution single nanoparticle-based influenza A virus (IAV) detection without the need of PCR amplification and sequencing. The initial step was to create a probe that could detect viral RNA intracellularly with sensitivity to single base RNA. We have demonstrated for the first time, both in buffer and at the single cell level, that the SERS signal intensity of a fluorophore covalently bonded to the beacon is an ideal reporter of mutations, as it has been shown to be dependent on the number of mutations present on the target viral RNA. We demonstrated the selectivity of the nanoparticle probe assay to its target by introducing other viral sequences and observing a measurable SERS signal only in the presence of the targeted strand.

To overcome obstacles with cellular uptake, and in particular to ensure that the nanostars would circulate in the cytosol (where the viral RNA is located) rather than being trapped in endosomes, we combined gold nanoparticles with trisaminocyclopropenium (TAC) ion-functionalized macro-molecules to provide an efficient route to nanoparticle endosomal escape. TAC polymers can be readily wrapped around nanoparticles through electrostatic interactions and have been shown to be less toxic than their counterpart poly(ethyleneimine) (PEI). We electrostatically layered TAC polymers onto gold nanostars for cellular uptake. These particles were able to escape the endosomal membrane and

diffuse within the cytoplasm without affecting cellular viability. In addition to being less toxic, the TAC coated nanostars diffused within the cytoplasm more rapidly than PEI-coated nanostars, making them an ideal tool to match the four-hour replication kinetics of IAV in cells. This platform will not replace current assays but rather become an invaluable tool to add to the virologist toolbox.

Acknowledgements:

I would first and foremost like to thank my advisor Dr. Laura Fabris for granting me the opportunity to study under her guidance and advisement. I am very fortunate to have had her support, guidance and encouragement. She has been a great role model for myself and others alike. I could not thank her enough and nothing will show the amount of gratitude and admiration I have for her.

I would like to thank my committee members, Dr. John Taylor, Dr. Lu wang, and Dr. Connie Chang. Dr. John Taylor has been a great support and mentor since I started in his lab as undergraduate student to starting a job a Pfizer to coming back as a graduate student and I look forward to continuing that relationship throughout my career. He also pushed, encouraged and inspired me to pursue a doctoral degree. Dr. Lu has been very encouraging and insightful through my process and I have always enjoyed our meetings. Dr. Chang has been an ideal collaborator, providing valuable feedback.

My group members have been very supportive and have made my experience enjoyable. I would like to thank them all, especially Manjari Bhamidipati, Matina Kallontzi, Ted Tsoulos, Sakshi Sardar and Supriya Atta. I would like to especially thank Manjari for all her constant support, fruitful collaborations, and more importantly her friendship though out the years.

I would also like to thank my friends in the chemistry and chemical biology department and throughout the campus. A special thanks to the CCB department, especially Allison Larkin, Arielle L'Esperance, and Shaneika Nelson, who made graduate life smooth. Also, a special thank you to Dr. Jean Baum, who dissolved difficult situations.

I would like to thank my family, Aida Dardir, Hanafi Dardir, Amira Dardir, Heba Dardir and Khaled Dardir for being my strength and showing patience and love. I would like to thank my boyfriend, Sean Coakley, who has been especially patient and supportive through the whole process. He has been nothing but encouraging and caring with every step.

Dedication:

This dissertation is dedicated to my family.

Table of Contents:

Abstract..... ii
Acknowledgements: v
Dedication:..... vii
List of Figures: xii
List of Schemes:..... xvii
List of Tables:..... xi
Table of Contents:..... viii

Chapter 1 **INTRODUCTION** 1
1.1 Background 2
1.2 Viruses and Viral Evolution.....3
1.3 Nanoparticle Tools for Intracellular Sensing 5
1.4 SERS and SERS Tags 7
1.5 Gold Nanostars.....9
1.6 Surface Coating and Bio-Conjugation 9
1.7 Targeting Molecules.....11
1.8 Application of SERS in Bio-Sensing 12
1.9 Dissertation Hypothesis and Overview.....13
1.10 References 17
Chapter 2 NANOPARTICLE SYNTHESIS 21
2.1 Abstract 22
2.2 Introduction 23
2.3 Materials and Method.....25
2.3.1 Surfactant Free Gold Nanostar Synthesis.....25
2.3.2 Silica Coated Nanostar Synthesis.....26
2.3.4 Polymer Coated Gold Nanostar synthesis 30
2.4 Results and discussion.....32
2.5 Conclusion.....38
2.6 References 40
Chapter 3 Polymer Facilitated Uptake 42
3.1 Abstract 43

3.2 Introduction 44
3.3 Materials and Method.....47
3.3.1 Preparation of Polymer Coated Gold Nanostar for Cellular Transfection 47
3.3.2 Characterization of Polymer Coated Gold Nanostars.....48
3.3.3 Cell Culture.....49
3.3.4 Cellular Viability 49
3.3.5 Fluorescent Labeling of Endosomes and Cellular Uptake 50
3.4 Results and discussion.....50
3.4.1 Preparation of Polymer Coated Nanostars.....50
3.4.2 *In Vitro* Cellular Viability Study 52
3.4.3 Endosomal Escape of Gold Nanostars.....56
3.5 Conclusion.....58
3.6 Acknowledgments 59
3.7 References 60
Chapter 4 SERS Nanoprobe 62
4.1 Abstract 63
4.2 Introduction 64
4.3 Materials and Method.....68
4.3.1 vRNA and Targeting Ligands.....68
4.3.2 Preparation of SERS Active Probe for vRNA Detection 69
4.3.3 Characterization of Si@AuNS and SANSPs.....70
4.3.4 Stability and Optimization of SANSPs 71
4.3.5 Viral RNA Mutation Detection 72
4.3.6 Cell Culture.....74
4.3.7 Viral RNA Detection in Cell Lysate.....74
4.3.8 Cellular Uptake of SANSPs 75
4.3.9 Viral RNA Detection in Single Cells 76
4.4 Results and discussion.....77
4.4.1 Demonstrating SANSPs RNA Detection 77
4.4.2 Stability and Optimization of SANSPs 80
4.4.3 Viral RNA Mutation Detection 86
4.4.4 Viral RNA Detection in Cell Lysate.....88

4.4.5 *In Vitro* Cellular Uptake of SANSPs: Viability and Fluorescence Microscopy90
4.4.6 Viral RNA Detection in Single Cells 91
4.5 Conclusion.....93
4.6 References 94
Chapter 5 Conclusion and Future Direction 96
5.1 Conclusion.....97
5.2 Future Direction 98
5.3 References 101
Appendix: Enhancement of MALDI-TOF Mass Spectroscopy via Gold Nanoparticle Integration 102
A.1 Abstract 103
A.2 Introduction 103
A.3 Materials and Methods 105
A.3.1 Nanoparticle Synthesis 105
A.3.2 Characterization of Nanoparticle 106
A.3.3 Preparation of Biomaterial Analysis.....107
A.4 Results and Discussion.....108
A.5 Conclusion.....112
A.6 Acknowledgments 113
A.7 References 114

List of Tables:

Table 2.1 The charge of each of the polymer coated nanostars and the controls. The table shows an increase in charge when gold nanostars are functionalized with ligands and polymers from -34.8 ± 0.2 mV to as high as 41.1 ± 0.5 mV. 37

Table 2.2 The hydrodynamic size of each of the polymer coated nanostars and the controls. The table shows an increase in size when gold nanostars are functionalized with ligands and polymers from 105.8 ± 1.7 nm to as high as 204.4 ± 11.5 nm. 38

Table 3.1 Cell Viability results with respect to the control for each of the six TAC polymers, PEI(Pep), PEI (Mo), PEI(iP), PMAS(Pep), PMAS(Mo), and PMAS(iP) coated gold nanostars. Each was tested at 10, 20 and 50 µg/mL of polymer and with a constant concentration of gold nanostars. 54

Table 4.1 The sequences synthesized and ordered from IDT to develop and test SANSPs. The sequences originate from 5'-TCA TTT TTG TTG CTT TTG TTT -3' located in the conserved region of IAV segment 4. 73

List of Figures:

Figure 1.1 Representation of viral reproduction. Once a cell is infected, the negative-sense RNA is used as a template for the positive-sense RNA, which is then used as template for the negative-sense RNA and viral protein production. The protein forms a capsid to encapsulate the negative-sense RNA to form progeny viruses. 5

Figure 1.2 Representation of localized surface plasmon resonance and oscillation of delocalized electrons.[43] 8

Figure 2.1 Step by step illustration of the silica coated gold nanostar synthesis. 27

Figure 2.2 Representation SERS nanostar probes (SANSPs), which consist of gold nanostars functionalized with a Raman tagged beacon DNA that is hybridized with a complementary oligo creating the SANSPs with the SERS signal quenched (off state). Upon addition of the viral RNA to SANSPs, the complementary oligo de-hybridizes and hybridizes with the viral RNA. The beacon then returns to its folded hairpin conformation with consequent increase in SERS signal intensity (on state). 30

Figure 2.3 a) UV-Vis spectra of 12 nm gold nanospheres dispersed in Milli-Q water. b) TEM micrograph of 12 nm gold nanospheres dispersed. c) SEM image of 12 nm gold nanospheres. 33

Figure 2.4 a) UV-Vis spectra of surfactant free gold nanostars dispersed in Milli-Q water. b) TEM image of surfactant free gold nanostars. 33

Figure 2.5 a) TEM micrograph of silica coated gold nanostars b) TEM micrograph of silica coated gold nanostars after 30 hours of etching. 34

Figure 2.6 SERS signal of Cy3 labeled beacon conjugated to silica coated gold nanostars and an illustrative representation of the particles in the top left corner. 36

Figure 3.1 Structures of the bis(dialkylamino)cyclopropenium chloride groups, morpholine (Mo), piperidine (Pep), and isopropyl (iP). Each are added via an amide bond to the backbone of poly(ethyleneimine) (PEI) and poly(methylaminostyrene) (PMAS). .46

Figure 3.2 The charge of each of the polymer coated nanostars and the controls. The graph shows a clear increase in charge when gold nanostars are functionalized with ligands and polymers from -34.8 ± 0.2 mV to as high as 41.1 ± 0.5 mV. 51

Figure 3.3 The hydrodynamic size of each of the polymer coated nanostars and the controls. The graph shows a clear increase in size when gold nanostars are functionalized with ligands and polymers from 105.8 ± 1.7 nm to as high as 204.4 ± 11.5 nm. 52

Figure 3.4 Comparison of the cell viability of the six TAC polymers, PEI(Pep), PEI (Mo), PEI(iP), PMAS(Pep), PMAS(Mo), and PMAS(iP) coated gold nanostars, PEI coated gold nanostars, and a control, gold nanostars without any polymer coatings. Each was tested at 10, 20 and 50 µg/mL of polymer and with a constant concentration of gold nanostars. 55

Figure 3.5 Images of FITC-PEG conjugated surfactant free gold nanoparticles, PEI coated FITC-PEG conjugated gold nanoparticles, and PMAS(Mo) coated FITC-PEG conjugated gold nanoparticles incubated in BMSC for 2 and 4 hours. The PMAS(Mo) coated nanostars showed significant improvement in endosomal escape over PEI coated nanostars and bare nanostars.....57

Figure 4.1 The SERS active nanoparticle probes were characterized via TEM. a) TEM micrograph of silica coated gold nanostars with exposed tips. The image shows a thin layer of silica around the core of the nanostars leaving the gold surface on the tips of exposed. b) A close-up image of the exposed tips.....78

Figure 4.2 a) Representation of the silica coated gold nanostars functionalized with the unhybridized beacon (top) and with the beacon hybridized to the complementary strand (bottom). b) SERS spectra of silica coated gold nanostars functionalized with Cy3 labeled beacon and PEG. The beacon is in the hairpin position, bringing the Cy3 Raman reporter in proximity of the gold surface resulting in an enhanced SERS signal ("On" state). c) SERS spectra of silica coated gold nanostars functionalized with PEG and Cy3 labeled beacon hybridized to the complementary strand. The beacon is no longer in the hairpin position, bringing the Cy3 Raman reporter away from the gold surface resulting in a decreased SERS signal ("Off" state).....79

Figure 4.3 Comparison of the "on-off" signal difference between unhybridized thiolated beacon functionalized (B) and after complementary strand addition (B+C) in a) surfactant free gold nanostars b) etched silica coated gold nanostars. The unspecified binding to the tips and the core on the surfactant free gold nanostars resulted in false "On" signals. 81

Figure 4.4 Representation of the SANSPs tested in solution. "B" indicates the nanostars conjugated to the beacon in its hairpin conformation. "B+C" represents the nanostars conjugated to the beacon hybridized to its complementary strand. "B+C+T" represents the configuration achieved after target RNA introduction, which leads to dehybridization of the complementary strand from the nanostar, followed by its hybridization to the target RNA and folding of the beacon back into hairpin conformation. "B+C+R" represents the case in which a random RNA sequence is introduced in the system.....83

Figure 4.5 Representation of the stability of SANSPs that were prepared at 37°C and tested against the target RNA at 37°C. "B" indicates the nanostars conjugated to the beacon in its hairpin conformation. "B+C" represents the nanostars conjugated to the

beacon hybridized to its complementary strand. “B+C+T” represents the configuration achieved after target RNA introduction, which leads to dehybridization of the complementary strand from the nanostar, followed by its hybridization to the target RNA and folding of the beacon back into hairpin conformation. 84

Figure 4.6 Stability of SANSPs over time for the configuration shown in the boxed illustration. 85

Figure 4.7 SANSPs interaction with the target RNA with different degree of base mismatch. The results showed a linear trend as the number of base pair modifications were made at SERS signal 1586 cm^{-1}. 88

Figure 4.8 The SERS spectrum shows the recovery of the SERS signal from Cy3 signal after exposing the SANSPs to target RNA-spiked HeLa cell lysate, demonstrating the SANSPs ability to target RNA even with intracellular obstacles such as nucleases and protein corona. 89

Figure 4.9 a) Cellular viability of 50, 75, 100, 125, and 150 µg/mL of SANSPs per well of HeLa cell. b) Fluorescence image of FITC labeled SANSPs showing efficient uptake of the probe. 90

Figure 4.10 The spectra show an intense SERS signal for single cell analysis of HeLa cells transfected with IAV H1N1 HA plasmid. This signal is not as strong as studies in solution but strong enough to differentiate the signal from HeLa cells transfected with IAV H1N1 PB1 plasmid, HeLa cells transfected with IAV H1N1 PB2 plasmid, and non-transfected HeLa cells. Additionally, the SANSPs were tested with PMAS(Mo) from chapter 3. The intense signal demonstrates a proof of concept study that the platform can successfully target specific vRNA without the need for amplification. The addition of a

PMAS(Mo) coating increases the amounts of SANSPs taken up the cell with minimal SERS response interference. 92

List of Schemes:

Scheme 4.1 Schematic diagram of the SERS nanostar probes (SANSPs). Gold nanostars are initially functionalized with a Raman tagged beacon DNA that is then hybridized with a complementary oligo creating the SANSPs. Upon exposure to the viral RNA, the complementary oligo de-hybridizes and hybridizes with the viral RNA, allowing the beacon to return to its original folded conformation. Upon addition of the complementary strand the SERS signal will be quenched (off state). Addition of the target RNA will lead to dehybridization of the complementary strand, re-folding of the beacon in its hairpin conformation with consequent increase in SERS signal intensity, which will depend on the number of base mutations in the vRNA (on state).....67

Chapter 1 INTRODUCTION

1.1 Background

Viral infections are a cause of increased morbidity and mortality. Despite efforts with vaccination, influenza A, a recurring seasonal epidemic, is highly contagious and causes thousands of deaths and billions of dollars in healthcare costs in the United States alone.[1] The Center for Disease Control and Prevention reported that the effectiveness of the 2016-2017 vaccine against the influenza A virus (IAV) ranged from 57% to as low as 13% depending on the age group.[2] The lack of efficacy in current preventative measures is due to the unpredictable nature of IAV which is highly prone to mutation as it replicates, leading it to grow resistant to drugs and vaccines.[3, 4] While the phenomenon is not a common occurrence among all viruses, and viral infections can be effectively controlled by vaccinations, IAV is not.[5, 6] Therefore, there has been extensive research on understanding viral mutation and evolution in IAV.

Current tools for virus detection progressed from the 1950s, when tissue culture systems were first developed, to current methods of immunoassays, such as polymerase chain reaction (PCR), serological detection, and molecular detection.[7] The recognition of viral markers with the use of antibodies is a common method for viral detection. Kits that assay for proteins and enzymes are widely used due to their commercial availability, relative safety, and limited cost. Serological detection became a standard method used for evaluating vaccines and antiviral therapies.[7] The current challenges with serological detection emerge from cross-reactivity of antibodies, which can produce false positive results.[7]

In more recent years, molecular techniques have become increasingly popular with the use of PCR and blot hybridization.[8] The majority of approaches employed in virus

detection are amplification-based molecular techniques. Non-amplified techniques are commonly applied in clinical samples for direct testing, reduced cost, and reduction of time consuming steps required during amplification of specific viruses[9]. These tools have led to promising automated detection systems that are used in clinical settings. However, due to high genetic variability and the unpredictable nature of IAV, these tools have limitations in sensitivity, reproducibility, and cost.[8]

Nanotechnology has emerged as a promising tool for viral detection.[10, 11] The surface chemistry of nanoparticles allows for facile conjugation of targeting viral-derived molecules, such as antibodies, peptides, and oligonucleotides, to create nanoparticle delivery systems, biosensors, and probes.[12] Specifically, gold nanoparticles are at the basis of countless examples in the literature as biosensors with high sensitivity. The preference of gold nanoparticles rather than other metallic and polymeric nanoparticles for biosensors, is owed to their stability, biocompatibility, signal amplification potential, and facile customization of size, morphology, and surface chemistry.[13]

1.2 Viruses and Viral Evolution

All living cells are subject to viral infections and diseases. IAV infections have been especially cumbersome to prevent, despite efforts with vaccines, due the high probability of the virus to mutate and adapt.[2-4] The rapid evolution of IAV is attributed to the size of mammalian populations that can quickly become infected by the airborne disease, its short replication times, and most importantly, high mutation rates.[14] IAV must successfully interacts with the host while evading immune recognition in order to survive.[15] IAV adaptation can be credited to three mechanisms: Mutation, re-assortment,

and recombination, with the latter two being the least common.[14] To that end, researchers are examining methods to interfere with or disrupt viral evolution.

One concept for an antiviral solution is "evolutionary suicide" of viral populations, which aims to disrupt the viral ecology and adaptive landscape of a viral population to push for decreased fitness via natural selection.[16] Brooke *et al.* were able to provide evidence that a predominant amount of IAV virions expresses incomplete sets of viral proteins rendering them incapable of multi-round replication.[17] *In vitro* studies have shown that defective interfering virus particles can interfere with the replication of infectious viruses and hold immense potential as antivirals.[18] These defective interfering particles (DIPs) are naturally formed through mutations and can possibly turn the very device used as a survival mechanism against them.

IAV consists of eight negative-sense single stranded RNA segments, which are all essential for productive infection of host cells.[19] They can only produce protein once they have infected a host from which they use the negative-sense RNA as a template for the positive-sense RNA. The positive-sense RNA can then produce viral proteins, the capsids, and can be used as a template for the negative-sense RNA. The IAV virus genome expresses 13 proteins. The capsids arrange to form a protein coat and encapsulate the negative-sense RNA forming a progeny virus that is ready to be released from the host. **(Figure 1.1)** During this process, the replicated RNA is prone to errors and mutations.

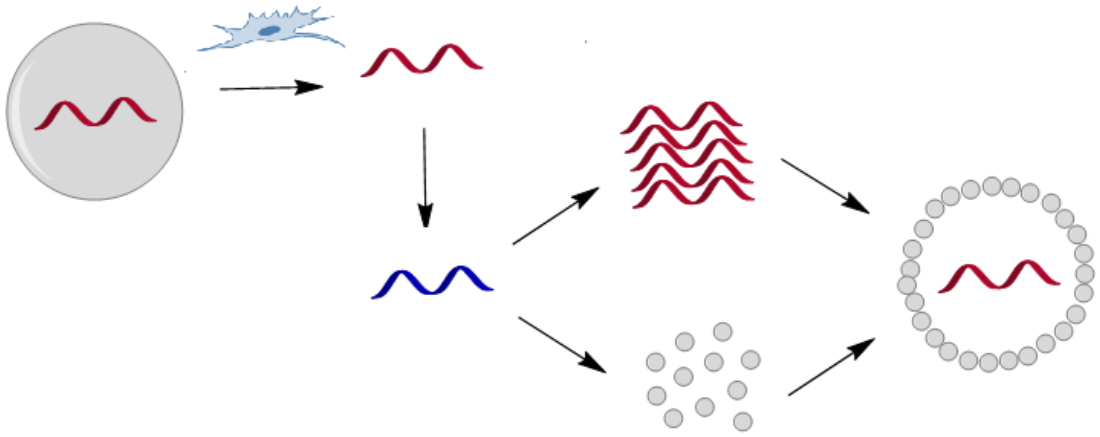

Figure 1.1 Representation of viral reproduction. Once a cell is infected, the negative-sense RNA is used as a template for the positive-sense RNA, which is then used as template for the negative-sense RNA and viral protein production. The protein forms a capsid to encapsulate the negative-sense RNA to form progeny viruses.

1.3 Nanoparticle Tools for Intracellular Sensing

Nanomaterials have gained attention for their significant role in the progression of nanotechnology as a whole.[20, 21] Specifically, gold nanoparticles have become a preferred material owing to their unique physical properties and plasmon resonance.[22-24] Gold nanoparticles were first discovered by Michael Faraday in 1857 and, in recent years, have carved a spot in various biomedical fields.[13, 22, 25-27] Various applications, such as targeted drug delivery, immunoassays, biosensing, optical imaging, and intracellular tracking have

been studied by exploiting the gold nanoparticle's surface chemistry, size, optical activity, and localized surface plasmon resonance.[28-32]

An important aspect to address to effectively employ nanoparticles for biomedical applications, specifically intracellular sensing, is their successful cell uptake and biocompatibility. Several studies have been conducted showing nanoparticle biocompatibility and low cytoxicity.[33] The size, shape, and surface chemistry of gold nanoparticles have been extensively studied to evaluate cytotoxic effects on healthy and diseased cells, with the conclusion that the shape has minimal impact on cell viability while surface chemistry plays a significant role in toxicity.[34] There are previously reported biocompatible surface ligands and coating options that allow for intracellular targeting, such as aptamers, antibodies, and proteins; for facilitated uptake, such as cell penetrating peptides, ligand mediated, and cationic polymers; and for nanoparticle stability, such as polyethylene glycol, within the cytoplasm.[35, 36] The shape of nanoparticles comes into effect for the analysis of biological specimens, such as tissues or blood, because their specific composition renders them semi-transparent in the near infrared (NIR) region of the electromagnetic spectrum. If one therefore wants to employ gold nanoparticles because of their unique plasmonic response, it is necessary to design them to absorb in the NIR. In this respect, the plasmonic resonance of gold nanostars can be suitably tuned in the NIR, making their morphology ideal in bioapplications.[37] Gold nanostars have been developed and studied as a tool for surface enhanced Raman spectroscopy (SERS)-based intracellular sensing.[38]

1.4 SERS and SERS Tags

Raman spectroscopy is a non-destructive spectroscopic technique that provides vibrational and rotational information to identify molecules based of inelastic scattering[39]. Despite being a useful tool for biomolecule analysis, its scattering intensity is low. Raman scattering cross sections are on the order of 10^{-30} cm^2/molecule, whereas typical fluorescence has cross sections on the order of 10^{-15} cm^2/molecule.[40] To overcome this challenge, several Raman techniques have been developed. One of the most notable techniques is SERS[39]. The Raman signal of an analyte is significantly increased with an enhancement factor of 10^8-10^{10} when it is placed in proximity to the surface of a noble metal nanoparticle, such as gold or silver[22, 40]. Gold nanoparticles (AuNPs) in particular, in addition to enhancing the Raman signal by several orders of magnitude, are also more biocompatible than their silver counterparts, making them an indispensable tool for biosensing.[41]

When AuNPs are exposed to electromagnetic waves, the free conduction electrons at the metal-dielectric interface coherently oscillate out of equilibrium in response to the oscillating electric field. The equilibrium is then re-established by coulombic restoring forces that form an oscillating dipole resonating at a specific frequency called localized surface plasmon resonance (LSPR) **(Figure 1.2)**.[42] Upon absorption of the incoming radiation, the electric field is scattered back out of the nanoparticle with intensity amplification that depends on the properties of the nanostructure, and is localized within a few nanometers from its surface. SERS is a spectroscopic technique that relies on the electric field enhancement provided by noble metals. If the analyte molecule is placed near the SERS-active surface of AuNPs, the intensity of scattered Raman signal is

amplified by several orders of magnitude.

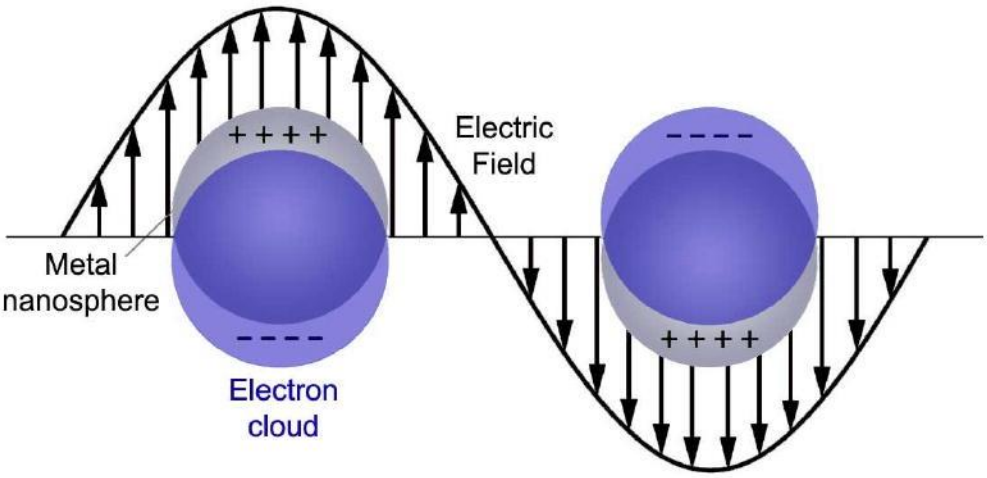

Figure 1.2 Representation of localized surface plasmon resonance and oscillation of delocalized electrons.[43]

A SERS-active noble metal can be combined with a Raman reporter molecule to create a SERS tag. Depending on the sample in question and the environment the SERS tag will function in, the Raman reporter would be a suitable molecule with a known spectroscopic fingerprint and the nanoparticle can be functionalized with ligands or coated for added stability. A SERS tag allows for indirect identification of an analyte by tracking its SERS signal, not the analyte itself, similar to what fluorescent dyes do. It is especially useful for identification of biological tissues which have weak intrinsic Raman signals or complex SERS patterns when enhanced by added gold nanoparticles.

1.5 Gold Nanostars

AuNPs have been studied in detail to achieve very precise control over their morphology and size, which in turn regulate their plasmonic response. Several bottom-up synthetic protocols have been developed for the synthesis of AuNPs, the most notable of which is the citrate capped protocol for spherical AuNPs developed in the 1950s, from which further modifications have led to various different morphologies, including nanospheres, nanorods, and nanostars.[44, 45] The localized surface plasmon resonance (LSPR) is tuned with the morphology and size of the nanoparticle, ranging from the visible for nanospheres to the NIR for nanostars. Nanostars have emerged as a significant material for the analysis of biological samples via SERS due to their LSPR resonance in the NIR region, as mentioned above.[46]

Placing a Raman active molecule in proximity to the gold surface of the nanoparticles enhances the SERS intensity by several orders of magnitude. The signal is even further enhanced when the Raman active molecule is near a hot spot, which is caused by the coupling of plasmon modes and found on junctions, vertices, and edges of nanoparticles.[47] Gold nanostars are capable of enhancing the intensity of Raman signals due to the gold spiky tips they possess. Additionally, core-shell structures such as silica coated nanostars can further improve bioanalysis of samples by limiting the contact of Raman active molecules to the hot spots located on the tips of nanostars.[48]

1.6 Surface Coating and Bio-Conjugation

Due to their surface chemistry, gold nanoparticles can readily be functionalized and coated with a number of ligands and materials.[49] Surface coatings include metallic and

semiconducting shells, which can be crystalline and amorphous, and polymer coatings. Core-shell systems can be synthesized via epitaxial deposition, sol-gel methods, and electrostatic interactions.[50, 51] Silica-coated inorganic nanoparticles are an example of a widely used core-shell system. Silica coated nanoparticles emerged due to their biocompatibility and stability in cell media.[52] Additionally, the thickness of the silica can be controlled to create either a thick shell or a shell thin enough to expose distinct features of the nanoparticles, such as exposing the gold surface of spike tips on gold nanostars.[48]

Polymer coatings have been used to improve drug delivery and cellular uptake. Polymers, such as poly(ethylenimine) (PEI) and its derivatives, have significantly improved the functionality of gold nanoparticles for intracellular applications. Electrostatically coating positively charged PEI to the surface of negatively charged gold nanostars, allows for facilitated cellular uptake and endosomal escape.[53] PEI-coated nanostars are just one of the many examples of how surface coating can drastically tune the gold nanoparticle properties.

Ligands contribute significantly to how nanoparticles interact with their surroundings, such as the effects of covalently bound poly(ethylene glycol) (PEG) to the surface of nanoparticles. PEG adds stability to nanoparticles, enhances biodistribution, increases cellular uptake, and prevents irreversible aggregation to ensure single particle SERS detection.[54] Ligands can also include targeting moieties that can recognize and selectively bind to cellular components of various nature.

1.7 Targeting Molecules

In order to add specificity to a nanoparticle probe, a targeting molecule is essential to allow the nanoparticle to recognize its target and bind to an area of interest. The targeting molecules are typically derived from a biomolecule expressed by the cell membrane, organelle, nucleic acid, or protein of interest. When nanotechnology was first developed for bio-targeting, antibodies pioneered the world of targeting moieties.[55] Other biomolecules and synthetic molecules such as peptides, protein domains, aptamers, and synthetic RNA, DNA, and PNA quickly followed.[22] Aptamers are short single stranded oligonucleotides that can potentially bind to several biological targets. RNA, DNA, and PNA segments can be customized and synthesized to target specific sequences and targets. Each of these targeted molecules have or can include moieties than bind to the surface of gold nanostars.

Unlike PEI, which can be electrostatically bound to the surface of nanoparticles, targeting molecules are covalently linked to ensure a strong association bond. Gold nanoparticles leverage their coatings and surface chemistry for covalent interactions. The covalent bonds are formed between the targeting molecule or linker molecules and the surface of the nanoparticles. Types of conjugation include: Amide bonds, gold-thiol bonds, thio-ether bonds, disulfide bonds, biotin/streptavidin, and triazole rings.[55] For instance, thiolated targeting molecules can bind directly to gold surfaces via a thiol-Au bond, while targeting molecules with amine groups, such as proteins and antibodies, can bind with the assistance of N-hydroxysuccinimide (NHS) terminated linkers forming an amide bond.[22] Some targeting molecules, such as custom oligonucleotides, can be synthesized to

include a functional group of interest for surface conjugation.

1.8 Application of SERS in Bio-Sensing

SERS is well suited for the detection of small analytes and biomarkers: It produces unique fingerprints for molecular structures and it is especially useful for water-based materials, since water has a very small Raman scattering cross-section.[40] Unlike other analytical methods, such as polymerase chain reaction (PCR), the analysis is quick, cost effective, and eliminates the need for amplification. Gold nanostar-based SERS tags are not susceptible to photobleaching and can achieve high signals upon indirect biomarker detection due to their resonance in the NIR region, also known as the biological transparent window.[46]

Small molecules such as antibodies, aptamers, and synthetic oligonucleotides have been employed as targeting moieties in SERS tags to develop biosensors for detection of cancer cells, glucose, antioxidants, mitochondrial diseases, and viral infections[55, 56]. For instance, Lim *et al.* utilized the sensitivity of SERS to identify mutated and emerging IAV strains.[56] The fingerprint information obtained from Raman scattering also provides information on a molecule of interest, enabling to closely monitor any changes or mutations to a biomarker. In their study,[54] Lim *et al.* developed a label-free IAV detection method using gold nanoparticles as SERS tags. They were able to rapidly identify newly emerging IAV strains by targeting surface proteins and lipids characteristic to each virus.

SERS based assays and biosensors are constantly progressing to include multiplex assays. Studies have demonstrated SERS-based multiplex assays with high sensitivity[57]. Neng *et*

al. developed a multiplexed detection method of surface envelope and capsid antigens from West Nile virus and Rift Valley fever virus using SERS by utilizing antibody recognition via a Raman reporter-coated gold nanoparticle.[57]

Additional medical applications include the detection of cell surface cancer biomarkers of two different cancer cell types with antibody-conjugated SERS tags using triphenylmethine and cyanine Raman reporters demonstrated by Maiti *et al*.[58] The detection of food-borne bacterial pathogens by Cam *et al.,*[59] and the detection of water borne bacterial pathogens by Rule *et al.*[60] validate the versatility of SERS sensors.

1.9 Dissertation Hypothesis and Overview

Overall, it has been demonstrated that gold nanoparticles hold tremendous potential for biomedical applications including SERS-based biosensing and intracellular targeting. Gold nanostars are biocompatible and offer unique optical properties. They can be designed as SERS tags for highly sensitive detection. Furthermore, with the help of transfection agents they can be designed for intracellular targeting.

We hypothesize that SERS-active gold nanostar probes will provide significant enhancement of SERS signals for targeted detection of viral RNA with high sensitivity to distinguish between wild type and defective RNA sequences and can track viral mutations intracellularly at the single cell level. Additionally, we hypothesize that the TAC polymer-mediated uptake will allow for rapid uptake and endosomal escape of the probes that will match the kinetics of viral infections.

In this dissertation, the overall objective was to develop a SERS-based intracellular biosensor for viral RNA identification and mutation detection. For this purpose, I have

developed three specific aims that would achieve the overall goals. The first specific aim was to identify synthetic methods for the development of intracellular targeting nanoparticles. The second specific aim was to device a method for cellular uptake and endosomal escape of gold nanoparticles with biodistribution within the cell. The third and last specific aim was to detect viral mutations and identify viral RNA at the single cell level in intact individual cells.

In the second chapter of this thesis the synthesis of nanoparticles is described in detail. Synthetic methods that influence shape, size, and surface chemistry are discussed to determine optimal nanostar platforms for *in vitro* studies. To test for cellular uptake, gold nanostars were synthesized and functionalized with a thiolated FITC PEG, for added stability and fluorescent labeling, then electrostatically coated with six different Trisaminocylcopropenium (TAC) polymers. These polymer-coated nanostars were each tested for stability, size, charge, and functionality. Additionally, surfactant free gold nanostars were synthesized and coated with a thin layer of silica to limit the location of functionalized ligands to the hot spots located at the tips of the spikes. The particles were then functionalized with PEG, for added stability, and Cy3-labeled oligonucleotides that function as recognition moieties. The stability and functionality of these particles were extensively tested and optimized.

The third chapter focuses on cellular uptake. Here we use TAC polymers for facilitated cellular uptake of gold nanostars. Each of the six TAC polymer-coated gold nanostars were synthesized, characterized, and compared to a control particle coated with the current standard polymer poly(ethylenimine) (PEI). The particles were tested in an *in vitro* study in human bone marrow stem cells (BMSC). The cell viability of the BMSC

exposed to the seven polymer-coated nanoparticles was determined by assessing metabolic activity with an MTT assay, which narrowed down the best of the six TAC polymers for further studies. The cellular uptake of the nanoparticles was analyzed by endosomal staining and fluorescence microscopy.

The fourth chapter focuses on the design and implementation of the SERS-based biosensor for the detection of viral mutations and the identification of viral RNA at the single cell level. Gold nanostars are functionalized with Raman reporter-labeled oligonucleotides to create a SERS tag that recognizes and detects its RNA target. The SERS-active nanoparticle probes were tested in solution and *in vitro*. To test for sensitivity towards viral RNA mutation, the target RNA was modified with base pair mismatches from the original target RNA. Each target RNA type was tested with the targeting moiety. Similarly, the recognition moiety was modified with base pair mismatches for its original version and tested against the original target RNA. Once detection sensitivity was established, the SERS-active nanoparticle probes were tested in both target RNA-spiked HeLa cell lysate and plasmid-transfected HeLa cells. The samples were analyzed via SERS to determine viral RNA detection and base pair mutation sensitivity.

The fifth chapter summarizes the conclusions of all the findings within this thesis. The results from the studies conducted satisfy the specific aims of identifying synthetic methods for the development of intracellular targeting nanoparticles, developing a method for cellular uptake and endosomal escape of gold nanoparticles with biodistribution within the cell, and detecting viral mutations and identifying viral RNA at the single cell level. The summary and future research direction of each is discussed.

The appendix sheds light onto an additional series of experiment that was not directly related to tools for viral RNA analysis, but has its benefits in the analysis of biomolecules. The integration of nanoparticles with bio-samples for matrix-assisted laser desorption/ionization –time of flight mass spectrometry (MALDI-TOF MS) is analyzed for signal enhancement. Samples that produce low signal-to-noise and low signal intensity, such as fatty acids, are extracted from vitamin supplements, such as fish oil and macadamia oil, and tested with gold nanostars. The samples showed significant enhancement compared to current methods in whichetched stainless-steel plates and gold-coated plates are used as substrates. The results demonstrate another approach to leveraging the enhancement produced by gold nanoparticles and an analytical technique that could benefit from it.

1.10 References

1. Gyllenberg, M. & Parvinen, K. Necessary and sufficient conditions for evolutionary suicide. *Bulletin of Mathematical Biology* **63**, 981-993 (2001).
2. in Seasonal Influenza (Flu) (Center for Disease Control and Prevention, 2018).
3. Hussain, M., Galvin, H.D., Haw, T.Y., Nutsford, A.N. & Husain, M. Drug resistance in influenza A virus: the epidemiology and management. *Infection and drug resistance* **10**, 121-134 (2017).
4. Taubenberger, J.K. & Morens, D.M. Influenza Viruses: Breaking All the Rules. *mBio* **4** (2013).
5. Brooke, C.B. Population Diversity and Collective Interactions during Influenza Virus Infection. *Journal of virology* **91** (2017).
6. Duffy, S., Shackelton, L.A. & Holmes, E.C. Rates of evolutionary change in viruses: patterns and determinants. *Nature Reviews Genetics* **9**, 267 (2008).
7. Ellis, J.S. & Zambon, M.C. Molecular diagnosis of influenza. *Reviews in medical virology* **12**, 375-389 (2002).
8. Ratcliff, R.M., Chang, G., Kok, T. & Sloots, T.P. Molecular diagnosis of medical viruses. *Current issues in molecular biology* **9**, 87-102 (2007).
9. Kaewphinit, T., Santiwatanakul, S., Promptmas, C. & Chansiri, K. Detection of non-amplified Mycobacterium tuberculosis genomic DNA using piezoelectric DNA-based biosensors. *Sensors (Basel, Switzerland)* **10**, 1846-1858 (2010).
10. Zehbe, I. et al. Sensitive in situ hybridization with catalyzed reporter deposition, streptavidin-Nanogold, and silver acetate autometallography: detection of single-copy human papillomavirus. *The American journal of pathology* **150**, 1553-1561 (1997).
11. Baptista, P. et al. Gold nanoparticles for the development of clinical diagnosis methods. *Anal Bioanal Chem* **391**, 943-950 (2008).
12. Wang, X., Liu, L.H., Ramstrom, O. & Yan, M. Engineering nanomaterial surfaces for biomedical applications. *Experimental biology and medicine (Maywood, N.J.)* **234**, 1128-1139 (2009).
13. Rosi, N.L. & Mirkin, C.A. Nanostructures in Biodiagnostics. *Chemical Reviews* **105**, 1547-1562 (2005).
14. Shao, W., Li, X., Goraya, M.U., Wang, S. & Chen, J.-L. Evolution of Influenza A Virus by Mutation and Re-Assortment. *International Journal of Molecular Sciences* **18**, 1650 (2017).
15. Taubenberger, J.K. & Kash, J.C. Influenza virus evolution, host adaptation, and pandemic formation. *Cell host & microbe* **7**, 440-451 (2010).
16. Parvinen, K. Evolutionary suicide. *Acta Biotheoretica* **53**, 241-264 (2005).
17. Brooke, C.B. et al. Most Influenza A Virions Fail To Express at Least One Essential Viral Protein. *Journal of virology* **87**, 3155-3162 (2013).
18. Dimmock, N.J. & Easton, A.J. Defective interfering influenza virus RNAs: time to reevaluate their clinical potential as broad-spectrum antivirals? *Journal of virology* **88**, 5217-5227 (2014).
19. Palese, P. Orthomyxoviridae : the viruses and their replication. *Fields Virology*, 1647-1689 (2007).

20. Breunig, M., Bauer, S. & Goepferich, A. Polymers and nanoparticles: intelligent tools for intracellular targeting? *European journal of pharmaceutics and biopharmaceutics : official journal of Arbeitsgemeinschaft fur Pharmazeutische Verfahrenstechnik e.V* **68**, 112-128 (2008).
21. Salata, O. Applications of nanoparticles in biology and medicine. *Journal of Nanobiotechnology* **2**, 3 (2004).
22. Laura, F. Gold-based SERS tags for biomedical imaging. *Journal of Optics* **17**, 114002 (2015).
23. Elahi, N., Kamali, M. & Baghersad, M.H. Recent biomedical applications of gold nanoparticles: A review. *Talanta* **184**, 537-556 (2018).
24. Das, M., Shim, K.H., An, S.S.A. & Yi, D.K. Review on gold nanoparticles and their applications. *Toxicology and Environmental Health Sciences* **3**, 193-205 (2011).
25. Faraday, M. X. The Bakerian Lecture. —Experimental relations of gold (and other metals) to light. *Philosophical Transactions of the Royal Society of London* **147**, 145-181 (1857).
26. Sharma, V., Park, K. & Srinivasarao, M. Colloidal dispersion of gold nanorods: Historical background, optical properties, seed-mediated synthesis, shape separation and self-assembly. *Materials Science and Engineering: R: Reports* **65**, 1-38 (2009).
27. Liu, X. et al. A one-step homogeneous immunoassay for cancer biomarker detection using gold nanoparticle probes coupled with dynamic light scattering. *Journal of the American Chemical Society* **130**, 2780-2782 (2008).
28. Chandran, P.R. & Thomas, R.T. in Nanotechnology Applications for Tissue Engineering. (eds. S. Thomas, Y. Grohens & N. Ninan) 221-237 (William Andrew Publishing, Oxford; 2015).
29. Bhamidipati, M., Lee, G., Kim, I. & Fabris, L. SERS-Based Quantification of PSMA in Tissue Microarrays Allows Effective Stratification of Patients with Prostate Cancer. *ACS Omega* **3**, 16784-16794 (2018).
30. Li, Y., Schluesener, H.J. & Xu, S. Gold nanoparticle-based biosensors. *Gold Bulletin* **43**, 29-41 (2010).
31. Wu, Y., Ali, M.R.K., Chen, K., Fang, N. & El-Sayed, M.A. Gold nanoparticles in biological optical imaging. *Nano Today* (2019).
32. Liu, M. et al. Real-time visualization of clustering and intracellular transport of gold nanoparticles by correlative imaging. *Nature Communications* **8**, 15646 (2017).
33. Dykman, L.A. & Khlebtsov, N.G. Uptake of Engineered Gold Nanoparticles into Mammalian Cells. *Chemical Reviews* **114**, 1258-1288 (2014).
34. Bhamidipati, M. & Fabris, L. Multiparametric Assessment of Gold Nanoparticle Cytotoxicity in Cancerous and Healthy Cells: The Role of Size, Shape, and Surface Chemistry. *Bioconjugate Chemistry* **28**, 449-460 (2017).
35. Xie, X., Liao, J., Shao, X., Li, Q. & Lin, Y. The Effect of shape on Cellular Uptake of Gold Nanoparticles in the forms of Stars, Rods, and Triangles. *Scientific Reports* **7**, 3827 (2017).

36. Ortega-Munoz, M. et al. Polyethyleneimine-Coated Gold Nanoparticles: Straightforward Preparation of Efficient DNA Delivery Nanocarriers. *Chemistry, an Asian journal* **11**, 3365-3375 (2016).
37. Li, W. & Chen, X. Gold nanoparticles for photoacoustic imaging. *Nanomedicine* **10**, 299-320 (2015).
38. Halas, N.J., Lal, S., Chang, W.S., Link, S. & Nordlander, P. Plasmons in strongly coupled metallic nanostructures. *Chem Rev* **111**, 3913-3961 (2011).
39. Ember, K.J.I. et al. Raman spectroscopy and regenerative medicine: a review. *npj Regenerative Medicine* **2**, 12 (2017).
40. Bantz, K.C. et al. Recent progress in SERS biosensing. *Physical chemistry chemical physics : PCCP* **13**, 11551-11567 (2011).
41. Fabris, L. SERS Tags: The Next Promising Tool for Personalized Cancer Detection? *ChemNanoMat* **2**, 249-258 (2016).
42. Liang, A., Liu, Q., Wen, G. & Jiang, Z. The surface-plasmon-resonance effect of nanogold/silver and its analytical applications. *TrAC Trends in Analytical Chemistry* **37**, 32-47 (2012).
43. Cobley, C.M. & Xia, Y. Engineering the Properties of Metal Nanostructures via Galvanic Replacement Reactions. *Mater Sci Eng R Rep* **70**, 44-62 (2010).
44. Turkevich, J., Stevenson, P.C. & Hillier, J. A study of the nucleation and growth processes in the synthesis of colloidal gold. *Discussions of the Faraday Society* **11**, 55-75 (1951).
45. Li, N., Zhao, P. & Astruc, D. Anisotropic Gold Nanoparticles: Synthesis, Properties, Applications, and Toxicity. *Angewandte Chemie International Edition* **53**, 1756-1789 (2014).
46. Zong, C. et al. Surface-Enhanced Raman Spectroscopy for Bioanalysis: Reliability and Challenges. *Chemical Reviews* **118**, 4946-4980 (2018).
47. Shiohara, A. et al. Plasmon Modes and Hot Spots in Gold Nanostar–Satellite Clusters. *The Journal of Physical Chemistry C* **119**, 10836-10843 (2015).
48. Atta, S., Tsoulos, T.V. & Fabris, L. Shaping Gold Nanostar Electric Fields for Surface-Enhanced Raman Spectroscopy Enhancement via Silica Coating and Selective Etching. *The Journal of Physical Chemistry C* **120**, 20749-20758 (2016).
49. Conde, J. et al. Revisiting 30 years of biofunctionalization and surface chemistry of inorganic nanoparticles for nanomedicine. *Frontiers in Chemistry* **2** (2014).
50. Ghosh Chaudhuri, R. & Paria, S. Core/Shell Nanoparticles: Classes, Properties, Synthesis Mechanisms, Characterization, and Applications. *Chemical Reviews* **112**, 2373-2433 (2012).
51. Elbakry, A. et al. Layer-by-layer coated gold nanoparticles: size-dependent delivery of DNA into cells. *Small (Weinheim an der Bergstrasse, Germany)* **8**, 3847-3856 (2012).
52. Guerrero-Martínez, A., Pérez-Juste, J. & Liz-Marzán, L.M. Recent Progress on Silica Coating of Nanoparticles and Related Nanomaterials. *Advanced Materials* **22**, 1182-1195 (2010).
53. Florea, B.I., Meaney, C., Junginger, H.E. & Borchard, G. Transfection efficiency and toxicity of polyethylenimine in differentiated Calu-3 and nondifferentiated COS-1 cell cultures. *AAPS pharmSci* **4**, E12-E12 (2002).

54. Jimenez de Aberasturi, D. et al. Surface Enhanced Raman Scattering Encoded Gold Nanostars for Multiplexed Cell Discrimination. *Chemistry of Materials* **28**, 6779-6790 (2016).
55. Friedman, A.D., Claypool, S.E. & Liu, R. The smart targeting of nanoparticles. *Current pharmaceutical design* **19**, 6315-6329 (2013).
56. Lim, J.Y. et al. Identification of Newly Emerging Influenza Viruses by Surface-Enhanced Raman Spectroscopy. *Anal Chem* **87**, 11652-11659 (2015).
57. Neng, J., Harpster, M.H., Wilson, W.C. & Johnson, P.A. Surface-enhanced Raman scattering (SERS) detection of multiple viral antigens using magnetic capture of SERS-active nanoparticles. *Biosensors & bioelectronics* **41**, 316-321 (2013).
58. Maiti, K.K. et al. Multiplex cancer cell detection by SERS nanotags with cyanine and triphenylmethine Raman reporters. *Chemical communications (Cambridge, England)* **47**, 3514-3516 (2011).
59. Çam, D., Keseroğlu, K., Kahraman, M., Sahin, F. & Culha, M. Multiplex Identification of Bacteria in Bacterial Mixtures with Surface-enhanced. (2009).
60. Rule, K.L. & Vikesland, P.J. Surface-Enhanced Resonance Raman Spectroscopy for the Rapid Detection of Cryptosporidium parvum and Giardia lamblia. *Environmental Science & Technology* **43**, 1147-1152 (2009).

Chapter 2 NANOPARTICLE SYNTHESIS

2.1 Abstract

Gold nanoparticles (AuNPs) have become one of the most extensively studied nanomaterials due to their unique physical and optical properties. The precise control over the morphology and size of AuNPs allows for fine tuning of their optical properties such as their plasmon resonance. These plasmonic nanoparticles have become an essential tool for Raman spectroscopy and have been an indispensable material for surface enhanced Raman spectroscopy (SERS). Several morphologies and sizes have been shown to enhance SERS signal intensity, with gold nanostars showing significant enhancement. Fine tuning gold nanostar synthesis allows for optimal SERS signal intensity as well as versatile surface chemistry. Therefore, in this chapter various forms of gold nanostars were developed for intracellular applications and SERS-based detection and assays. The synthesis of gold nanostars in this chapter was developed to provide highly sensitive SERS-based biosensing and efficient cellular uptake. Gold nanostars with high spike numbers were functionalized with a silica coating leaving the gold surface exposed at the tips in order to localize ligand conjugation at the hot spots. The particles were functionalized with polyethylene glycol (PEG), for added stability and biodispersity, and target-specific Raman labeled oligonucleotides, creating SERS-active nanoparticle probes for viral RNA detection with high sensitivity to base pair mismatches. In parallel, gold nanostars were prepared for efficient cellular uptake and endosomal escape. Negatively charged gold nanostars were functionalize with a FITC-labeled PEG and electrostatically coated with positively charged trisaminocyclopropenium (TAC) ion-functionalized polymers and compared to the widely used transfecting agent polyethyleneimine (PEI). After optimization of the

nanoparticle-based platform, the particles were successfully characterized and showed stability in cell media and tissue culture incubation conditions. Additionally, the particles showed intense SERS signals when in a Raman reporter was located in close proximity to their surface. Overall, the synthetic versatility of gold nanostars allowed for facile surface coating and functionalization for the development of an effective biocompatible nanoparticle-based biosensor for viral RNA detection.

2.2 Introduction

Nanomaterials have carved their place in various applications, including biomedical applications.

They have become an essential building block for the field of nanotechnology.[1, 2] Of the various types of nanomaterials, gold nanoparticles (AuNPs) have become the preferred material for biomedical studies due to their unique physical properties and plasmon resonance.[3-5] AuNPs have been around before the establishment of nanotechnology as a scientific field. In the past, AuNPs were used for their decorative colors and incorporated into pottery and stained glass.[6, 7] For modern uses, AuNPs were first discovered by Michael Faraday in 1857, who studied their optical properties.[8] Since then, researchers developed fascinating theories, morphologies, and applications.[9]

Despite the long history of AuNPs, their use in biological studies was only propelled by Faulk *et al.* in 1971.[10] The group introduced a method of antibody conjugation to the surface of AuNPs, establishing the start of extensive research dedicated to functionalizing nanoparticles for a wide range of biological applications, including biosensors, targeted delivery, phototherapy, genomics, and diagnostics.[11]

AuNPs have also been developed for signal enhancement in analytical techniques, such as Raman spectroscopy. With the help of plasmonic nanoparticles, surface enhanced Raman spectroscopy (SERS) has become a widely used technique.[5, 12] In proximity to a plasmonic surface, the signal intensity of a Raman active molecule is significantly enhanced by several orders of magnitude.[13] Moreover, the signal can be further enhanced by synthesizing nanoparticles with hot spots, which are locations at edges, tips, and junctions on the nanoparticles where the local scattered electric field reaches the highest values.[14] AuNPs in particular, have been shown to enhance the Raman signal while being a suitable material for manipulation of biological samples.[15] The surface plasmon resonance of AuNPs ranges from 520 nm for nanospheres to the near infrared region for nanostars, putting them in an ideal wavelength to analyze and monitor biological events. Through the combination of a surface chemistry amenable to straightforward bioconjugation and a plasmonic response that leads to substantial SERS enhancement factors, AuNPs have become an indispensable tool for biosensing.

The development of AuNPs has led to precise synthetic control over the morphology and size. This precision allows for tune-ability of shape, size, surface chemistry, and surface plasmon resonance. Each of these properties factor in when choosing an appropriate nanoparticle for a given study. In this dissertation, we discuss developing a SERS-active gold nanostar probe and an enhanced method for AuNP cellular uptake for intracellular targeting. Hence, a robust synthetic protocol for the synthesis of the functionalized nanoparticles is highly desirable to develop a biocompatible sensor.

Herein, we describe the synthetic methods for the synthesis of gold nanostars with various coatings and ligands. Surfactant free gold nanostars were synthesized via a seed

mediated method described by Yuan *et al.*[16] The particles were then coated with a thin layer of silica to limit the location of functionalized ligands to the hot spots.[17] The silica-coated particles were functionalized with polyethylene glycol (PEG), for added stability, and targeting moieties to create a nanoparticle probe. The stability and efficiency of the nanoparticle probes were extensively tested and optimized.

To optimize cellular uptake, gold nanostars were functionalized with a FITC-PEG polymer, for added stability and fluorescent labeling, then electrostatically coated with six different Trisaminocylcopropenium (TAC) polymers. These polymer-coated nanostars were each tested for stability, size, charge, and cytotoxicity.

2.3 Materials and Method

2.3.1 Surfactant Free Gold Nanostar Synthesis

Surfactant free gold nanostars were synthesized using modifications of established protocols from the literature.[16-18] The gold nanostars were prepared via a seed mediated method described by Yuan *et al.*[16] The seeds, citrate capped gold nanospheres, were synthesized according to a modified synthesis described by Turkevich.[18] Gold nanospheres were prepared by adding 8 mL of 0.025 M $HAuCl_4$ salt to 477 mL of Milli-Q water. The diluted gold salt was heated up to a boil under stirring, to which 15 mL of 1% citric acid trisodium salt was added and left to boil for 5 minutes. After the 5 minutes, the solution turned a deep red and was allowed to cool to room temperature. The cooled product was purified by centrifugation at 6000 g for 30 to 45 minutes. The nanospheres settled at the bottom in a pellet, which was collected.

Using the synthesized nanospheres, the gold nanostars were synthesized via a seed-

mediated protocol by adding 2 mL of 0.025 M $HAuCl_4$ salt solution, 200 µL of 1 N HCl, 48 mL of Milli-Q water, and 125 µL of 12 nm citrate capped spheres with an absorbance value of 2.81 at a 1 mm path length under gentle stirring. To the mixture, 2 mL of 3 mM $AgNO_3$ and 1 mL of 100 mM ascorbic acid were added simultaneously. The reaction was left to stir for 7 minutes, after which it turned a deep blue color. The resulting product was purified by centrifugation at 3000 g for 15 minutes.

2.3.2 Silica Coated Nanostar Synthesis

To prepare the silica coated gold nanostars, a modified version of the protocol from Atta *et al.*[17] was used. Briefly, the synthesized nanostars were capped with cetyltrimethyl ammonium bromide (CTAB) by mixing the gold nanostar solution with 10 mL of 0.2 M CTAB under gentle stirring and purified via centrifugation at 6500 g for 20 minutes. A modified Stöber method was used to recap the CTAB capped nanostars with silica. 50 µL of tetraethyl orthosilicate (TEOS) were added to 40 mL of 0.8 nM CTAB capped nanostars and stirred gently. After an hour of stirring, the pH of the mixture was adjusted to 8.6 by NH_4OH addition under gentle stirring for 24 hours. The resulting product was purified by centrifugation at 6500 g for 30-45 minutes.

The silica coating on the silica coated gold nanostars was then etched by adding 300 mg of $NaBH_4$ to 10 mL of 0.4 nM silica-coated gold nanostars under gentle stirring for 30 hours. The 30 hours of etching produced a silica shell covering the core of the stars and leaving the tips of the stars exposed. **Figure 2.1** illustrates a schematic diagram of the synthesis.

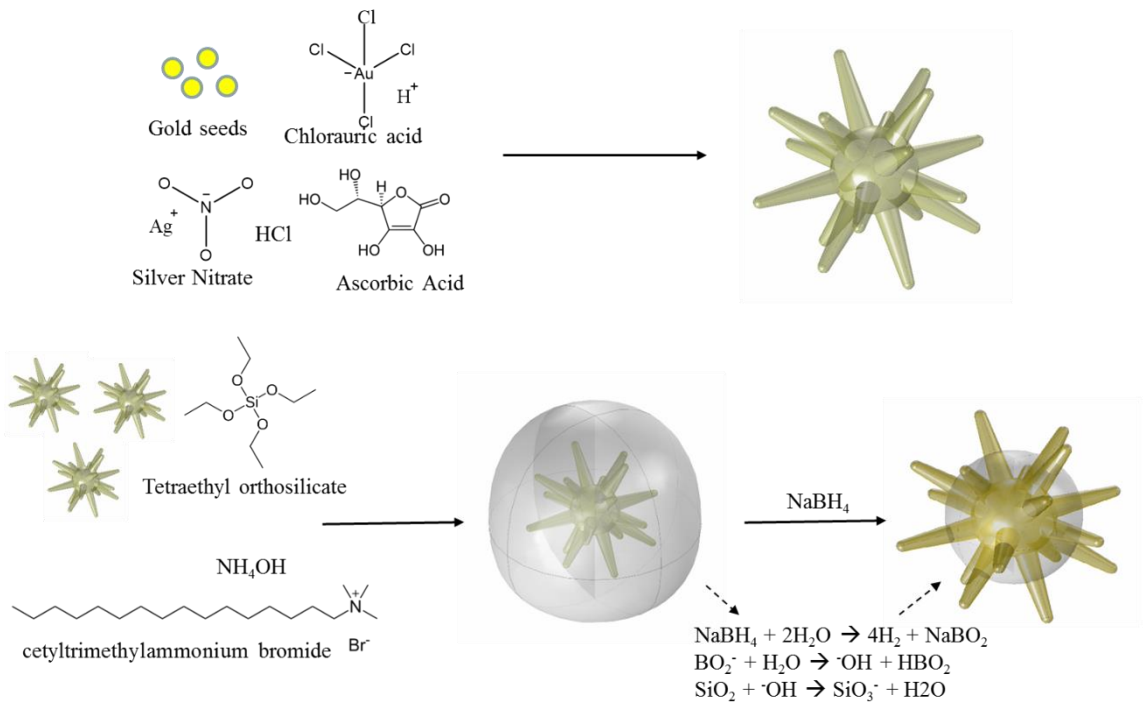

Figure 2.1 Step by step illustration of the silica coated gold nanostar synthesis.

2.3.3 SERS Active Gold Nanostar Probe Synthesis

To create the SERS active gold nanostars, the surface was functionalized with oligonucleotides with target specificity. This specificity was established through functionalization via an RNA beacon that was determined from one of the influenza A virus (IAV) H1N1 genomic virion sequences (vRNA). The sequence was chosen from the conserved region of the hemagglutinin (HA) glycoprotein expressing genome, segment 4, namely 5'-TCA TTT TTG TTG CTT TTG TTT-3'.[19] The beacon's design allows for targeting specificity to distinguish segment 4 from the other seven segments. Additionally, to create the SERS active beacon, the 21 base pair sequence was flanked on each end with a short complementary sequence that allowed it to fold into a hairpin

structure; furthermore, it was tagged with a Cy3 dye at the 3' end to provide both a fluorescent and Raman response depending on its folding status.[20] The beacon length and composition were determined for optimal folding to form a hairpin structure using the binding affinity calculated by an ad hoc tool freely available on the IDT website, the company we use to acquire the oligoucleotides. The overall sequence of beacon was: 5'-Thiol-MC6-CGTGCG TCA TTT TTG TTG CTT TTG TTT CGCACG-Cy3-3'. The complementary strand 5'-AAA CAA AAG CAA CAA AAA TGA-3' and target sequence 5'-TCA TTT TTG TTG CTT TTG TTT-3' were also purchased from IDT.

For added stability, a thiolated poly(ethylene glycol) (PEG) was conjugated onto the gold surface of the exposed tips of the etched silica coated gold nanostar (Si@AuNS) following a method described by Jimenez *et al.*[21] Si@AuNS were concentrated via centrifugation and re-suspended to 3 nM. The thiolated PEG was added to the 3 nM Si@AuNS under mild shaking for 30 minutes. The particles were purified via centrifugation at 3000 g for 10 minutes and re-suspended. The thiolated beacon and complementary strand were each dissolved separately in RNase-free DCEP-treated water (Thermo Fisher). They were each diluted in 1X phosphate buffer solution (PBS), heated to 70°C and combined to hybridize. The hybridized oligonucleotides were then added to the Si@AuNS at a final concentration of 500 nM and purified thoroughly through centrifugation at 3000 g for 10 minutes. The final product is a SERS active nanostar probe (SANSP). Additionally, to confirm the SERS signal with the un-hybridized beacon, the thiolated beacon was dissolved in RNase-free DCEP-treated water and added to Si@AuNS at a concentration of 500 nM and purified thoroughly through centrifugation

at 3000 g for 10 minutes. These nanoparticles are beacon conjugated Si@AuNS without the complementary strand found in the SANSPs. (**Figure 2.2**)

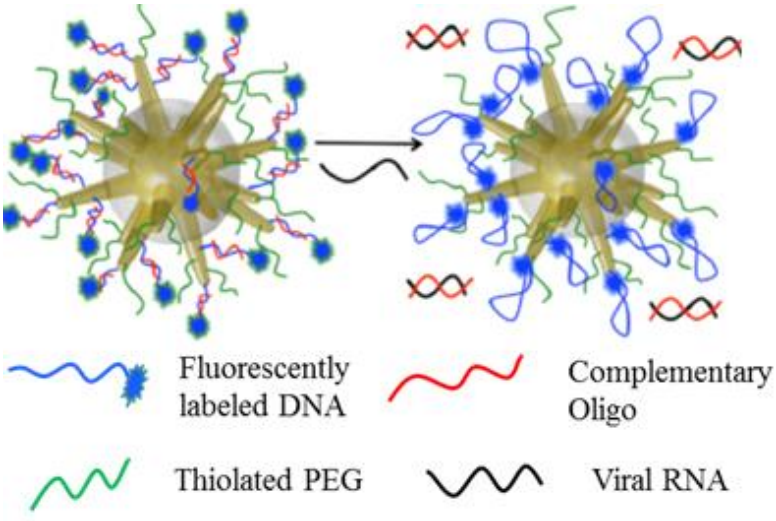

Figure 2.2 Representation SERS nanostar probes (SANSPs), which consist of gold nanostars functionalized with a Raman tagged beacon DNA that is hybridized with a complementary oligo creating the SANSPs with the SERS signal quenched (off state). Upon addition of the viral RNA to SANSPs, the complementary oligo de-hybridizes and hybridizes with the viral RNA. The beacon then returns to its folded hairpin conformation with consequent increase in SERS signal intensity (on state).

2.3.4 Polymer Coated Gold Nanostar synthesis

The protocol for surfactant free gold nanostars used to synthesize the polymer coated gold nanostars for the SERS active nanostar probe (SANSP) previously described in section 2.3.3, was followed with modifications. As an initial proof of concept, the silica coating was not added, instead surfactant free nanostars were used. Additionally, the thiolated PEG previously mentioned was substituted with a thiolated FITC tagged PEG to fluorescently monitor the location of the SANSPs within the cell. Six different TAC ion-functionalized polymers, PEI(Mo), PEI(iP), PEI(Pep), PMAS(Mo), PMAS(iP) and

PMAS(Pep), were synthesized by Dr. Luis Campos's group at Columbia University.[22, 23] The positively charged polymers were each separately electrostatically coated onto the negatively charged gold nanostars according to a modified protocol from Elbakry *et al.*[24] Briefly, the polymers were added at varying concentration to 3 nM gold nanostars under gentle shaking for 1 hour. The particles were then thoroughly purified via centrifugation at 3000 g for 15 minutes. PEI-coated gold nanostars, which are commonly found in literature,[24] were prepared using the same protocol as the TAC polymer coatings and used as controls.

2.3.5 Characterization of Gold Nanostars

Optical characterization of the nanoparticles was carried out via UV-Vis spectrophotometry using a Thermo Scientific Nanodrop 2000 and SI Photonics Model 440 CCD Array UV-Vis spectrophotometer.

Transmission electron microcopy (TEM) images were taken using a Philips CM12 transmission electron microscope. This was used to evaluate the morphology and size. The samples were drop casted onto carbon TEM grids (Ted Pella).

The concentration of the particles was calculated using beer lambert's law and the equation from Liu *et al.*[25]

The hydrodynamic size and the charge were measured using DLS and zeta potential using a Malvern Zetasizer Nano-S. The size was measured by diluting the samples in Milli-Q water in a disposable cuvette and were calculated by relating particle size to particle motion. The charge was measured by diluting the samples in Milli-Q water in a

folded capillary zeta cell and calculated using Smoluchowski theory.[26]

2.4 Results and discussion

The citrate capped nanospheres were synthesized by citrate reduction of $HAuCl_4$ salt using the modified Turkevich method.[18] The nanospheres showed the characteristic LSPR peak at 521 nm via UV-Vis analysis. **(Figure 2.3a)** The morphology and size of the nanospheres were confirmed using transmission electron microscopy (TEM) and scanning electron microscopy (SEM). **(Figure 2.3b and Figure 2.3c)**

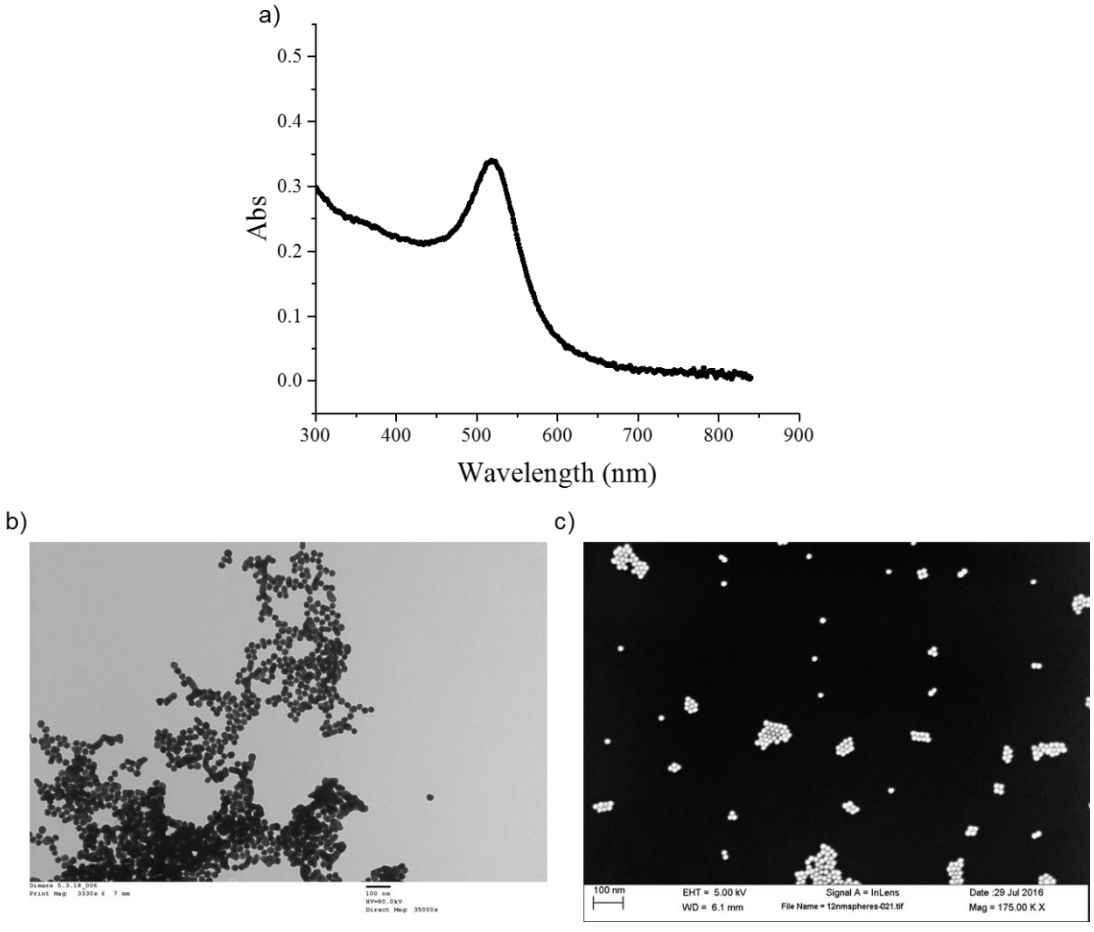

Figure 2.3 a) UV-Vis spectra of 12 nm gold nanospheres dispersed in Milli-Q water. b) TEM micrograph of 12 nm gold nanospheres dispersed. c) SEM image of 12 nm gold nanospheres.

The citrate capped nanospheres were used to synthesize the seed mediated surfactant free gold nanostars following a modified protocol from Yuan *et al*.[16] The surfactant free nanostars showed their broad characteristic plasmon resonance peak at around 750 nm. (**Figure 2.4a)** The TEM image of the gold nanostars verified the morphology and size. (**Figure 2.4b)** The concentration was calculated using Beer Lambert law, $C = \frac{A}{(\varepsilon \times l)}$.[27]

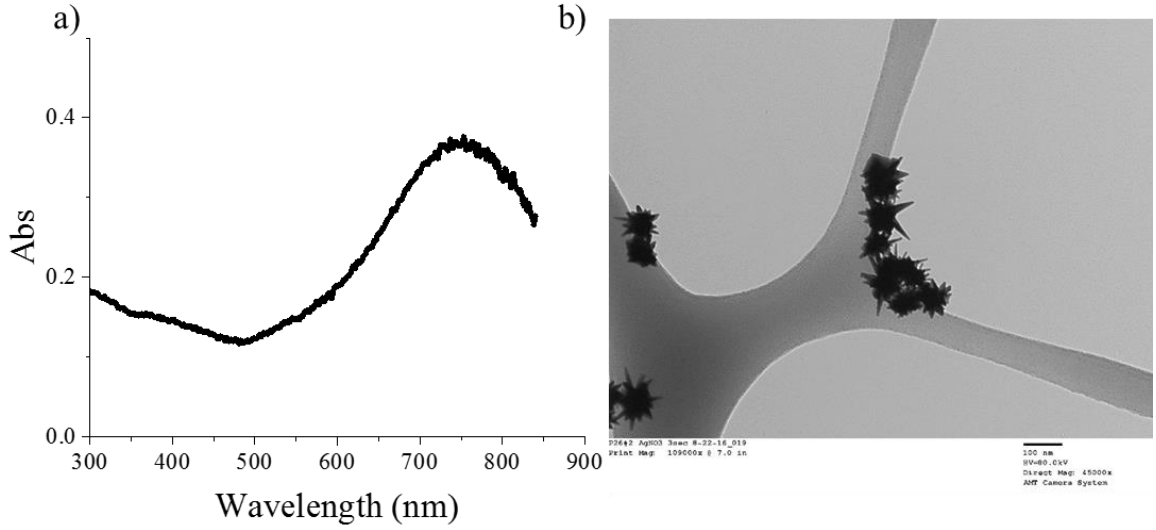

Figure 2.4 a) UV-Vis spectra of surfactant free gold nanostars dispersed in Milli-Q water. b) TEM image of surfactant free gold nanostars.

The silica coated gold nanostars and the partially coated silica gold nanostars were synthesized using a modified protocol adopted from *Atta et al.*[17] Both the silica coated gold nanostars and the partially coated silica gold nanostars showed their broad characteristic UV-vis LSPR at around 750 nm. The TEM image confirmed the silica coating of the CTAB coated nanostars and the 30-hour etching of the resulting silica coated gold nanostars. (**Figure 2.5a** and **2.5b**). Figure 2.5b shows a clearly exposed gold surface at the tips of the nanoparticles.

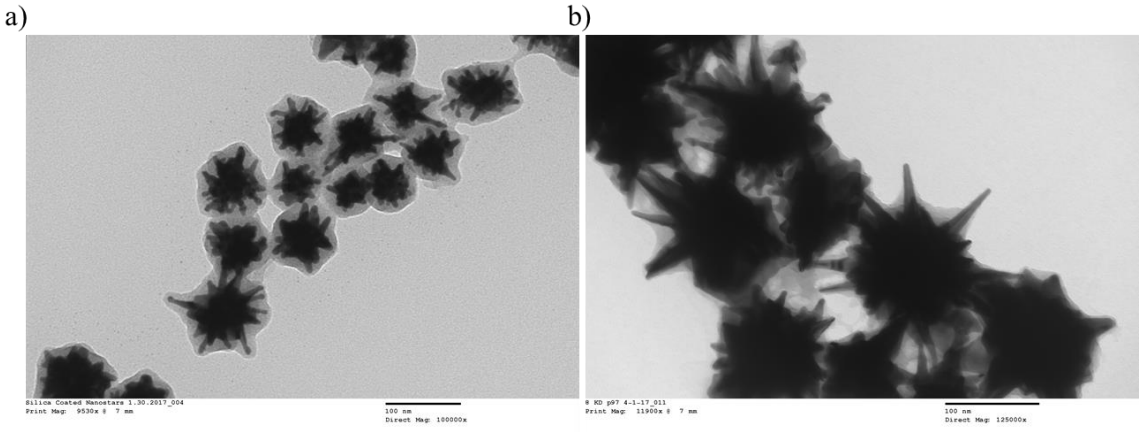

Figure 2.5 a) TEM micrograph of silica coated gold nanostars b) TEM micrograph of silica coated gold nanostars after 30 hours of etching.

For verification of the SERS active nanostar probes, the conjugation of the oligonucleotides to the Si@AuNS were confirmed by determining their SERS signal from the un-hybridized beacon conjugated nanoparticles (**Figure 2.6**). Figure 2.6 shows a representation of the un-hybridized beacon conjugated nanoparticles and the SERS verification of the conjugation using a 633 nm HeNe laser excitation, at 0.101 mW laser power and 3 accumulations. The SERS spectra show a clear fingerprint of Cy3, the Raman reporter at the 3' end of the beacon, 5'-Thiol-MC6-CGTGCG TCA TTT TTG TTG CTT TTG TTT CGCACG-Cy3-3', when it is un-hybridized from the complementary strand and folded into a hairpin structure. The proximity of Cy3 to the gold surface significantly enhances the Raman signal while quenching its fluorescence. This strong signal indicates the successful conjugation of the beacon to the gold surface.

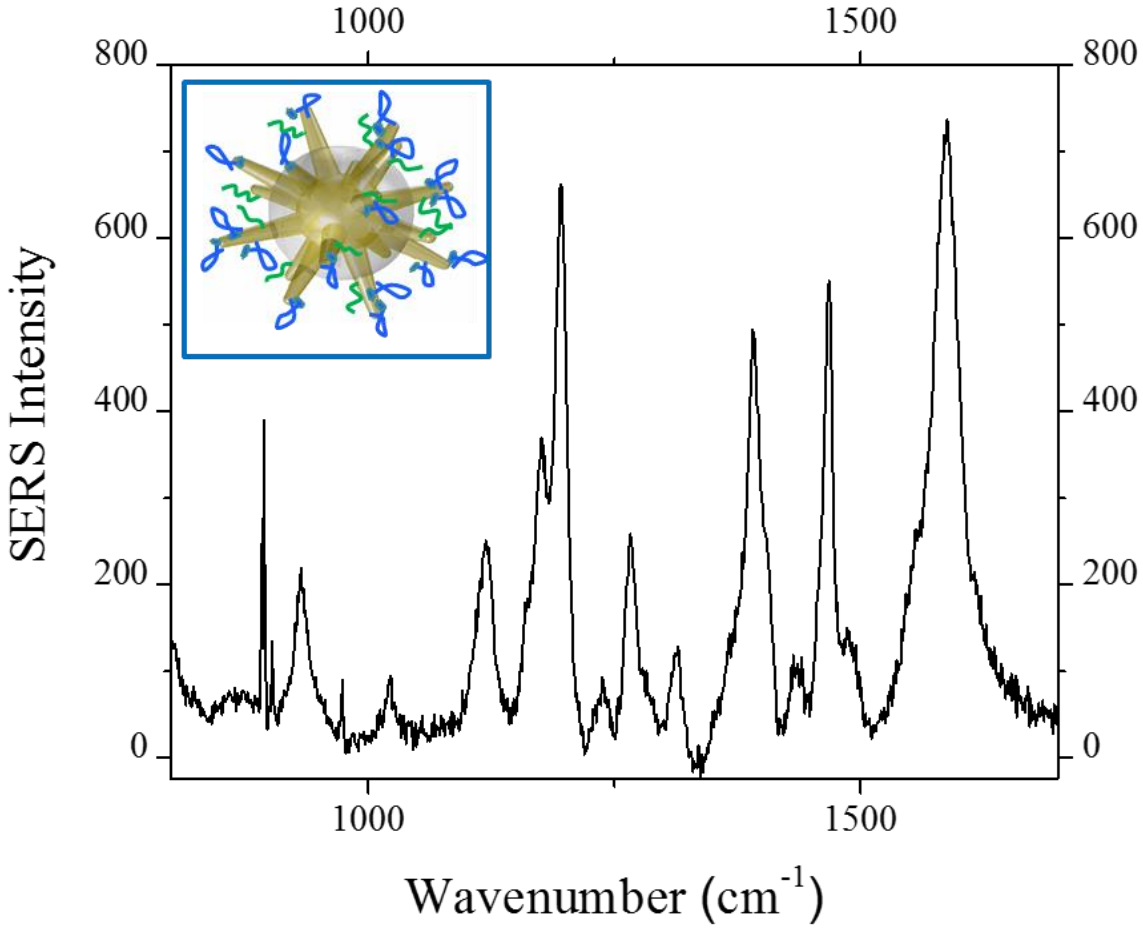

Figure 2.6 SERS signal of Cy3 labeled beacon conjugated to silica coated gold nanostars and an illustrative representation of the particles in the top left corner.

The polymer coated nanoparticles were synthesized using a modified protocol from Elbakry *et al.*[24] The TAC polymers were synthesized by Dr. Luis Campos's group at Columbia University and coated on nanostars at 10, 20, and 50 µg/mL of polymer. To verify the addition of the polymer and the ligands to the surfactant free nanostars, DLS

and zeta potential were measured to monitor the size, charge, surface ligand exchange, and coating addition. Bare surfactant free nanostars measured at a hydrodynamic size of 105.8 ± 1.7 nm and a charge of -34.8 ± 0.2 mV. Upon addition of PEG the size is shifted to 143.8 ± 2.8 nm and the further shifted to 146.1 ± 3.8 nm with the addition of the oligonucleotide and the charge shifted to -25.2 ± 0.4 mV. Once the charge has been confirmed to remain negative, the positively charged TAC polymers were added and the resulting charges became increasingly positive, ranging from 18.8 ± 0.4 mV to 31.2 ± 1.2 mV at 10 µg/mL, 22.4 ± 0.7 mV to 42.7 ± 0.3 mV at 20 µg/mL, and 23.0 ± 0.8 mV to 41.1 ± 0.5 mV at 50 µg/mL. **(Table 2.1)** The size increased with a range of 111.7 ± 1.1 nm to 204.4 ± 11.5 at 10 µg/mL, 113.9 ± 1.4 nm to 160.8 ± 4.9 at 20 µg/mL, and 118.3 ± 1.9 nm to 149.7 ± 2.2 at 50 µg/mL. **(Table 2.2)**

TAC Polymer	10 µg/mL	20 µg/mL	50 µg/mL
	Charge (mV)	Charge (mV)	Charge (mV)
PEI(PEP)	26.6 ± 0.5	27.9 ± 0.4	35.8 ± 0.8
PEI(Mo)	19.5 ± 0.5	22.4 ± 0.7	23.0 ± 0.8
PEI(iP)	18.8 ± 0.4	22.6 ± 0.6	24.1 ± 1.4
PMAS(PEP)	26.6 ± 1.2	36.3 ± 0.6	28.1 ± 0.8
PMAS(Mo)	21.7 ± 0.4	29.4 ± 0.2	41.1 ± 0.4
PMAS(iP)	31.2 ± 1.2	42.7 ± 0.3	38.7 ± 0.3
PEI	29.7 ± 0.2	37.7 ± 0.4	48.9 ± 0.4

Table 2.1 The charge of each of the polymer coated nanostars and the controls. The table shows an increase in charge when gold nanostars are functionalized with ligands and polymers from -34.8 ± 0.2 mV to as high as 41.1 ± 0.5 mV.

TAC Polymer	10 µg/mL	20 µg/mL	50 µg/mL
	Size (nm)	Size (nm)	Size (nm)
PEI(PEP)	116.1 ± 1.2	124.6 ± 0.4	126.8 ± 1.7
PEI(Mo)	119.6 ± 1.4	133.8 ± 2.3	118.3 ± 1.2
PEI(iP)	113.0 ±1.0	113.9 ± 1.4	124.3 ± 2.3
PMAS(PEP)	111.7 ± 1.1	116.8 ± 1.2	164.6 ± 1.4
PMAS(Mo)	125.8 ± 2.9	138.1 ± 6.1	143.1 ± 4.1
PMAS(iP)	204.4 ± 11.5	160.8 ± 4.9	149.7 ± 2.2
PEI	127.3 ± 1.8	141.8 ± 1.7	183.2 ± 5.2

Table 2.2 The hydrodynamic size of each of the polymer coated nanostars and the controls. The table shows an increase in size when gold nanostars are functionalized with ligands and polymers from 105.8 ± 1.7 nm to as high as 204.4 ± 11.5 nm.

2.5 Conclusion

In summary, plasmonic gold nanostars have immense potential for biomedical applications. Their unique optical and physical properties make them ideal for studying cellular components and intracellular events. The gold nanostars developed in this dissertation work are readily coated, and readily functionalized for cellular uptake and viral RNA detection, as will be further discussed in later chapters. By adjusting the capping agents, surface coating, and ligands, the nanoparticles were designed to leverage their field enhancing capabilities for SERS-based biodetection applications. Using the

silica coated gold nanostars, the gold surface on the tips of the spikes are exposed to strategically bind ligands at the hot spots via thiol-gold chemistry. By conjugating target-specific oligonucleotides, the gold nanostars were transformed into probes for viral RNA detection. An additional method to customize gold nanostar was to coat them with TAC ion-functionalized polymers. As we will discuss in the third chapter, the TAC polymers enable facilitated uptake of nanoparticles and endosomal escape, a necessary condition to detect and quantify viral RNA freely circulating in the cytosol. Each of the surface coatings and ligands dictate how gold nanostars interact with their environments and determine the type of tool they will become.

2.6 References

1. Salata, O. Applications of nanoparticles in biology and medicine. *Journal of Nanobiotechnology* **2**, 3 (2004).
2. Breunig, M., Bauer, S. & Goepferich, A. Polymers and nanoparticles: intelligent tools for intracellular targeting? *European journal of pharmaceutics and biopharmaceutics : official journal of Arbeitsgemeinschaft fur Pharmazeutische Verfahrenstechnik e.V* **68**, 112-128 (2008).
3. Elahi, N., Kamali, M. & Baghersad, M.H. Recent biomedical applications of gold nanoparticles: A review. *Talanta* **184**, 537-556 (2018).
4. Das, M., Shim, K.H., An, S.S.A. & Yi, D.K. Review on gold nanoparticles and their applications. *Toxicology and Environmental Health Sciences* **3**, 193-205 (2011).
5. Laura, F. Gold-based SERS tags for biomedical imaging. *Journal of Optics* **17**, 114002 (2015).
6. Padeletti, G. & Fermo, P. How the masters in Umbria, Italy, generated and used nanoparticles in art fabrication during the Renaissance period. *Applied Physics A* **76**, 515-525 (2003).
7. Wagner, F.E. et al. Before striking gold in gold-ruby glass. *Nature* **407**, 691 (2000).
8. Faraday, M. X. The Bakerian Lecture. —Experimental relations of gold (and other metals) to light. *Philosophical Transactions of the Royal Society of London* **147**, 145-181 (1857).
9. Li, N., Zhao, P. & Astruc, D. Anisotropic Gold Nanoparticles: Synthesis, Properties, Applications, and Toxicity. *Angewandte Chemie International Edition* **53**, 1756-1789 (2014).
10. Faulk, W.P. & Taylor, G.M. An immunocolloid method for the electron microscope. *Immunochemistry* **8**, 1081-1083 (1971).
11. Dykman, L.A. & Khlebtsov, N.G. Gold nanoparticles in biology and medicine: recent advances and prospects. *Acta naturae* **3**, 34-55 (2011).
12. Ember, K.J.I. et al. Raman spectroscopy and regenerative medicine: a review. *npj Regenerative Medicine* **2**, 12 (2017).
13. Bantz, K.C. et al. Recent progress in SERS biosensing. *Physical chemistry chemical physics : PCCP* **13**, 11551-11567 (2011).
14. Halas, N.J., Lal, S., Chang, W.S., Link, S. & Nordlander, P. Plasmons in strongly coupled metallic nanostructures. *Chem Rev* **111**, 3913-3961 (2011).
15. Fabris, L. SERS Tags: The Next Promising Tool for Personalized Cancer Detection? *ChemNanoMat* **2**, 249-258 (2016).
16. Yuan, H. et al. Gold nanostars: surfactant-free synthesis, 3D modelling, and two-photon photoluminescence imaging. *Nanotechnology* **23**, 075102 (2012).
17. Atta, S., Tsoulos, T.V. & Fabris, L. Shaping Gold Nanostar Electric Fields for Surface-Enhanced Raman Spectroscopy Enhancement via Silica Coating and Selective Etching. *The Journal of Physical Chemistry C* **120**, 20749-20758 (2016).
18. Frens, G. Controlled Nucleation for the Regulation of the Particle Size in Monodisperse Gold Suspensions. *Nature Physical Science* **241**, 20 (1973).

19. Breen, M., Nogales, A., Baker, S.F. & Martinez-Sobrido, L. Replication-Competent Influenza A Viruses Expressing Reporter Genes. *Viruses* **8** (2016).
20. Cheng, Y. et al. Fluorescence Near Gold Nanoparticles for DNA Sensing. *Analytical Chemistry* **83**, 1307-1314 (2011).
21. Jimenez de Aberasturi, D. et al. Surface Enhanced Raman Scattering Encoded Gold Nanostars for Multiplexed Cell Discrimination. *Chemistry of Materials* **28**, 6779-6790 (2016).
22. Freyer, J.L. et al. Clickable Poly(ionic liquids): A Materials Platform for Transfection. *Angewandte Chemie (International ed. in English)* **55**, 12382-12386 (2016).
23. Brucks, S.D., Freyer, J.L., Lambert, T.H. & Campos, L.M. Influence of Substituent Chain Branching on the Transfection Efficacy of Cyclopropenium-Based Polymers. *Polymers* **9**, 79 (2017).
24. Elbakry, A. et al. Layer-by-layer coated gold nanoparticles: size-dependent delivery of DNA into cells. *Small (Weinheim an der Bergstrasse, Germany)* **8**, 3847-3856 (2012).
25. Liu, X., Atwater, M., Wang, J. & Huo, Q. Extinction coefficient of gold nanoparticles with different sizes and different capping ligands. *Colloids and surfaces. B, Biointerfaces* **58**, 3-7 (2007).
26. Gudowska-Nowak, E., Lindenberg, K. & Metzler, R. Preface: Marian Smoluchowski's 1916 paper—a century of inspiration. *Journal of Physics A: Mathematical and Theoretical* **50**, 380301 (2017).
27. Swinehart, D.F. The Beer-Lambert Law. *Journal of Chemical Education* **39**, 333 (1962).

Chapter 3 Polymer Facilitated Uptake

3.1 Abstract

Bio-active nanomaterials have significant therapeutic and diagnostic potential. Their unique features provide opportunities for targeted intracellular drug delivery, biomolecule detection, and cellular imaging. Due to their size and composition, they have limited access to the cytoplasm during cellular uptake and get trapped in the endosomes. Current methods to avoid endosomal uptake leverage cell penetrating peptides or cationic polymers, such poly(ethyleneimine) (PEI). These peptides need to be covalently bound to the gold nanoparticle or to be tethered to an electrostatically-bound PEI, which is toxic at higher dosages. To that end, developing a less toxic, yet efficient, method for endosomal escape would allow for quicker and safer nanoparticle access to the cytoplasm. To overcome obstacles with cellular uptake, we functionalized gold nanoparticles with trisaminocyclopropenium (TAC) ion-functionalized macro-molecules to provide an efficient route to nanoparticle endosomal escape. The efficiency of TAC polymers has been previously demonstrated in their free form for endosomal escape and biocompatibility. With synthetic optimization, six different TAC polymers derived from PEI and poly(methylaminostyrene) (PMAS) were electrostatically coated onto gold nanoparticles and tested for their effects on viability. Of those polymers, poly(methylaminostyrene)funtionalized with morpholine PMAS(Mo) showed a combination of high stability in solution and in cellular media and high viability with respect to the control. By conjugating FITC-PEG for added biodispersity, stability, and fluorescence tracking, the particles were monitored intracellularly. These particles were able to escape the endosomes and diffuse within the cytoplasm without aggregation and with high biodistribution. Moreover, the TAC-coated nanostars were less toxic at higher

loading compared to the PEI-coated counterpart, and diffused within the cytoplasm faster than the widely used transfection agent, PEI, when similarly coated onto gold nanostars. The delivery platform has immense potential for rapid cellular uptake and endosomal escape, specifically for time restricted biological processes such as viral infection.

3.2 Introduction

Nanomaterials have emerged as promising tools for biomedical applications. They have significantly progressed since their début for biological studies in 1971.[1] Since then, nanoparticles have become a preferred method for various studies including drug delivery, bio-sensing, diagnostics, phototherapy, and mechanistic studies.[2] While some nanoparticle based studies only need access to biomolecules secreted from cells or to external markers on the cell membrane, other require intracellular maneuvering.[3] Like other bioactive macromolecules, such as nucleic acids and proteins, nanoparticles are presented with the obstacle of entry into the cytoplasm of a cell.[4] Thus, understanding and developing methods for cellular uptake has been and is still in the process of being perfected.[5]

After a material or substance is first taken up by a cell via one of the endocytic pathways, phagocytosis, pinocytosis, or receptor mediated endocytosis, it is then encased and trapped by a vesicle. Each of these pathways determine the fate of the ingested material or substance.[6] There have been several proposed mechanisms for evading endocytosis such as small molecule based transfection agents, peptide based transfection agents, and polymer based transfection agents.[4, 5, 7]

Polymer based transfection agents such as the cationic poly(ethyleneimine) (PEI) have

been demonstrated by various researchers including Elbakry *et al.* where DNA was delivered via size dependent uptake of gold nanoparticles (AuNPs) by coating the nanoparticles in a layer-by layer-approach with both nucleic acid and PEI.[7] Once PEI enters the endosomal membrane, its un-protonated amines attract protons which are pumped into the endosome resulting in an influx of chloride ions and water. The increase in influx results in swelling from the osmatic pressure and the repulsion between negatively and positively charged ions, ultimately rapturing the endosomal membrane and releases its contents. This process is known as a the proton-sponge effect[8]. Despite PEI's effectiveness, it has been shown to be toxic at higher concentrations.[9, 10] To that end, developing a biocompatible method for endosomal escape would allow for a quicker and a less toxic method for nanoparticles access to the cytoplasm.

Fryer *et al.* reported a post-polymerization click reaction to synthesize trisaminocyclopropenium (TAC) ion-functionalized macro-molecules for an efficient transfection material platform. The TAC polymers are derived from the polymer backbones of PEI and poly(methylaminostyrene) (PMAS) and compared to the widely used transfection agent, linear PEI. The group showed that the TAC polymers are comparable to PEI in toxicity profile at low dosages but are less toxic at higher dosages. They also demonstrated their efficiency as transfection agents by testing them for luciferase expression.

Herein, we describe a method for enhanced cellular uptake of gold nanostars by integrating TAC polymers in their bioconjugation schemes. Six different TAC polymers derived from PEI and PMAS functionalized with various bis(dialkylamino)cyclopropenium chloride were provided by Dr. Campos's group from

Columbia University. **(Figure 3.1)** PEI and PMAS were each functionalized with morpholine (Mo), piperidine (Pep), and isopropyl (iP) to form PEI(Mo), PEI(Pep), PEI(iP), PMAS(Mo), PMAS(Pep), and PMAS(iP). The polymers were electrostatically coated onto gold nanostars and tested for stability and cell viability with PMAS(Mo) showing a combination of high stability in solution and in cellular media and high viability in bone marrow stem cells (BMSC) with respect to the control. Additionally, to track the particles intracellularly, the particles were conjugated with FITC PEG and the endosomes were stained using pHrodo Red Dextran. This method allowed for biodispersity and diffusion of the particles within the cytoplasm, which is relevant with respect to future applications of AuNPs in monitoring intracellular events.

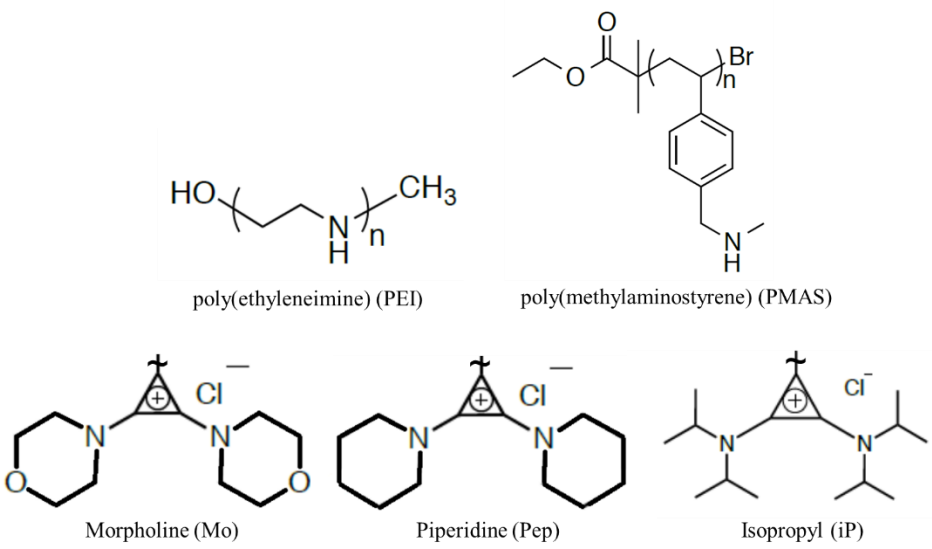

Figure 3.1 Structures of the bis(dialkylamino)cyclopropenium chloride groups, morpholine (Mo), piperidine (Pep), and isopropyl (iP). Each are added via an amide bond to the backbone of poly(ethyleneimine) (PEI) and poly(methylaminostyrene) (PMAS).

3.3 Materials and Method

3.3.1 Preparation of Polymer Coated Gold Nanostar for Cellular Transfection

Surfactant free gold nanostars were synthesized using modifications of established protocols from the literature starting with the synthesis of citrate capped gold nanospheres.[11, 12] Gold nanospheres were synthesized by citrate reduction of $HAuCl_4$ salt using a modified Turkevich method.[11] Briefly, 8 mL of 0.025 M $HAuCl_4$ salt and 477 mL of Milli-Q deionized water were heated up to a boil under stirring, followed by addition of 15 mL of 1 % citric acid trisodium salt. The mixture was left to boil for 5 minutes and then cooled to room temperature. The resulting deep red suspension was purified by centrifugation at 6000 g for 30 to 45 minutes.

Using the citrate capped gold nanospheres, the gold nanostars were prepared via a seed mediated method described by Yuan *et al.*[12] Briefly, 2 mL of 0.025 M $HAuCl_4$ salt solution, 200 µL of 1 N HCl, 48 mL of milli-Q water, and 125 µL of 12 nm citrate capped spheres with an absorbance of 2.81 at a 1 mm path length were mixed under gentle stirring. 2 mL of 3 mM $AgNO_3$ and 1 mL of 100 mM ascorbic acid were simultaneously added to the mixture, stirred gently for 7 minutes, and then purified by centrifugation at 3000 g for 15 minutes.

The gold nanostars were sequentially conjugated with a thiolated FITC PEG[13] and a thiolated RNA beacon, 5'-Thiol-MC6-CGTGCG TCA TTT TTG TTG CTT TTG TTT CGCACG-3', and thoroughly purified after each step via centrifugation at 3000 g for 10 minutes. For initial testing, the particles were also prepared without the beacon.

The resulting platform was coated by six different Trisaminocylcopropenium (TAC) ion functionalized polymers, PEI(Mo), PEI(iP), PEI(Pep), PMAS(Mo), PMAS(iP) and PMAS(Pep) (**Figure 3.1**), as well as PEI using a modified protocol from Elbakry *et al.*[7] The TAC polymers were synthesized by Dr. Luis Campos's group at Columbia University.[9, 14] Each of the seven polymers were added to 3 nM nanostars at final concentrations of 10, 20, and 50 µg/mL under gentle shaking for 1 hour. The particles were then thoroughly purified via centrifugation at 3000 g for 15 minutes.

3.3.2 Characterization of Polymer Coated Gold Nanostars

To characterize the nanoparticles, the UV-Vis spectra were recorded using a Thermo Scientific Nanodrop 2000 and SI Photonics Model 440 CCD Array UV-Vis spectrophotometer.

Transmission electron microcopy (TEM) images were taken using a Topcon 002B TEM. This was used to evaluate the morphology and size. The samples were drop casted onto carbon-coated TEM grids (Ted Pella).

The concertations of the particles were calculated using Beer Lambert's law.[15]

The hydrodynamic size and the charge were measured using DLS and zeta potential using a Malvern Zetasizer Nano-S. The size was measured by diluting the samples in Milli-Q water in a disposable cuvette and were calculated by relating particle size to particle motion. The charge was measured by diluting the samples in Milli-Q water in a folded capillary zeta cell and calculated using Smoluchowski theory.

3.3.3 Cell Culture

Human bone marrow-derived mesenchymal stem cells (BMSC) were purchased from ATCC. The cell line was cultured in Gibco Minimum Essential Medium, Alpha (MEM α) (Fisher Scientific) that was supplemented with 5% Penstrep (Thermo Fisher) and 10% Fetal Bovine Serum (Thermo Fisher). The cells were grown at 37°C at 5% CO_2. Upon reaching 70-80% confluency, the BMSCs were washed with 1X phosphate buffer solution (PBS), trypsinized, and re-suspended in fresh MEM α. For experiments and assays, BMSCs were counted and seeded appropriately.

3.3.4 Cellular Viability

To test *in vitro* cell viability, an MTT assay was conducted. BMSCs were counted and seeded in a 96-well tissue culture plate and incubated for 24 hours at 37°C at 5 % CO_2 to allow proper attachment. The media was then replaced and 100 µg/mL of polymer coated nanoparticles, with varying polymer concentration of 10, 20, and 50 µg/mL, were added and incubated for 24 hours. Each of the seven polymer concentrations ranged from 10-50 µg/mL; we used this approach to determine the optimal concentration for coating the nanoparticles. After 24 hours of incubation, the cell viability was measured using a Vybrant MTT cell proliferation assay kit (V13154 Thermo Fisher) following the manufacturer's protocol. The media in each well was replaced with 100 µL of fresh media with 10 µL of 12 mM 3-(4,5-dimethylthiazol-2-yl)-2,5-diphenyltertazolium bromide (MTT) and incubated at 37°C and 5 % CO_2 for 4 hours. 85 µL of media were removed and 75 µL of DMSO were added to each well. The concentration of live cells was determined by measuring the density at 540 nm of the formazan dye crystals

produced as a result of metabolic activity of live cells.

3.3.5 Fluorescent Labeling of Endosomes and Cellular Uptake

To test for cellular uptake and endosomal escape of the polymer coated gold nanostars, BMSCs were exposed to the nanoparticles and stained for fluorescence imaging. BMSCs were counted and seeded in an 8-well chambered cover-glass tissue culture plate and incubated for 24 hours at 37°C and 5 % CO_2 to allow proper attachment. The media was then replaced and the cells were pre-treated with pHrodo Red Dextran, 10,000 MW, for endocytosis (Thermo Fisher) following the manufacturer's protocol. 10 µL of 1 mg/mL pHrodo dextran stock solution were added to each well for 15 minutes. The solution was removed, the cells were washed with 1X PBS, and fresh media was added. 100 µg/mL of polymer coated nanoparticles were then added and incubated. After 2 and 4 hours of incubation the cells were fixed in 4% formaldehyde in PBS for 10 minutes in room temperature. The cells were washed with 1X PBS and wrapped in foil. The cells were examined under fluorescence imaging using a Nikon Eclipse TE2000-S microscope.

3.4 Results and discussion

3.4.1 Preparation of Polymer Coated Nanostars

The polymer coated nanoparticles were synthesized using a modified protocol from Elbakry *et al.*[7] The TAC polymers were synthesized by Dr. Luis Campos's group at Columbia University.[9, 14] In Dr. Campos's study, the TAC polymer are synthesized on the postulation that modifying PEI, a cationic polyelectric polymer that is widely used as a cellular transfection agent,[16, 17] with cyclopropenium moieties, will result in a transfection

agent that is less toxic and more efficient than PEI. The group showed that TAC polymers exhibit similar cellular viability to linear PEI at low dosages and higher cellular viability than linear PEI at higher loadings.[9] Those results are reflected when the TAC polymers are coated onto the nanostars.

To verify the addition of the polymer and the ligands to the surfactant free nanostars, dynamic light scattering (DLS) was used to monitor the size change, and zeta potential was measured to monitor surface ligand exchange as well as ligand and coating addition. For an indepth analysis refer to section 2.4. The shift of size and charge verify the addition of both ligands and the polymer. **(Figure 3.2** and **Figure 3.3)**

Figure 3.2 The charge of each of the polymer coated nanostars and the controls. The graph shows a clear increase in charge when gold nanostars are functionalized with ligands and polymers from -34.8 ± 0.2 mV to as high as 41.1 ± 0.5 mV.

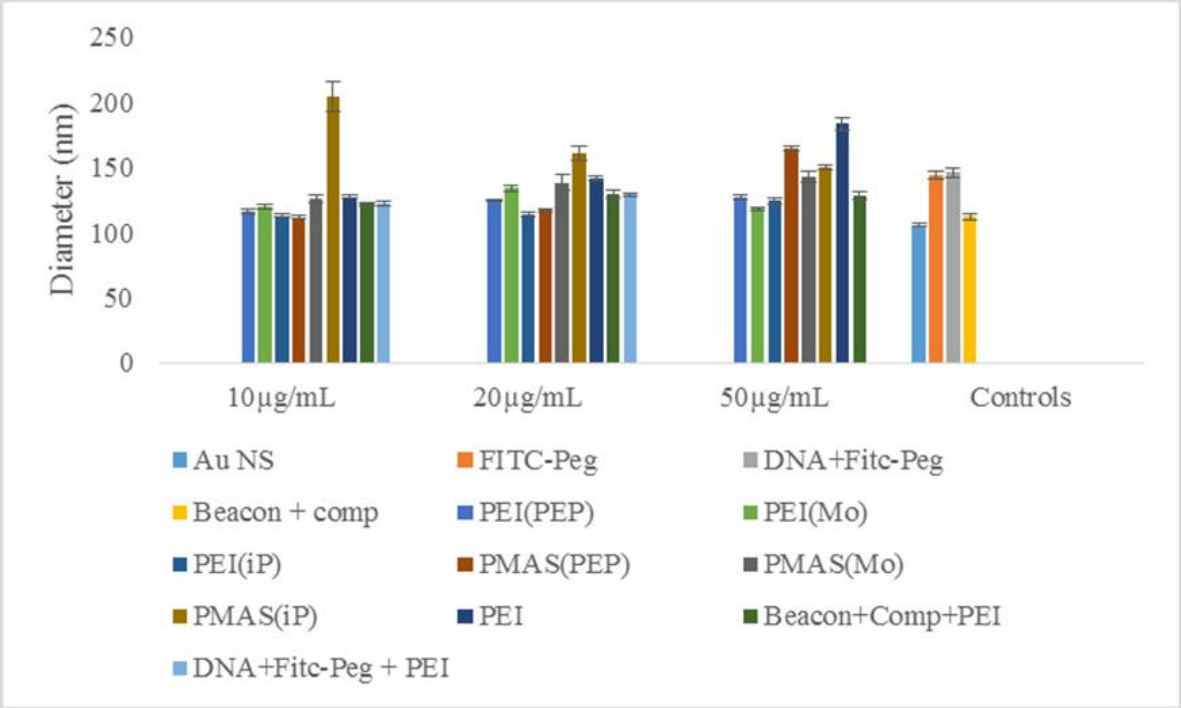

Figure 3.3 The hydrodynamic size of each of the polymer coated nanostars and the controls. The graph shows a clear increase in size when gold nanostars are functionalized with ligands and polymers from 105.8 ± 1.7 nm to as high as 204.4 ± 11.5 nm.

3.4.2 *In Vitro* Cellular Viability Study

To test for endosomal escape, the polymer coated nanostars were first tested for cellular toxicity. Dr. Campos's group was able to confirm lower toxicity of free TAC polymers compared to the widely used liner PEI polymer.[7] An MTT assay was conducted to test for cellular viability of the polymer coated nanostars. The values of the TAC polymer coated gold nanostars are listed in **Table 3.1**. At a lower dose of 10 µg/mL of each polymer with

a constant nanostar concentration, PEI-coated nanostars had the highest average viability at 163.6 ± 9.8 % with respect to the control, however, with no significant differences observed between the different polymers. PMAS(iP) had the next highest viability at 152.9 ± 5.3 %, followed by PMAS(Mo) at 148.0 ± 16.8 %, PEI(Pep) at 132.4 ± 12.5 %, PEI(iP) 122.0 ± 6.0 %, PMAS(Pep) at 117.7 ± 11.5 %, and PEI(Mo) at 111.8 ± 13.1 % with respect to the control. As the dosage increased to 20 µg/mL the same observation was made as that of 10 µg/mL concentration, PEI coated nanostars had the highest average viability at 134.5 ± 5.7 % with respect to the control, however, with no significant differences observed between the different polymers. PMAS(Mo) had the next highest viability at 131.0 ± 21.0 %, followed by PMAS(Pep) at 124.4 ± 2.8 %, PMAS(iP) at 123.9 ± 11.7 %, PEI(Mo) 1118.6 ± 3.4 %, PEI(iP) at 109.9 ± 2.0 %, and PEI(Pep) at 96.3 ± 10.1 % with respect to the control. The dose was then increased to 50 µg/mL of polymer, to which PEI had the lowest average viability at 85.3 ± 43.6 %. PMAS(iP) had the highest viability at 126.0 ± 12.1 %, followed by PMAS(Mo) at 120.2 ± 7.9 %, PEI(Pep) at 109.0 ± 20.3 %, PEI(Mo) 102.5 ± 9.8 %, PMAS(Pep) at 96.2 ± 3.6 %, and PEI(iP) at 94.4 ± 4.0 % with respect to the control. **(Figure 3.4)**

	10 ug/mL	**20 ug/mL**	**50 ug/mL**
PEI (Pep)	132.4 ± 12.5	96.3 ± 10.1	109.0 ± 20.2
PEI (Mo)	111.8 ± 13.1	118.6 ± 3.9	102.5 ± 9.8
PEI (IP)	122.0 ± 6.0	109.9 ± 2.0	94.4 ± 4.0
PMAS (Pep)	117.7 ± 9.6	124.4 ± 2.8	96.2 ± 3.6
PMAS (Mo)	148.0 ± 16.8	131.0 ± 21.0	120.2 ± 7.9
PMAS (IP)	152.9 ± 5.3	123.9 ± 11.7	126.0 ± 12.1
PEI	163.6 ± 9.8	134.5 ± 5.7	109.9 ± 43.6

Table 3.1 Cell Viability results with respect to the control for each of the six TAC polymers, PEI(Pep), PEI (Mo), PEI(iP), PMAS(Pep), PMAS(Mo), and PMAS(iP) coated gold nanostars. Each was tested at 10, 20 and 50 µg/mL of polymer and with a constant concentration of gold nanostars.

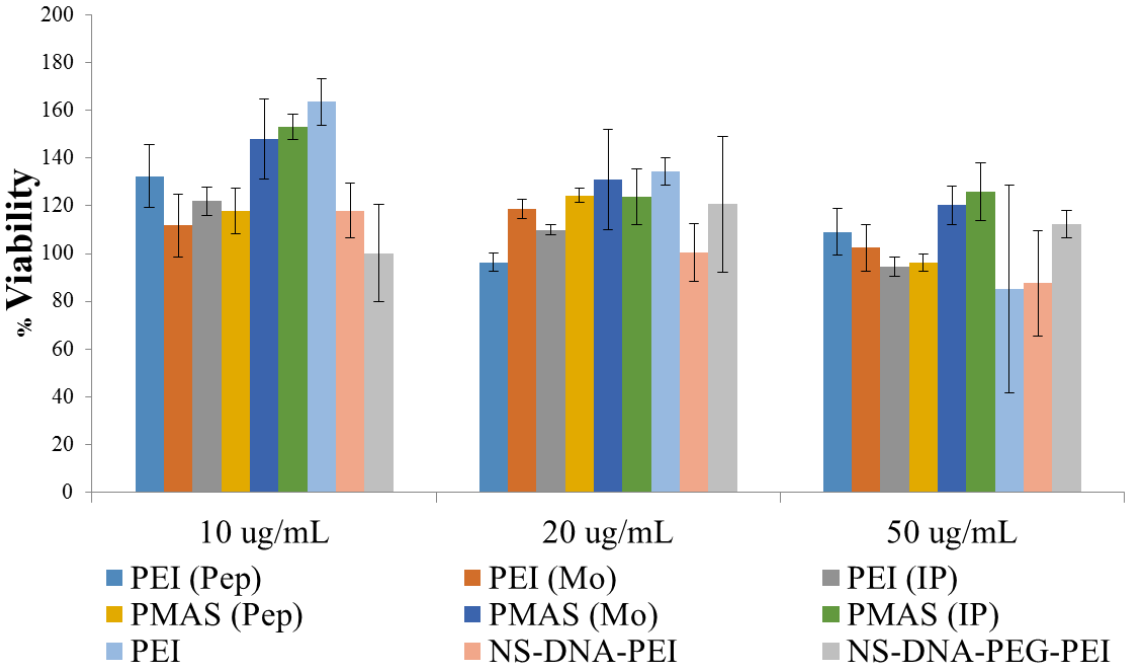

Figure 3.4 Comparison of the cell viability of the six TAC polymers, PEI(Pep), PEI (Mo), PEI(iP), PMAS(Pep), PMAS(Mo), and PMAS(iP) coated gold nanostars, PEI coated gold nanostars, and a control, gold nanostars without any polymer coatings. Each was tested at 10, 20 and 50 µg/mL of polymer and with a constant concentration of gold nanostars.

PMAS(Mo) was chosen to continue cell studies due to its combination of low toxicity and stability it provided to the nanostars. Despite PMAS(iP) having the highest cellular viability, the nanostars were not stable in solution and aggregated when coated with PMAS(iP).

3.4.3 Endosomal Escape of Gold Nanostars

Once the polymer coated nanostars were tested for biocompatibility, the next step was to test for the polymer's effectiveness as a transfection agent for nanostar endosomal escape. Dr. Campos's paper demonstrated similar transfection efficiency of free TAC polymers as linear PEI via a proof of concept luciferase assay.[9] As the concentration of TAC polymer was increased, the transfection efficiency decreased. This was attributed to the hydrophobicity of the molecules. PMAS(Mo) coated nanostars were transfected into cells to test the transfection efficiency of the polymer when it is coated around nanostars and compared to PEI, which is widely used in the literature. It was also compared to a control, gold nanostars without transfection agents. Prior to transfection, the endosomes were fluorescently labeled using lysotracker red. After 2 and 4 hours of incubation with the polymer coated nanostars, the cells were fixed and examined under fluorescence microscopy. **(Figure 3.5).**

The fluorescence images of gold nanostars without transfection agents showed clear overlap of the FITC labeled nanostars with the red stained endosomes, indicating the entrapment of gold nanoparticles in the endosomal membrane. Additionally, there were nanostars that did not enter the cell at both 2 and 4 hours of incubation. The transfection efficiency was enhanced with the addition of PEI. The PEI coated nanostars showed more overlap of the FITC labeled nanostars and the cytoplasm with slight improvement at 4-hour incubation. However, there still remained overlap between the FITC labeled nanostars and the red stained endosomes. PMAS(Mo) coated nanostars showed significant improvement of FITC labeled gold nanostars transfection. At 2-hour

incubation there is a clear overlap of FITC labeled gold nanostars and the cytoplasm. However, the particles are not fully diffused. At 4-hour incubation the transfection is once again improved and the FITC labeled gold nanostars are diffused within the cytoplasm. (**Figure 3.5)**

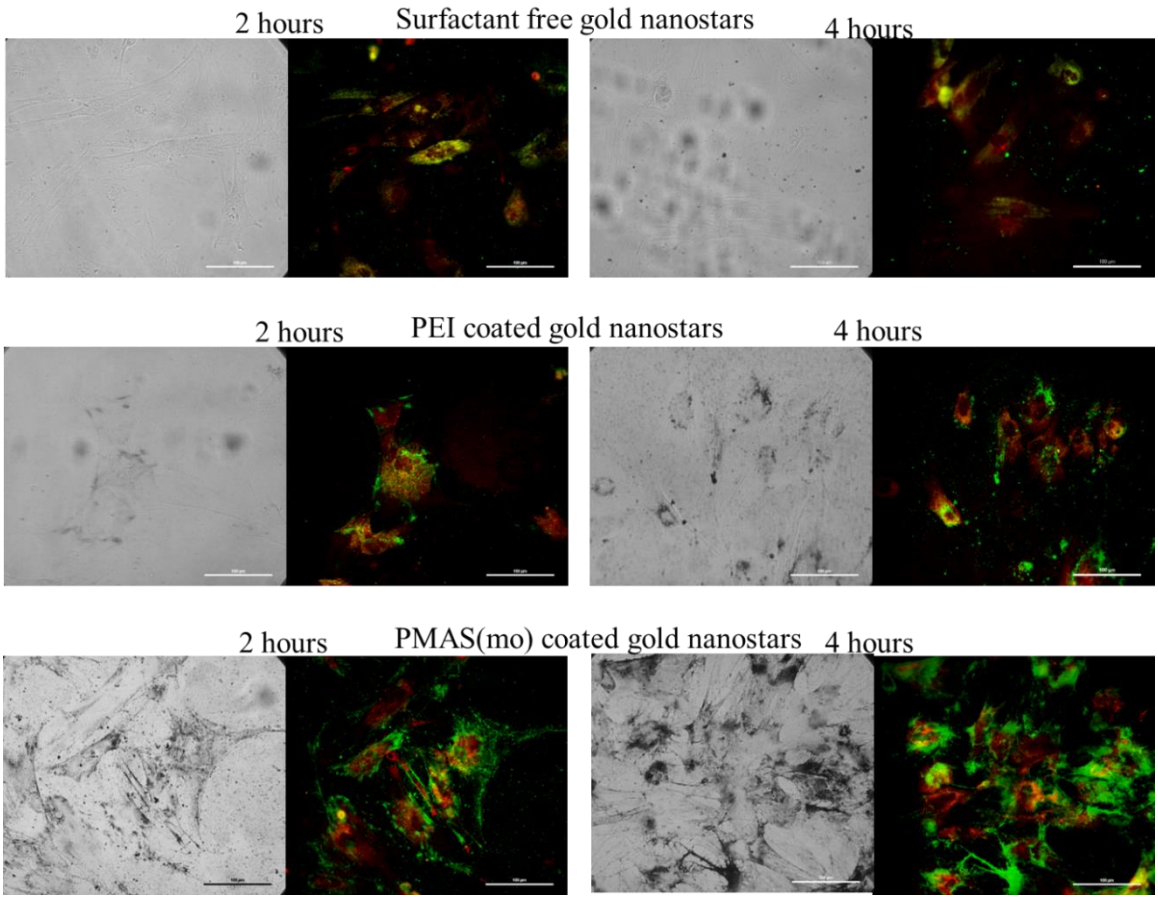

Figure 3.5 Images of FITC-PEG conjugated surfactant free gold nanoparticles, PEI coated FITC-PEG conjugated gold nanoparticles, and PMAS(Mo) coated FITC-PEG conjugated gold nanoparticles incubated in BMSC for 2 and 4 hours. The PMAS(Mo)

coated nanostars showed significant improvement in endosomal escape over PEI coated nanostars and bare nanostars.

3.5 Conclusion

In conclusion, we demonstrated a less toxic, yet efficient, approach to improve nanoparticle uptake and endosomal escape. With the aid of a synthetic cationic polymer with high amine density, trisaminocylcopropenium (TAC) ion functionalized polymers, functionalized gold nanostars readily escaped the endosome and diffused into the cytoplasm within 4 hours of incubation. The TAC polymers were electrostatically bound to the gold nanostars and leveraged their high amine density to function as a proton sponge to attract positively charged ions into the endosome, which enabled the rupture of the endosomal membrane and the escape of the nanoparticles into the cytoplasm. Gold nanostars diffused in the cytoplasm as opposed to aggregating within the endosomal membrane. Additionally, the TAC polymers were found to be less toxic at higher dosages and more efficient at shorter incubation times than the widely used transfection agent, poly(ethylenimine). The polymer coated nanoparticles can be utilized for quicker endosomal escape when testing time sensitive biological activities such as viral infection and replication in healthy cells.

3.6 Acknowledgments

I would like to acknowledge Dr. Luis Campos and Dr. Spencer Brucks for providing the trisaminocylcopropenium ion functionalized polymers.

3.7 References

1. Faulk, W.P. & Taylor, G.M. An immunocolloid method for the electron microscope. *Immunochemistry* **8**, 1081-1083 (1971).
2. Elahi, N., Kamali, M. & Baghersad, M.H. Recent biomedical applications of gold nanoparticles: A review. *Talanta* **184**, 537-556 (2018).
3. Dykman, L.A. & Khlebtsov, N.G. Gold nanoparticles in biology and medicine: recent advances and prospects. *Acta naturae* **3**, 34-55 (2011).
4. Lönn, P. et al. Enhancing Endosomal Escape for Intracellular Delivery of Macromolecular Biologic Therapeutics. *Scientific Reports* **6**, 32301 (2016).
5. Iversen, T.-G., Skotland, T. & Sandvig, K. Endocytosis and intracellular transport of nanoparticles: Present knowledge and need for future studies. *Nano Today* **6**, 176-185 (2011).
6. Marsh, M. & McMahon, H.T. The structural era of endocytosis. *Science (New York, N.Y.)* **285**, 215-220 (1999).
7. Elbakry, A. et al. Layer-by-layer coated gold nanoparticles: size-dependent delivery of DNA into cells. *Small (Weinheim an der Bergstrasse, Germany)* **8**, 3847-3856 (2012).
8. Benjaminsen, R.V., Mattebjerg, M.A., Henriksen, J.R., Moghimi, S.M. & Andresen, T.L. The possible "proton sponge " effect of polyethylenimine (PEI) does not include change in lysosomal pH. *Molecular therapy : the journal of the American Society of Gene Therapy* **21**, 149-157 (2013).
9. Freyer, J.L. et al. Clickable Poly(ionic liquids): A Materials Platform for Transfection. *Angewandte Chemie (International ed. in English)* **55**, 12382-12386 (2016).
10. Moghimi, S.M. et al. A two-stage poly(ethylenimine)-mediated cytotoxicity: implications for gene transfer/therapy. *Molecular therapy : the journal of the American Society of Gene Therapy* **11**, 990-995 (2005).
11. Frens, G. Controlled Nucleation for the Regulation of the Particle Size in Monodisperse Gold Suspensions. *Nature Physical Science* **241**, 20 (1973).
12. Yuan, H. et al. Gold nanostars: surfactant-free synthesis, 3D modelling, and two-photon photoluminescence imaging. *Nanotechnology* **23**, 075102 (2012).
13. Jimenez de Aberasturi, D. et al. Surface Enhanced Raman Scattering Encoded Gold Nanostars for Multiplexed Cell Discrimination. *Chemistry of Materials* **28**, 6779-6790 (2016).
14. Brucks, S.D., Freyer, J.L., Lambert, T.H. & Campos, L.M. Influence of Substituent Chain Branching on the Transfection Efficacy of Cyclopropenium-Based Polymers. *Polymers* **9**, 79 (2017).
15. Liu, X., Atwater, M., Wang, J. & Huo, Q. Extinction coefficient of gold nanoparticles with different sizes and different capping ligands. *Colloids and surfaces. B, Biointerfaces* **58**, 3-7 (2007).
16. Boussif, O. et al. A versatile vector for gene and oligonucleotide transfer into cells in culture and in vivo: polyethylenimine. *Proceedings of the National Academy of Sciences of the United States of America* **92**, 7297-7301 (1995).

17. Florea, B.I., Meaney, C., Junginger, H.E. & Borchard, G. Transfection efficiency and toxicity of polyethylenimine in differentiated Calu-3 and nondifferentiated COS-1 cell cultures. *AAPS pharmSci* **4**, E12-E12 (2002).

Chapter 4 SERS Nanoprobe

4.1 Abstract

Similarly to other RNA viruses, the influenza A virus (IAV) rapidly evolves and adapts to evade therapeutic treatments and vaccines. While common practices to monitor viral evolution involve lysing cells and sequencing their RNA content to extract genetic information at the population level, detection and quantification of RNA mutations at the single cell level may be critical for tracking population outliers, such as cell superspreaders, and for carrying out detailed monitoring of the effect of evolutionary pressures on phenotypically different cells. Ultimately, the insight obtained at the single cell level may aid in achieving viral population control and for the development of effective next generation vaccines. This is especially important for the highly mutating IAV, but could be leveraged for other important viruses, such as HIV, dengue, or ebola. The unpredictable evolutionary nature of IAV has allowed it to grow resistant to current preventative methods. Thus, studying the mechanisms underlying viral evolution is essential, and we hypothesize that creating a highly sensitive and selective nanostructured tool that can track viral mutations intracellularly at the single cell level will enable us to obtain some important mechanistic insight into this process. We have designed, synthesized, and tested a nanoparticle probe that can detect viral RNA in intact cells with sensitivity to mutations in the targeted RNA sequence. The probe consists of gold nanostars functionalized with surface enhanced Raman spectroscopy (SERS) active beacons allowing for accurate and high resolution single particle-based IAV screening. The SERS-based assay allows detection of viral RNA without the need of PCR amplification. The target-specific SERS-active nanoparticle probe is designed to emit an intense SERS signal in the presence of viral RNA targets, whose intensity will vary with the number of mutations present on the

target RNA. Additionally, the platform has been developed to account for viral population diversity by accommodating multiplexed intracellular imaging and sensing of various IAV gene sequences in the future. It was also designed with a fluorescent Raman reporter for the option to develop a switchable SERS - fluorescent system. The SERS-active nanoparticle probe is not meant to replace current methods, but rather to function as a building block for a specialized tool to add to the virologist toolbox.

4.2 Introduction

The influenza A virus (IAV) is a highly mutating RNA virus that is the source of a reoccurring seasonal epidemic, causing thousands of deaths and billions of dollars in healthcare expenditures in the United States alone.[1] Despite the efforts with vaccination, the Center for Disease Control and Prevention (CDC) reported that the effectiveness of the 2016-2017 vaccine against IAV ranged from 57% to as low as 13% depending on the age group.[2] Unlike other viral infections that are effectively controlled by vaccinations, IAV is an unpredictable human pathogen and grows resistant to drugs and vaccines as it mutates and replicates.[3-6] The continuous evolution and mutation of IAV is not a common characteristic of most viruses, which is the cause of low effective rates of the flu vaccines.[3, 4] To this end, countless studies have been conducted to understand viral anatomy, ecology, and evolution. Current methods include immunoassays, serological detection, and molecular detection.[7] The challenges faced by current methods are due to high genetic variability and the unpredictable nature of IAV, leading to limitations in sensitivity, reproducibility, and cost.[8] Hence, a facile method for effectively studying

genetic variability, mutation, and evolution of viral RNA would be highly desirable for virologists.

In particular, there is a need to study single point RNA mutations to predict and understand the mechanisms of viral mutation and evolution and how they correlate to evolutionary pressures. Quantifying RNA modifications at the single cell level is critical for the detection of viral mutations and would provide a tool to study viral evolution and ultimately crack the code for viral population control.[9, 10] Effective treatments and preventative measures can be developed by understanding the sequence of events and the factors that contribute to IAV's evolutionary success and drug resistance.

Nanomaterial-based approaches have emerged as promising tools for biomedical applications including detection and analysis of viruses.[11, 12] Since their development in 1875 and implementation in biological applications in 1971, gold nanoparticle (AuNP) platforms have been developed with increasingly high sensitivity, rapid detection, tunable properties, and cost efficiency.[13-15] AuNPs are advantageous due to their unique physical and optical properties.[16-18] Their biocompatibility, size, morphology, and optical properties have established their role in biomedical imaging and sensing. Their plasmonic properties make them essential for signal enhancement in Surface Enhanced Raman Spectroscopy (SERS).[19, 20] In particular, biological applications have benefited from the use of SERS tags. A SERS tag can readily gain access to various cellular components for intracellular monitoring and indirect labeling.[18] Their specific targeting capabilities, implemented via the use of antibodies, aptamers, or peptides, can be leveraged to design biomolecule delivery systems and biosensors to detect and quantify cellular membrane biomarkers and intracellular components such as proteins or nucleic acids.[21-24]

Furthermore, SERS-active nanoparticle platforms provide a method for single cell analysis that overcomes the challenges brought by the unpredictable nature of viral replication, which causes inter-cellular variability. The single cell applicability allows for a mechanistic insight into viral evolution that is obscured in whole population studies. It affords an advantage of analyzing RNA in outliers that can provide additional awareness to the viral ecosystem.

Herein, we describe a method for intracellular viral RNA detection and quantification via a SERS active nanostar probe (SANSP). Our method is not only extremely sensitive and selective but is uniquely equipped for identification of single base mutations in the target RNA. The nanostar probe was functionalized with a SERS-active DNA beacon to allow for high resolution single particle-based screening without the need for PCR amplification. **Scheme 4.1** illustrates the steps that were followed to synthesize the SANSPs. The SANSPs were designed with targeting moieties to become SERS-active in the presence of their viral RNA target while showing sensitivity to base pair mutations.

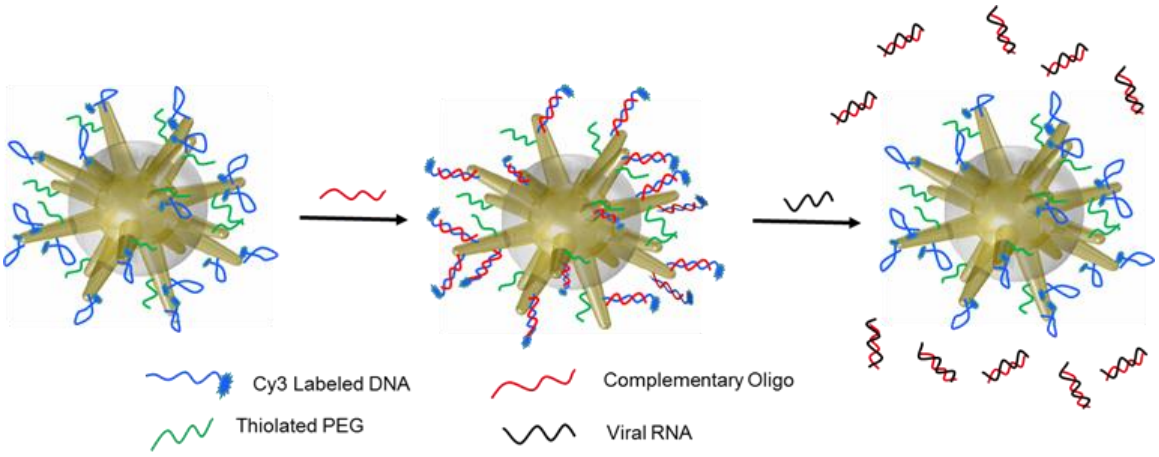

Scheme 4.1 Schematic diagram of the SERS nanostar probes (SANSPs). Gold nanostars are initially functionalized with a Raman tagged beacon DNA that is then hybridized with a complementary oligo creating the SANSPs. Upon exposure to the viral RNA, the complementary oligo de-hybridizes and hybridizes with the viral RNA, allowing the beacon to return to its original folded conformation. Upon addition of the complementary strand the SERS signal will be quenched (off state). Addition of the target RNA will lead to dehybridization of the complementary strand, re-folding of the beacon in its hairpin conformation with consequent increase in SERS signal intensity, which will depend on the number of base mutations in the vRNA (on state).

To synthesize the SANSPs, the particles are initially functionalized with a Raman reporter (i.e. Cy3)-labeled beacon, that will yield an intense SERS signal when folded into a hairpin confirmation. The intense SERS signal is a result of bringing the Raman reporter in close proximity to the gold surface. The beacon is then hybridized with a complementary strand creating what we call SANSPs. In this configuration, the Raman

reporter will no longer be in close contact to the gold surface and the SERS signal will significantly decrease. When the SANSPs are exposed to their target, the complementary oligo will de-hybridize from the beacon and hybridize with the target sequence, returning the beacon to its original folded conformation which will result in the recovery of the SERS signal. This series of events creates the "on-off-on" response series.

4.3 Materials and Method

4.3.1 vRNA and Targeting Ligands

IAV RNA genome is divided into 8 separate segments of genomic virion (vRNA). Each segment consists of 1) terminal coding regions, which are highly conserved and found at the terminal end of each segment, 2) packaging regions, located within the conserved region, and 3) a central coding region, which is a region highly prone to mutations.[10] To first develop a sensor that targets viral RNA, conserved sequences in the terminal coding regions are the ideal target aim. The vRNA segment chosen in this work as the target RNA to test the SERS active probe is a 21 base pair segment in the conserved region of the hemagglutinin (HA) glycoprotein expressing genome, segment 4. The target RNA sequence is 5'-TCA TTT TTG TTG CTT TTG TTT-3'. The beacon length and composition were determined for optimal folding to form a hairpin using the ΔH calculated using the tool available on IDT's website, the company supplying all our oligonucleotides, including the beacon (5'-Thiol-MC6-CGTGCG TCA TTT TTG TTG CTT TTG TTT CGCACG-Cy3-3') and its complementary strand (5'-AAA CAA AAG CAA CAA AAA TGA-3').[25]

4.3.2 Preparation of SERS Active Probe for vRNA Detection

The SERS active nanostar probes (SANSPs) were prepared using the silica coated gold nanostars with exposed tips previously described. Surfactant free gold nanostars were synthesized using modifications of established protocols via seed mediated method described by Yuan *et al.*[26] 2 mL of 0.025 M $HAuCl_4$ salt solution, 200 µL of 1 N HCl, 48 mL of milliQ water, and 125 µL of 12 nm citrate capped spheres with an absorbance of 2.81 at a 1 mm path length under gentle stirring were added to a flask. To the mixture, 2 mL of 3 mM $AgNO_3$ and 1 mL of 100 mM ascorbic acid were added simultaneously. The reaction was left to stir for 7 minutes, after which it turned a deep blue.

For the silica coating preparation, a modified version of the protocol reported by Atta *et al.* was used.[27] The gold nanostars were capped with CTAB by mixing the gold nanostar solution with 10 mL of 0.2 M CTAB under gentle stirring and purified via centrifugation at 6500 g for 20 minute. 50 µL of tetraethylorthosilicate (TEOS) were added to 40 mL of 0.8 nM CTAB capped nanostars and stirred gently. After an hour of stirring, the pH of the mixture was adjusted to 8.6 by NH_4OH addition under gentle stirring for 24 hours. The resulting product was purified by centrifugation at 6500 g for 30-45 minutes, resulting in exposed tips and a silica coated core.

The silica coating on the silica coated gold nanostars was then etched by adding 300 mg of $NaBH_4$ to 10 mL of 0.4 nM silica coated gold nanostars under gentle stirring for 30 hours.

The functionalized particles were prepared by conjugating PEG, for added stability,[28] and the oligonucleotides. Briefly, thiolated PEG was added to 3 nM Si@AuNS under mild shaking for 30 minutes to allow proper PEG conjugation to the gold surface of the

exposed tips and centrifuged at 3000g for 10 min. The particles were re-suspended and the thiolated oligonucleotides, 5'-Thiol-MC6-CGTGCG TCA TTT TTG TTG CTT TTG TTT CGCACG-Cy3-3' and 5'-TCA TTT TTG TTG CTT TTG TTT-3', were dissolved in RNAse free DCEP-treated water (Thermo Fisher) and added at a final concertation of 500 nM. The particles were purified and re-suspended.[29]

Two version of the particles were made. The first was to verify the "ON" state, i.e. with the unhybridized beacon in its hairpin conformation, which leads the Cy3 reporter to be in close proximity to the gold surface, and give rise to an enhanced SERS signal. For that version, only the unhybridized beacon was conjugated to the Si@AuNs. The second version was the actual SANSPs, i.e. with the beacon hybridized to its complementary strand, resulting in the Cy3 dye to be away from the gold surface with a quenched SERS signal ("OFF" state). For that version, the beacon was conjugated to the Si@AuNs and hybridized to the complementary strand.

4.3.3 Characterization of Si@AuNS and SANSPs

To optically characterize the nanoparticles, UV-Vis spectra were recorded using a Thermo Fisher Nanodrop 2000 and a SI Photonics Model 440 CCD Array UV-Vis spectrophotometer.

Transmission electron microcopy (TEM) images were taken using a Philips CM12 transmission electron microscope. This was used to evaluate the morphology and size. The samples were drop casted onto carbon-coated TEM grids (Ted Pella).

4.3.4 Stability and Optimization of SANSPs

Before conducting extensive experiments, Si@AuNS were confirmed to be the optimal selection for preparation of the SANSPs. Si@AuNS were compared to surfactant free nanostars to determine if Si@AuNS are capable of reducing false "On" signals.

Surfactant free gold nanostars were synthesized using modifications of established protocols such as the seed mediated method described by Yuan *et al.*[26] Briefly, 2 mL of 0.025 M $HAuCl_4$ salt solution, 200 µL of 1 N HCl, 48 mL of milliQ water, and 125 µL of 12 nm citrate capped spheres with an absorbance of 2.81at a 1 mm path length under gentle stirring. 2 mL of 3 mM $AgNO_3$ and 1 mL of 100 mM ascorbic acid were added simultaneously to the mixture. The reaction was left to stir for 7 minutes and purified via centrifugation. The particles were then functionalized in a similar fashion as the Si@AuNS were. Thiolated PEG was added to 3 nM Si@AuNS under mild shaking for 30 minutes to allow proper PEG conjugation to the gold surface of the exposed tips and centrifuged at 3000g for 10 min. The particles were re-suspended and the thiolated oligonucleotides, 5'-Thiol-MC6-CGTGCG TCA TTT TTG TTG CTT TTG TTT CGCACG-Cy3-3' and 5'-TCA TTT TTG TTG CTT TTG TTT-3', were dissolved in RNAse free DCEP-treated water (Thermo Fisher) and added at a final concertation of 500 nM. The particles were purified and re-suspended.

To confirm temperature stability at tissue culture incubation, 37°C, the SANSPs were prepared at 37°C and tested against the target RNA at 37°C using a Fisher Scientific Microtube Thermal Mixer.

To test for the SANSPs stability over time, the unhybridized beacon functionalized Si@AuNs was shielded from light and left at room temperature for 1 month.

Additionally, the SANSPs were shielded from light and also left at room temperature for 1 month.

4.3.5 Viral RNA Mutation Detection

To demonstrate the SANSPs sensitivity towards nucleotide mutations, modified beacon and target RNA sequences were purchased from IDT. The beacon with 0 modifications was compared to a beacon with 2 and 4 base mismatches, 5'-/5ThioMC6-D/ <u>CGTGCG</u> TCA TTT TTG TTG CTT TTG TTT <u>CGCACG</u> /3cy3P/ -3', 5'-/5ThioMC6-D/ <u>CGTGCG</u> TCA TTT TTG **A**TG CTT TTG **A**TT <u>CGCACG</u> /3cy3P/ -3' and 5'-/5ThioMC6-D/ <u>CGTGCG</u> **A**CA TTT **A**TG TTG **G**TT TTG **A**TT <u>CGCACG</u> /3cy3P/ -3' with the modified base pairs in bold and the flank regions underlined. Each of the three beacons were hybridized to the complementary strand, 5'- AAA CAA AAG CAA CAA AAA TGA -3' and tested against the target RNA and the control/random sequence, 5'- TTT TAT CCT TCA TCT CTT GTA -3'. Likewise, the target with 0 modifications, 5'-TCA TTT TTG TTG CTT TTG TTT-3', was compared to the target with 2, 4, 6, and 8 mismatches 5'-TCA TTT TTG TTG CTT TTG TTT-3', 5'- TCA T**<u>G</u>**T TTG TTG C**<u>G</u>**T TTG TTT-3', 5'- T**<u>A</u>**A TTT T**<u>C</u>**G TTG C**<u>G</u>**T TTG T**<u>C</u>**T-3', 5'- T**A**A TT**<u>A</u>** T**C**G TT**<u>A</u>** C**<u>G</u>**T TTG T**<u>C</u>**T - 3', and 5'-T**<u>A</u>**A TT**<u>A</u>** T**C**G **<u>A</u>**T**<u>A</u>** C**<u>G</u>**T T**<u>A</u>**G T**<u>C</u>**T-3', with the modified base pairs underlined. Each target was tested against a single beacon. In each case a target strand is introduced to the SANSPs that are comprised of a beacon hybridized to the complementary strand and conjugated to a PEG coated Si@AuNS. The resulting mixture is dried and analyzed via surface enhanced Raman spectroscopy (SERS).

Sequence Name	**Sequence**
0-Mismatch Beacon	5'-/5ThioMC6-D/ CGTGCG TCA TTT TTG TTG CTT TTG TTT CGCACG /3cy3P/ -3
2-Mismatch Beacon	5'-/5ThioMC6-D/ CGTGCG TCA TTT TTG ATG CTT TTG ATT CGCACG /3cy3P/ -3’
4-Mismatch Beacon	5'-/5ThioMC6-D/ <u>CGTGCG</u> **A**CA TTT **A**TG TTG **G**TT TTG **A**TT <u>CGCACG</u> /3cy3P/ -3’
Complementary	5'- AAA CAA AAG CAA CAA AAA TGA -3'
Control/Random	5'- TTT TAT CCT TCA TCT CTT GTA -3'
0-Mismatch Target	5’-TCA TTT TTG TTG CTT TTG TTT-3’
2-Mismatch Target	5’- TCA T**G**T TTG TTG C**G**T TTG TTT-3’,
4-Mismatch Target	5’- T**A**A TTT T**C**G TTG C**G**T TTG T**C**T-3’
6-Mismatch Target	5’- T**A**A TT**A** T**C**G TT**A** C**G**T TTG T**C**T - 3’
8-Mismatch Target	5’-T**A**A TT**A** T**C**G **A**T**A** C**G**T T**A**G T**C**T-3’

Table 4.1 The sequences synthesized and ordered from IDT to develop and test SANSPs. The sequences originate from 5'-TCA TTT TTG TTG CTT TTG TTT -3’ located in the conserved region of IAV segment 4.

4.3.6 Cell Culture

HeLa cells were purchased from ATCC and cultured in Eagle's minimum essential medium (EMEM, ATCC) that was supplemented with 5% Penstrep (Thermo Fisher) and 10% Fetal Bovine Serum (Thermo Fisher). The cells were grown at 37°C at 5% CO_2. Upon reaching 70-80% confluency, the HeLa cells were washed with 1X phosphate buffer solution (PBS), trypsinized and re-suspended in fresh EMEM. For experiments and assays, HeLa cells were counted and seeded appropriately.

4.3.7 Viral RNA Detection in Cell Lysate

HeLa cell were seeded in a 10 cm dish at a seeding density of 2.0 X 10^6 in 5% Penstrep and 10% Fetal Bovine Serum supplemented EMEM. The cells were allowed to grow and attach for 24 hours at 37°C and 5% CO_2. The media was removed and the cells were washed with 1X PBS. To lysate the cells, Cell Lysis Buffer (Cell Signaling Technology) was used following the manufacturer's protocol. Briefly, 400 μL of 1X lysis buffer was added to the dish and incubated on ice for 5 minutes. The cells were then scraped and transferred to a 2 mL centrifuge tube. The cell were sonicated and centrifuged at 14,000 g. The supernatant was extracted for use. A fraction of extracted cell lysate, equivalent to 25,000 cells (amount seeded in an 8-well chambered coverglass), was spiked with target RNA, 5'-TCA TTT TTG TTG CTT TTG TTT-3'. The SANSPs were introduced to the cell lysate and allowed to interact prior to SERS analysis.

4.3.8 Cellular Uptake of SANSPs

To confirm cellular uptake, cells were exposed to SANSPs decorated with FITC-labeled PEG. The SANSPs with FITC labeled PEG were prepared by sequentially conjugating FITC labeled PEG, for added stability and fluorescence tagging,[28] and then conjugating oligonucleotides. Briefly, thiolated FITC labeled PEG was added to 3 nM Si@AuNS under mild shaking for 30 minutes to allow proper PEG conjugation to the gold surface of the exposed tips and centrifuged at 3000g for 10 min. The particles were re-suspended, and the thiolated oligo nucleotides (5'-Thiol-MC6-CGTGCG TCA TTT TTG TTG CTT TTG TTT CGCACG-Cy3-3' and 5'-TCA TTT TTG TTG CTT TTG TTT-3') were dissolved in RNAse free DCEP treated water (Thermo Fisher) and added to the nanostar suspension at a final concertation of 500 nM. The particles were purified and re-suspended.[29]

To determine the optimal concentration of SANSPs to be delivered to each tissue culture well, various concentrations were tested. HeLa cell were seeded in a 96-well plate tissue culture dish (ThermoFisher) at a seeding density of 10,000 cell / well in the supplemented EMEM. The cells were allowed to grow and attach for 24 hours at 37°C and 5% CO_2. Upon reaching 70-80% confluency, the HeLa cells were washed with 1X phosphate buffer solution (PBS) and fresh EMEM was added. 50, 75, 100, 125, and 150 µg/mL of SANSPs were added to 3 wells each. After 24 hours of incubation, the cell viability was measured using a Vybrant MTT cell proliferation assay kit (V13154 Thermo Fisher) following the manufacturer's protocol. The media in each well was replaced with 100 µL of fresh media and10 µL of 12 mM 3-(4,5-dimethylthiazol-2-yl)-2,5-diphenyltertazolium bromide (MTT). The cells were then incubated at 37°C and 5% CO_2 for 4 hours. 85 µL of

media were removed and 75 µL of DMSO were added to each well. The concentration of live cells was determined by measuring the density at 540 nm of the formazan dye crystals produced as a result of metabolic activity of live cells.

Once the optimal concentration of SANSPs was determined, HeLa cell were seeded in an 8-well chambered coverglass (ThermoFisher) at a seeding density of 25,000 cell / well in the supplemented EMEM. The cells were allowed to grow and attach for 24 hours at 37°C and 5% CO_2. Upon reaching 70-80% confluency, the HeLa cells were washed with 1X phosphate buffer solution (PBS) and fresh EMEM was added. 50 µg/mL of SANSPs were added and incubated for 4 hours. After the 4-hour incubation, the media was removed and cells were washed with 1X PBS. To fix the cells, 4% formaldehyde in 1X PBS was added to cover the surface of the cells and left to incubate for 10 minutes at room temperature. The solution was removed and the cells were washed with 1X PBS. The cells were allowed to dry and analyzed via fluorescence microscopy.

4.3.9 Viral RNA Detection in Single Cells

HeLa cell were seeded in an 8-well chambered coverglass (ThermoFisher) at a seeding density of 25,000 cell / well in the supplemented EMEM. The cells were allowed to grow and attach for 24 hours at 37°C and 5% CO_2. The cell were transfected with IAV H1N1 HA plasmid to express the HA segment. Three controlexperiments were designed: 1) cells transfected with PB1 plasmid, 2) cells transfected with PB2 plasmid and 3) non-transfected cells. The controls were tested to demonstrate SANSP sensitivity. JetPRIME transfection reagent (Polyplus transfection) was used following the manufacturer's protocol. The plasmids were each diluted in 25 µL jet prime buffer then vortexed to mix.

Jet prime reagent was then added to the mixture and mixed. 0.5 µL of the mixture were added to each appropriate well and incubated for 24 hours. The media was removed, the cells were washed with 1X PBS, and fresh media was added. 50 µg/mL of SANSPs were added and incubated for 4 hours. After the 4-hour incubation, the media was removed and cells were washed with 1X PBS. To fix the cells, 4 % formaldehyde in 1X PBS was added to cover the surface of the cells and left to incubate for 10 minutes at room temperature. The solution was removed and the cells were washed with 1X PBS. The cells were allowed to dry and analyzed via SERS.

4.4 Results and discussion

4.4.1 Demonstrating SANSPs RNA Detection

Surfactant free gold nanostars were synthesized using a previously reported seed mediated protocol,[26] and then partially coated with silica shell to form Si@AuNS.[27] The Si@AuNS were then functionalized with thiolated PEG[28] and the unhybridized thiolated beacon via a thiol-Au bond. The beacon was labeled with Cy3, as its SERS profile is well established in the literature and the fluorescence capability can be utilized for future progression of the SANSPs as switchable SERS-fluorescent tags.[29] Another batch of Si@AuNS was functionalized with thiolated PEG and thiolated beacon, followed by hybridization to the complementary strand. The morphology, size, and the On-OFF-On switching of the particles were verified by TEM and SERS. (**Figure 4.1** and **Figure 4.2**).

a) b)

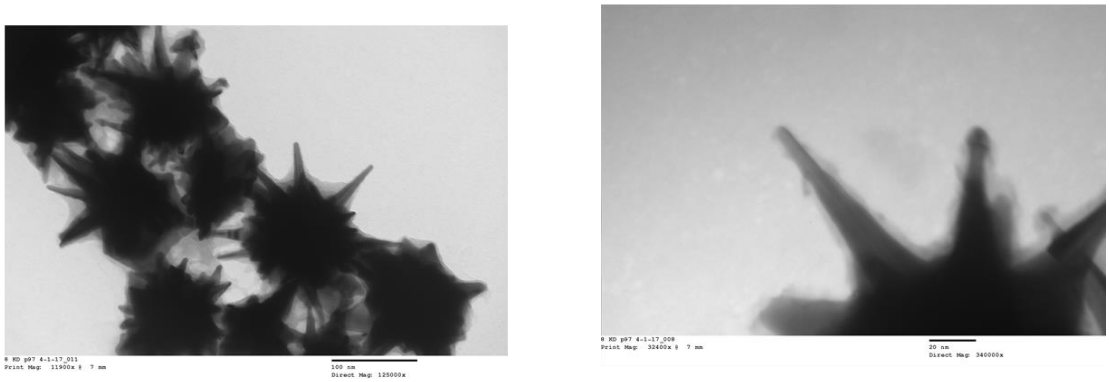

Figure 4.1 The SERS active nanoparticle probes were characterized via TEM. a) TEM micrograph of silica coated gold nanostars with exposed tips. The image shows a thin layer of silica around the core of the nanostars leaving the gold surface on the tips of exposed. b) A close-up image of the exposed tips.

The particles conjugated to the unhybridized thiolated beacon were analyzed via SERS using 633 nm HeNe laser excitation, at 0.101 mW laser power and 3 accumulations. The SERS measurements, collected through 4 maps, revealed strong peaks correlating to the Cy3 SERS profile.[29] This demonstrates the "ON" position. (**Figure 4.2b**) The particles conjugated to the thiolated beacon hybridized to the complementary strand were analyzed via SERS using a 633 nm HeNe laser at 0.101 mW laser power and 3 accumulations. The SERS measurements, taken in 4 maps, revealed an absence of an intense Cy3 signal

(**Figure 4.2c**). The "off" signal is not completely absent and this can be due to a number of beacons that have remained in contact with the gold surface.

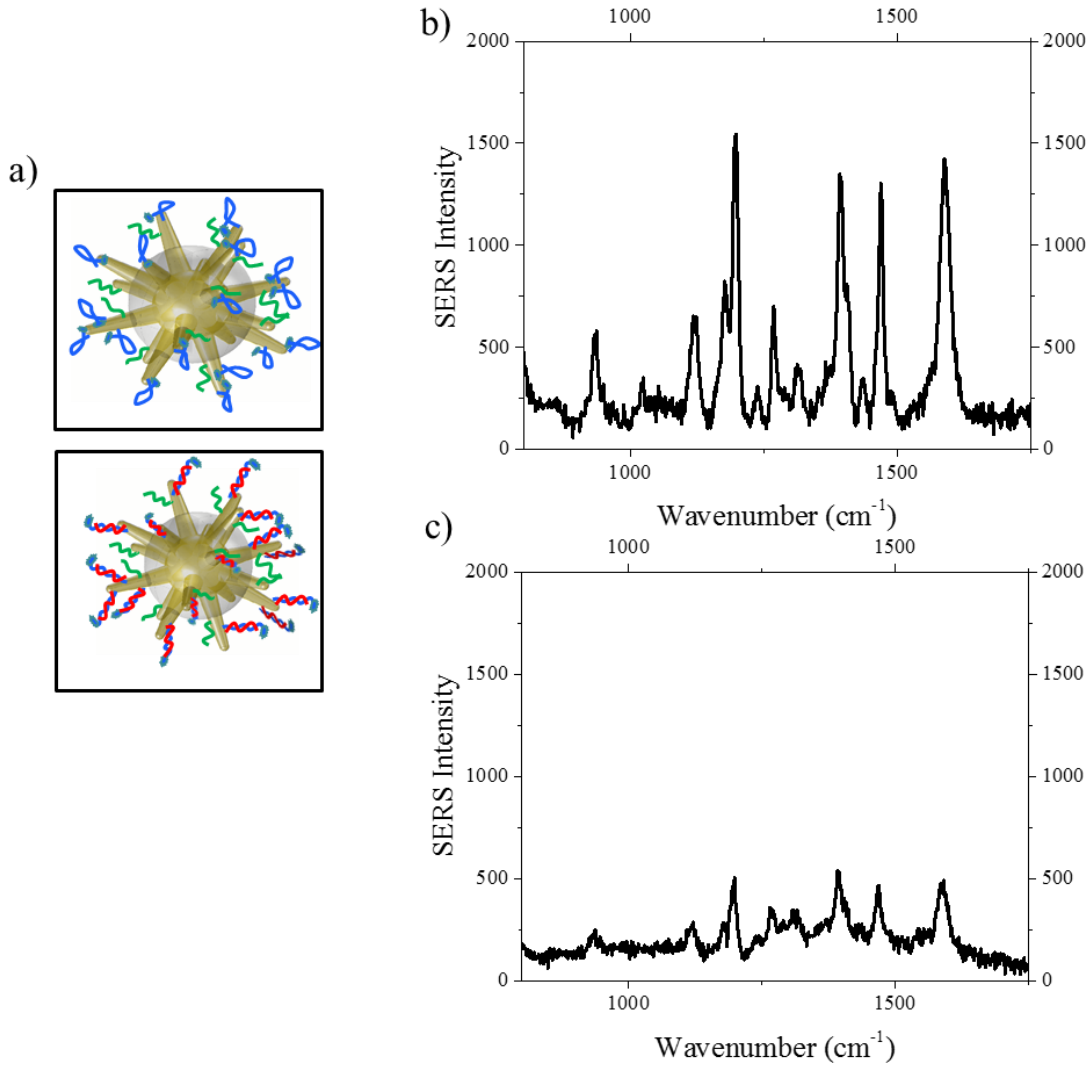

Figure 4.2 a) Representation of the silica coated gold nanostars functionalized with the unhybridized beacon (top) and with the beacon hybridized to the complementary strand (bottom). b) SERS spectra of silica coated gold nanostars functionalized with Cy3 labeled beacon and PEG. The beacon is in the hairpin position, bringing the Cy3 Raman reporter

in proximity of the gold surface resulting in an enhanced SERS signal ("On" state). c) SERS spectra of silica coated gold nanostars functionalized with PEG and Cy3 labeled beacon hybridized to the complementary strand. The beacon is no longer in the hairpin position, bringing the Cy3 Raman reporter away from the gold surface resulting in a decreased SERS signal ("Off" state).

4.4.2 Stability and Optimization of SANSPs

Before conducting extensive experiments, it was important to confirm that Si@AuNS was the best particle for the experiments. The rationale for using Si@AuNS was to have strategic placement of the ligands at the hot spots located on the tips of the gold nanostars and preventing false signals, which can be explained as follows.[20, 30, 31] Si@AuNS provide the advantage of coating the core of gold nanostars with silica and allowing for only gold exposure at the tips of the spikes. When the ligands bind to Si@AuNS via a thiol-Au bond, they are limited to the exposed gold surfaces located at the tip of the spikes. Surfactant free gold nanostars without this partial silica coating will have unspecified ligand binding to the core, to the sides of the spikes, and to the tips of the spikes, leading to false "on" signals.

The surfactant free gold nanostars were synthesized using a previously reported seed mediated protocol,[26] and Si@AuNS were prepared using a protocol from Atta *et al.*[27] Both particles were then functionalized with thiolated PEG[28] and both were each separately functionalized with the unhybridized thiolated beacon and the hybridized thiolated beacon with the complementary strand. The 4 total samples, 1) unhybridized

thiolated beacon functionalized nanostars, 2) hybridized thiolated beacon functionalized nanostars, 3) unhybridized thiolated beacon functionalized Si@AuNS and 4) hybridized thiolated beacon functionalized Si@AuNS (SANSPs), were analyzed vis SERS(**Figure 4.3).** The "On-Off" signal of the Si@AuNS was stronger than the "On-Off" signal of the surfactant free stars. This indicates that even though the beacons on the surfactant free stars are hybridized to the complementary strand and no longer in a hairpin confirmation, their unspecified placement in the core of the nanostars as opposed to the tips of the nanostars resulted in false "On" signals. The Raman tags on the hybridized beacons that are conjugated to the core would remain in close proximity to the gold surface and thus giving off a stronger signal than if it was located on the tips and extended away for the gold surface.

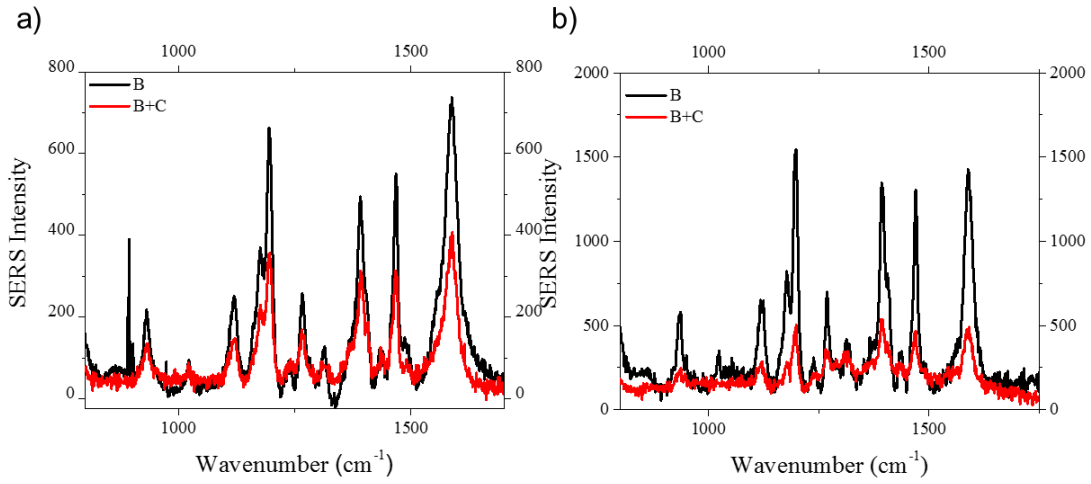

Figure 4.3 Comparison of the "on-off" signal difference between unhybridized thiolated beacon functionalized (B) and after complementary strand addition (B+C) in a) surfactant

free gold nanostars b) etched silica coated gold nanostars. The unspecified binding to the tips and the core on the surfactant free gold nanostars resulted in false “On” signals.

Next, the “On-OFF-On” switch in solution was tested to see that the SANSPs can in fact detect its target RNA. **Figure 4.4** shows a clear intense signal with beacon conjugated nanoparticles. Once the beacon is hybridized to the complementary strand, the signal significantly decreases. When the target RNA is introduced, the signal is then recovered. Introduction of a random RNA sequence as opposed to the target RNA sequence led to no signal recovery, demonstrating the selectivity of the probe to only the intended target RNA.

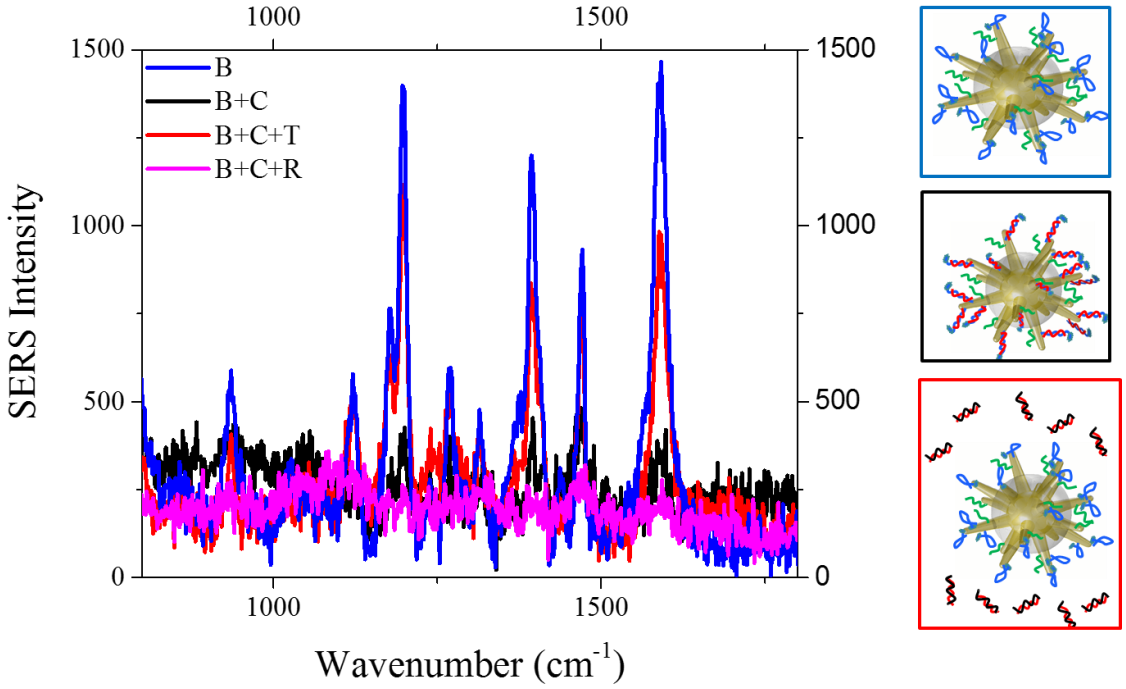

Figure 4.4 Representation of the SANSPs tested in solution. "B" indicates the nanostars conjugated to the beacon in its hairpin conformation. "B+C" represents the nanostars conjugated to the beacon hybridized to its complementary strand. "B+C+T" represents the configuration achieved after target RNA introduction, which leads to dehybridization of the complementary strand from the nanostar, followed by its hybridization to the target RNA and folding of the beacon back into hairpin conformation. "B+C+R" represents the case in which a random RNA sequence is introduced in the system.

The temperature stability in tissue culture incubation conditions, 37°C, was confirmed. The SANSPs were prepared at 37°C and tested against the target RNA at 37°C. The SANSPs show comparable stability and efficiency at 37°C. **(Figure 4.5)**

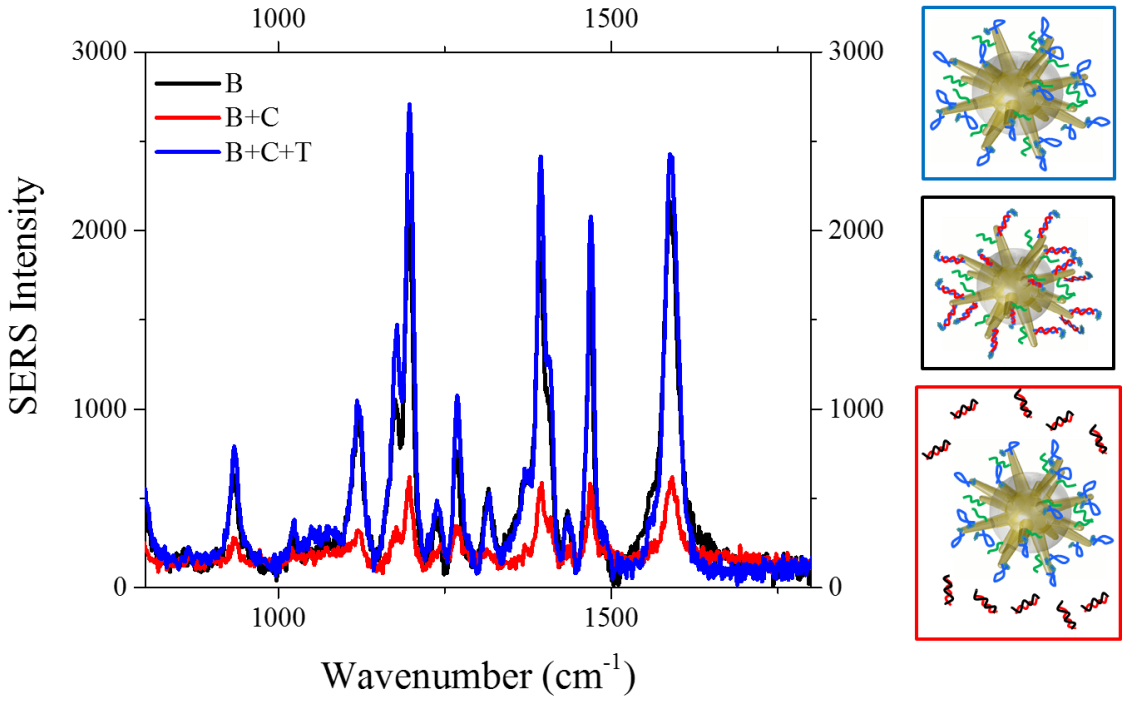

Figure 4.5 Representation of the stability of SANSPs that were prepared at 37°C and tested against the target RNA at 37°C. "B" indicates the nanostars conjugated to the beacon in its hairpin conformation. "B+C" represents the nanostars conjugated to the beacon hybridized to its complementary strand. "B+C+T" represents the configuration achieved after target RNA introduction, which leads to dehybridization of the complementary strand from the nanostar, followed by its hybridization to the target RNA and folding of the beacon back into hairpin conformation.

The shelf life of the SANSPs was tested over time at 1 day, 1 week, 2 weeks, and 1 month time points. The SANSPs showed consistent activity and stability. **(Figure 4.6)**

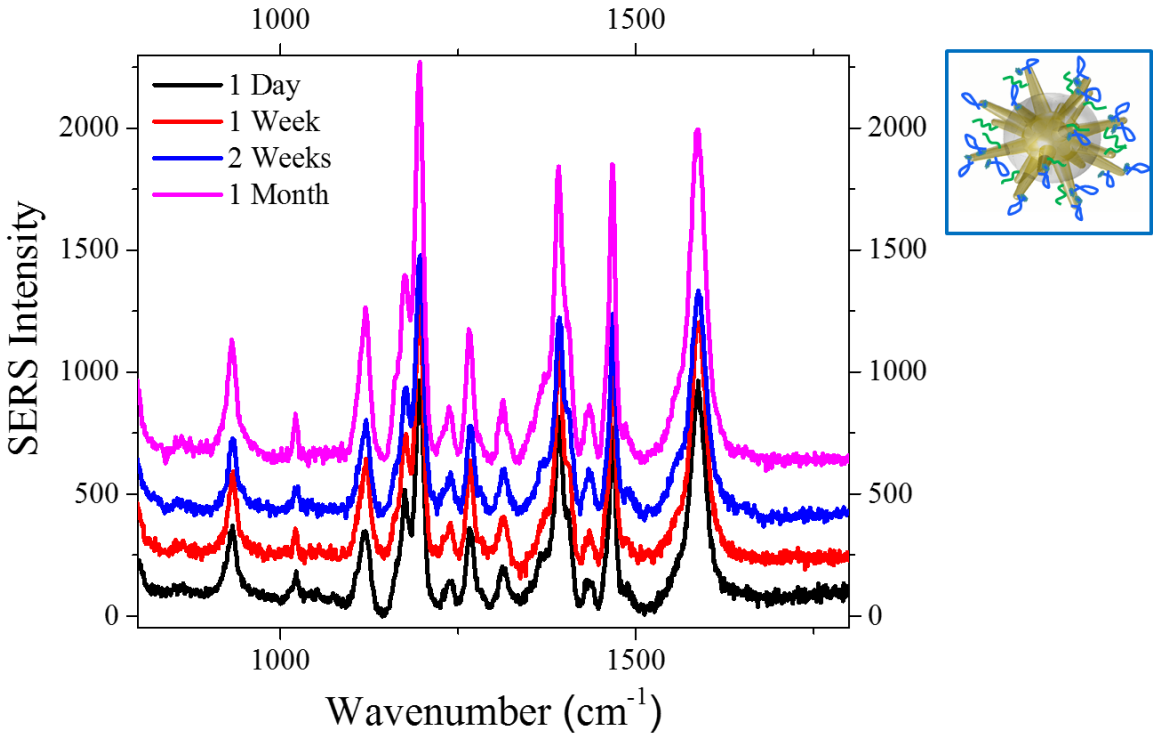

Figure 4.6 Stability of SANSPs over time for the configuration shown in the boxed illustration.

4.4.3 Viral RNA Mutation Detection

The sensitivity of the SANSPs towards RNA detection was demonstrated by testing out the SANSPs with non-modified and modified beacons, 5'-/5ThioMC6-D/ CGTGCG TCA TTT TTG TTG CTT TTG TTT CGCACG /3cy3P/ -3', 5'-/5ThioMC6-D/ CGTGCG TCA TTT TTG **A**TG CTT TTG **A**TT CGCACG /3cy3P/ -3' and 5'-/5ThioMC6-D/ CGTGCG **A**CA TTT **A**TG TTG **G**TT TTG **A**TT CGCACG /3cy3P/ -3'. Each beacon type was hybridized to its complementary strand, conjugated to the Si@AuNS, and exposed to the target RNA, 5'-TCA TTT TTG TTG CTT TTG TTT-3'. The samples were tested via SERS using a 633 nm HeNe laser excitation, at 0.101 mW laser power and 3 accumulations. The SERS measurements were taken in 4 maps, averaged, plotted and compared to show a linear dependence between the SERS signal intensity and the number of mismatches in the target. As the number of modifications increased, the ratio between the SERS signal of 1) the particles conjugated to the unhybridized thiolated beacon prior to complementary strand hybridization and exposure to the target and 2) the particles conjugated to the unhybridized thiolated beacon subsequent to complementary strand hybridization and exposure to the target decreased. The percent recovery of the "on" signal decreased as the number of base pair modifications increased, from 94.95 % at 0 modifications, to 76.01 % at 2 modifications, and 40.87 % at 4 base pair modifications.

Likewise, the target with 0 modifications was compared to the target with 2, 4, 6, and 8 base pair modifications, 5'-TCA TTT TTG TTG CTT TTG TTT-3', 5'- TCA T**G**T TTG

TTG C**G**T TTG TTT-3', 5'- T**A**A TTT T**C**G TTG C**G**T TTG T**C**T-3', 5'- T**A**A TT**A** T**C**G TT**A** C**G**T TTG T**C**T - 3', and 5'-T**A**A TT**A** T**C**G **A**T**A** C**G**T T**A**G T**C**T-3'. Each target was tested against a single beacon. In each case the target was added to SANSPs that are comprised of the beacon hybridized to the complementary strand and conjugated to a PEG coated Si@AuNS,. The samples were tested via SERS using a 633 nm HeNe laser excitation, at 0.101 mW laser power and 3 accumulations. The SERS measurements were taken in 4 maps, averaged, plotted, and compared to show a linear trend as the number of base pair modifications were made at SERS signal 1586 cm^{-1}. **(Figure 4.7)** SERS signal 1586 cm^{-1} was chosen since it is a characteristic Cy3 band and is unique in the event of multiplexing, which is a promising feature of SANSPs.[32] As the number of modifications increased the ratio between the SERS signal of 1) the particles conjugated to the unhybridized thiolated beacon prior to complementary strand hybridization and exposure to the target and 2) the particles conjugated to the unhybridized thiolated beacon subsequent to complementary strand hybridization and exposure to the target decreased. The percent recovery of the "on" signal decreased as the number of base pair modifications increased, from 80.2 % at 0 modifications, 75.4 % at 2 modifications, 68.6 % at 4 base pair modifications, 52.0 % at 6 base pair modifications and 35.5 % at 8 base pair modifications.

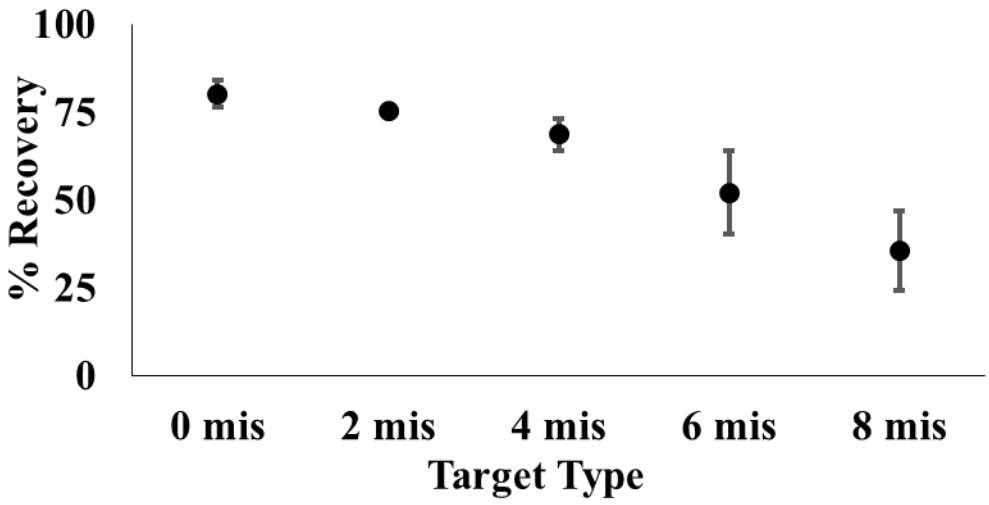

Figure 4.7 SANSPs interaction with the target RNA with different degree of base mismatch. The results showed a linear trend as the number of base pair modifications were made at SERS signal 1586 cm^{-1}.

4.4.4 Viral RNA Detection in Cell Lysate

HeLa cells were seeded in a 10 cm dish and their lysate was extracted for initial testing of SANSPs in cytoplasm. The cell lysate was spiked with the target RNA, 5'-TCA TTT TTG TTG CTT TTG TTT-3', in a concertation of 500 nM to replicate previous experimental conditions. The SANSPs were introduced to a fraction of the cell lysate, equivalent to 25,000 cells (amount seeded in an 8-well chambered coverglass), and analyzed via SERS, using a 633 nm HeNe laser excitation, at 0.101 mW laser power and 3 accumulations. The SERS measurements were collected in 4 maps, averaged, and

plotted. The SERS spectra showed strong Cy3 SERS signal recovery, demonstrating the SANSPs ability to target RNA even with the presence of intracellular obstacles such as nucleases and protein corona. (**Figure 4.8**)

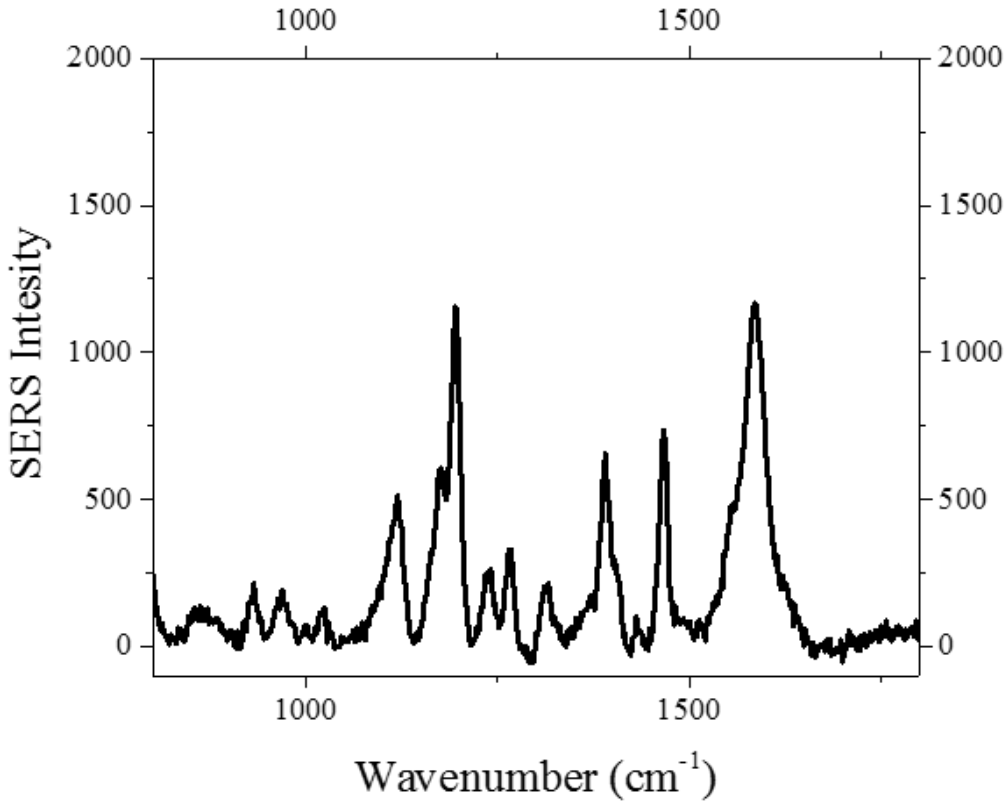

Figure 4.8 The SERS spectrum shows the recovery of the SERS signal from Cy3 signal after exposing the SANSPs to target RNA-spiked HeLa cell lysate, demonstrating the SANSPs ability to target RNA even with intracellular obstacles such as nucleases and protein corona.

4.4.5 *In Vitro* Cellular Uptake of SANSPs: Viability and Fluorescence Microscopy

To confirm cellular uptake of the SANSPs, the particles were initially tested for optimal dosage. An MTT assay was conducted to test for cellular viability of 50, 75, 100, 125, and 150 µg/mL of SANSPs per well. 50 µg/mL had the highest average viability at 76.38 % with respect to the control and was chosen to continue the *in vitro* studies (**Figure 4.9a**).

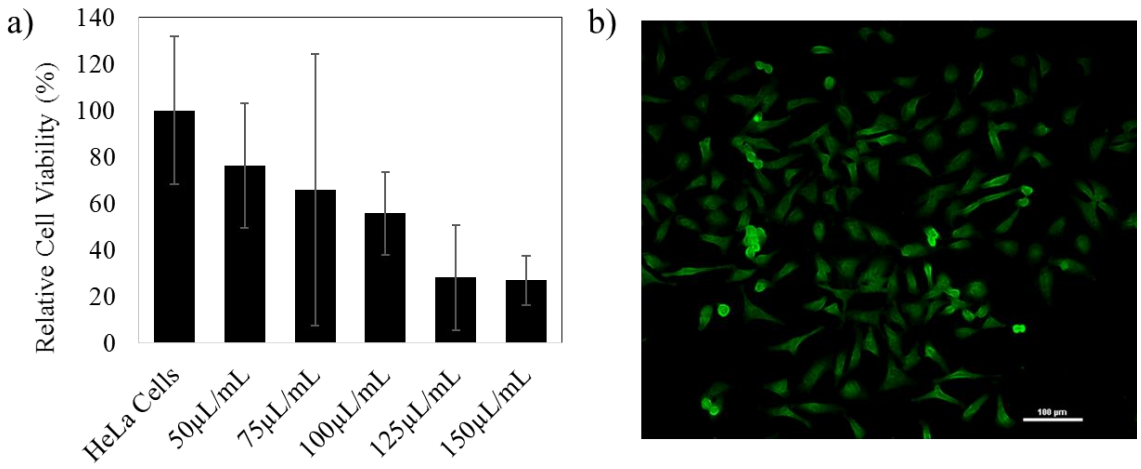

Figure 4.9 a) Cellular viability of 50, 75, 100, 125, and 150 µg/mL of SANSPs per well of HeLa cell. b) Fluorescence image of FITC labeled SANSPs showing efficient uptake of the probe.

The SANSPs with FITC labeled PEG were prepared by conjugating FITC labeled PEG and beacon to Si@AuNS. Other than the added stability PEG provides,[28] a FITC labeled PEG allows for monitoring the beacon conjugated Si@AuNS via fluorescence microscopy. Upon cellular take up, the HeLa cells were fixed and analyzed. The fluorescence images show a clear uptake of the SANSPs (**Figure 4.9b**).

4.4.6 Viral RNA Detection in Single Cells

Viral RNA was detected via SERS in HeLa cells transfected with HA-expressing plasmids. HeLa cell were seeded in an 8-well chambered coverglass and were allowed to grow and attach for 24 hours at 37°C and 5% CO_2. The cell were transfected with IAV H1N1 HA plasmid as well as PB1 plasmid and PB2 plasmid as controls demonstrate SANSP sensitivity. Next, they were incubated with SANSPs, washed and fixed for SERS analysis. SERS measurements were acquired for each test and averaged. **(Figure 4.10)**

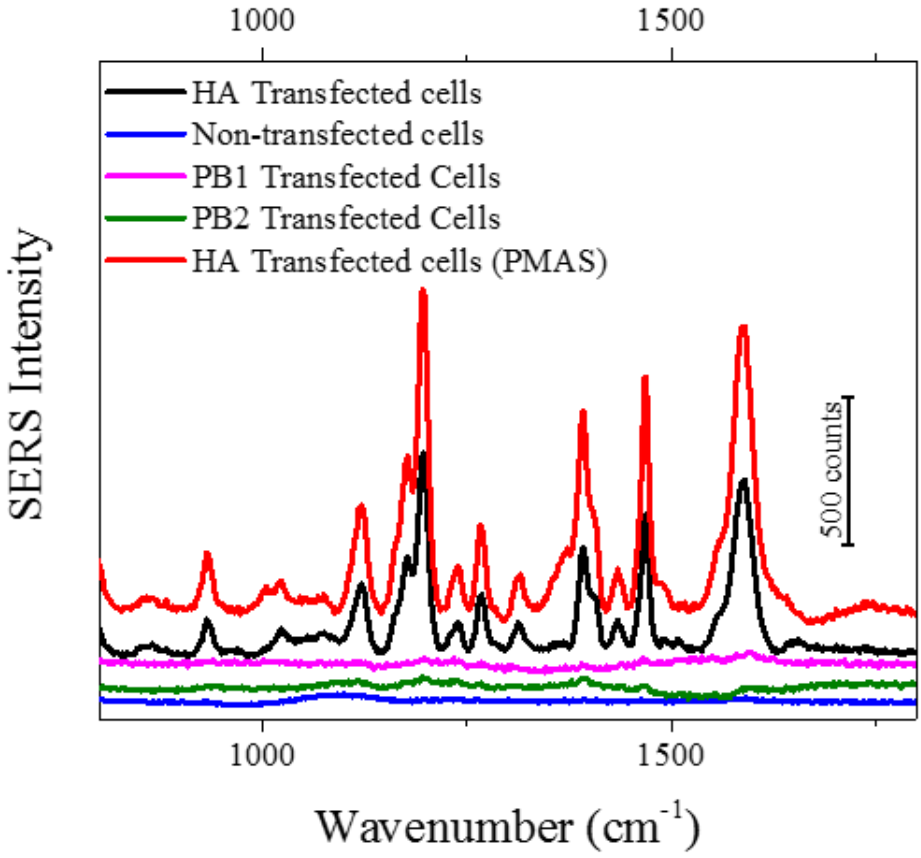

Figure 4.10 The spectra show an intense SERS signal for single cell analysis of HeLa cells transfected with IAV H1N1 HA plasmid. This signal is not as strong as studies in solution but strong enough to differentiate the signal from HeLa cells transfected with IAV H1N1 PB1 plasmid, HeLa cells transfected with IAV H1N1 PB2 plasmid, and non-transfected HeLa cells. Additionally, the SANSPs were tested with PMAS(Mo) from chapter 3. The intense signal demonstrates a proof of concept study that the platform can successfully target specific vRNA without the need for amplification. The addition of a PMAS(Mo) coating increases the amounts of SANSPs taken up the cell with minimal SERS response interference.

4.5 Conclusion

In conclusion, we demonstrated a promising new method to study viral evolution at the single cellular level. The plasmonic nanoparticle platform advances SERS microscopic techniques for tissue application and propose a novel strategy that virologists could leverage in the future to study viral evolution and ecology. This is one of many building blocks to create a specialized tool box to study viral mutations. The SERS active nanoparticle probe affords a detection platform with high signal to noise ratio and rapid target recognition. The field-enhancing properties of gold nanostars are strategically utilized by leveraging the morphology of the particles and placing the ligands at the hot spots located at the tip of the spikes. This approach enables improved recognition of viral RNA and detection at the single cell level, enabling the isolation of population outliers, important to decipher new pathways of viral infection. The platform has high sensitivity to modifications in RNA sequences with linear trends as the number of mismatched base pairs increase, making it not only effective for viral detection but also a potential tool for tracking the evolution of IAV. The ligands on the SANSPs can readily be customized for other segments, allowing one to envision a complete analysis and study of all eight viral RNA segments. Importantly, this SERS-based approach does not require amplification or extraction of RNA from the cells, which reduces detection time and can be easily implemented by virologists and foreseeably, by physicians.

4.6 References

1. Gyllenberg, M. & Parvinen, K. Necessary and sufficient conditions for evolutionary suicide. *Bulletin of Mathematical Biology* **63**, 981-993 (2001).
2. in Seasonal Influenza (Flu) (Center for Disease Control and Prevention, 2018).
3. Duffy, S., Shackelton, L.A. & Holmes, E.C. Rates of evolutionary change in viruses: patterns and determinants. *Nature Reviews Genetics* **9**, 267 (2008).
4. Brooke, C.B. Population Diversity and Collective Interactions during Influenza Virus Infection. *Journal of virology* **91** (2017).
5. Hussain, M., Galvin, H.D., Haw, T.Y., Nutsford, A.N. & Husain, M. Drug resistance in influenza A virus: the epidemiology and management. *Infection and drug resistance* **10**, 121-134 (2017).
6. Taubenberger, J.K. & Morens, D.M. Influenza Viruses: Breaking All the Rules. *mBio* **4** (2013).
7. Ellis, J.S. & Zambon, M.C. Molecular diagnosis of influenza. *Reviews in medical virology* **12**, 375-389 (2002).
8. Ratcliff, R.M., Chang, G., Kok, T. & Sloots, T.P. Molecular diagnosis of medical viruses. *Current issues in molecular biology* **9**, 87-102 (2007).
9. Cella, L.N., Blackstock, D., Yates, M.A., Mulchandani, A. & Chen, W. Detection of RNA viruses: current technologies and future perspectives. *Critical reviews in eukaryotic gene expression* **23**, 125-137 (2013).
10. Hutchinson, E.C., von Kirchbach, J.C., Gog, J.R. & Digard, P. Genome packaging in influenza A virus. *The Journal of general virology* **91**, 313-328 (2010).
11. Baptista, P. et al. Gold nanoparticles for the development of clinical diagnosis methods. *Anal Bioanal Chem* **391**, 943-950 (2008).
12. Zehbe, I. et al. Sensitive in situ hybridization with catalyzed reporter deposition, streptavidin-Nanogold, and silver acetate autometallography: detection of single-copy human papillomavirus. *The American journal of pathology* **150**, 1553-1561 (1997).
13. Faraday, M. X. The Bakerian Lecture. —Experimental relations of gold (and other metals) to light. *Philosophical Transactions of the Royal Society of London* **147**, 145-181 (1857).
14. Faulk, W.P. & Taylor, G.M. An immunocolloid method for the electron microscope. *Immunochemistry* **8**, 1081-1083 (1971).
15. Draz, M.S. & Shafiee, H. Applications of gold nanoparticles in virus detection. *Theranostics* **8**, 1985-2017 (2018).
16. Das, M., Shim, K.H., An, S.S.A. & Yi, D.K. Review on gold nanoparticles and their applications. *Toxicology and Environmental Health Sciences* **3**, 193-205 (2011).
17. Elahi, N., Kamali, M. & Baghersad, M.H. Recent biomedical applications of gold nanoparticles: A review. *Talanta* **184**, 537-556 (2018).
18. Fabris, L. SERS Tags: The Next Promising Tool for Personalized Cancer Detection? *ChemNanoMat* **2**, 249-258 (2016).
19. Indrasekara, A.S. et al. Gold nanostar substrates for SERS-based chemical sensing in the femtomolar regime. *Nanoscale* **6**, 8891-8899 (2014).

20. Laura, F. Gold-based SERS tags for biomedical imaging. *Journal of Optics* **17**, 114002 (2015).
21. Giljohann, D.A. et al. Gold nanoparticles for biology and medicine. *Angewandte Chemie (International ed. in English)* **49**, 3280-3294 (2010).
22. Liu, M. et al. Highly sensitive protein detection using enzyme-labeled gold nanoparticle probes. *The Analyst* **135**, 327-331 (2010).
23. Lu, W. et al. Multifunctional oval-shaped gold-nanoparticle-based selective detection of breast cancer cells using simple colorimetric and highly sensitive two-photon scattering assay. *ACS nano* **4**, 1739-1749 (2010).
24. Mirkin, C.A., Letsinger, R.L., Mucic, R.C. & Storhoff, J.J. A DNA-based method for rationally assembling nanoparticles into macroscopic materials. *Nature* **382**, 607-609 (1996).
25. Cheng, Y. et al. Fluorescence Near Gold Nanoparticles for DNA Sensing. *Analytical Chemistry* **83**, 1307-1314 (2011).
26. Yuan, H. et al. Gold nanostars: surfactant-free synthesis, 3D modelling, and two-photon photoluminescence imaging. *Nanotechnology* **23**, 075102 (2012).
27. Atta, S., Tsoulos, T.V. & Fabris, L. Shaping Gold Nanostar Electric Fields for Surface-Enhanced Raman Spectroscopy Enhancement via Silica Coating and Selective Etching. *The Journal of Physical Chemistry C* **120**, 20749-20758 (2016).
28. Jimenez de Aberasturi, D. et al. Surface Enhanced Raman Scattering Encoded Gold Nanostars for Multiplexed Cell Discrimination. *Chemistry of Materials* **28**, 6779-6790 (2016).
29. Faulds, K., Smith, W.E. & Graham, D. Evaluation of surface-enhanced resonance Raman scattering for quantitative DNA analysis. *Anal Chem* **76**, 412-417 (2004).
30. Halas, N.J., Lal, S., Chang, W.S., Link, S. & Nordlander, P. Plasmons in strongly coupled metallic nanostructures. *Chem Rev* **111**, 3913-3961 (2011).
31. Indrasekara, A.S.D.S. et al. Gold nanostar substrates for SERS-based chemical sensing in the femtomolar regime. *Nanoscale* **6**, 8891-8899 (2014).
32. Gracie, K. et al. Simultaneous detection and quantification of three bacterial meningitis pathogens by SERS. *Chemical Science* **5**, 1030-1040 (2014).

Chapter 5 Conclusions and Future Directions

5.1 Conclusions

The studies carried out in this thesis aimed to develop a sensitive and efficient method for detection (and ultimately quantification) of viral mutations in intact individual cells. Additionally, it aimed to design and implement an effective bioconjugation scheme for cellular uptake, endosomal escape, and intracellular targeting. To develop an effective nanoparticle tool, it is essential to precisely synthesize the desired morphology, since it drastically impacts other physical and optical properties, such as surface area, extinction coefficient, and plasmonic resonances. Electing to synthesize gold nanostars for a SERS-based assay is based on their plasmonic hot spots located at the tips, which enable achieving SERS signal enhancements on the order of $10^8 – 10^9$. To further develop the nanoparticle tool is then necessary to determine the surface chemistry and direct how it will interact with its surroundings. For *in vitro* testing, the stability of the nanoparticles and their ability to escape endosomes is crucial. A non-toxic method that does not impact the surface chemistry and functionality of the nanoparticles has been an emphasis of many studies focusing on endosomal escape into the cytoplasm. In the case of a biosensor, its selectivity, targeting efficiency, and stability all need to be accounted for when functionalizing the surface.

In this dissertation work, gold nanostars were functionalized with Raman-active moieties to quantify viral RNA and detect the presence of mutations at the single cell level. This work started with the design and synthesis of the nanoparticle platforms used for cellular uptake and the design of the SERS active biosensor. The particles synthesized and functionalized were stable in both solution and media, and were biocompatible,

displaying low cytotoxicity. Gold nanostars were functionalized with a previously developed transfecting agent, trisaminocyclopropenium (TAC) polymers, to obtain a platform yielding quick and efficient nanoparticle uptake and endosomal escape into the cytoplasm with minimal cytotoxic effects. The TAC polymer-coated nanoparticles displayed faster and more efficient diffusion into the cytoplasm compared to when current standard nanoparticle transfection agents, such as poly(ethyleneimine), PEI, are used. Gold nanostars were used to design the SERS active nanoparticle probe (SANSPs). The SANSPs were sensitive to nucleotide mismatches in their target oligonucleotides. Furthermore, single cell analysis was possible using the SANSPs for detection of viral RNA, which may be critical for tracking population outliers that would otherwise go unnoticed with whole population analysis. These findings can contribute to the mechanistic study of viral evolution and for the development of effective next generation vaccines.

5.2 Future Directions

In the second chapter we discussed nanoparticle synthesis for *in vitro* studies and SERS-based assays. Nanoparticles come in various morphologies and applications.[1] They have tremendous potential as SERS tags and for SERS-based assays.[2] While in this synthetic procedure we discuss utilizing surfactant free gold nanostars, which possess a multitude of spikes, other forms of newly developed nanostars should be explored. For instance, six-branched gold nanostars, which were first developed by Pallavicini *et al.*[3] and refined for improved purity and monodispersity by Atta *et al.*[4] in 2019, can be explored as a

potential nanoparticle of choice for developing bioactive nanoparticle platforms. Having only six spikes can limit and allow greater control over ligand conjugation. Future work could examine other synthetic procedures to enhance the nanoparticle platform for cellular uptake and for biosensing.

The third chapter discusses optimization of nanoparticle delivery to the cytoplasm. In order to fully extend the potential of gold nanoparticles, an efficient method for cellular uptake is essential.[5] Bhamidipati *et al.*[6] established the low cytotoxicity and biocompatibility of gold nanostars, which confirmed their safety for use in *in vitro* studies. This study aimed to develop a method for efficient and quick endosomal escape of gold nanostars into the cytosol. While this study provided a basic demonstration of cellular uptake, endosomal escape, and diffusion of nanostars in the cytoplasm in cultured cells, it would be useful to understand the polymer's fate after endosomal escape. Although this study was successful *in vitro*, it may not accurately reflect *in vivo* studies. Previous studies have shown *in vivo* success for nanoparticles coated in PEI, which leaves one optimistic that it may be possible for TAC polymers as well.[7] Future work could focus on studying the fate of the TAC polymers after endosomal escape and applying the polymers onto target specific nanoparticles for *in vivo* studies.

In the fourth chapter we developed a nanoparticle probe for viral RNA detection with sensitivity to mutations and base pair modification on the targeted RNA sequence. The platform was developed with future work in mind. It was designed to accommodate multiplexing to target the various IAV gene sequences.[8, 9] Additionally, the Raman reporter used for the study is also fluorescently active.[10] Our initial vision was to create a switchable SERS-fluorescent nanostar probe, however we were only successful in

creating a SERS active probe and found challenges in the fluorescent response, as reported by others. Although we successfully demonstrated the nanoparticle probe's specific targeting in plasmid transfected cells, it would be beneficial to test the particles in IAV infected cells. Future work could aim to develop a switchable SERS-fluorescent platform with multiplexing capability that responds well to the presence of both IAV wild type and mutated segments *in vitro,* and eventually, *in vivo*. Additionally, the application of the SERS-active nanostar probe can be expanded to other viral infections and other intracellular targeting.

Overall, the work completed in this thesis provides a foundation for the development of a highly sensitive viral RNA sensor with immense potential as a tool for the mechanistic study of viral evolution. It also lays out methods for nanoparticle uptake that can be applied to nanoparticle sensing and intracellular platforms.

5.3 References

1. Salata, O. Applications of nanoparticles in biology and medicine. *Journal of Nanobiotechnology* **2**, 3 (2004).
2. Laura, F. Gold-based SERS tags for biomedical imaging. *Journal of Optics* **17**, 114002 (2015).
3. Pallavicini, P. et al. Triton X-100 for three-plasmon gold nanostars with two photothermally active NIR (near IR) and SWIR (short-wavelength IR) channels. *Chemical Communications* **49**, 6265-6267 (2013).
4. Supriya, A. & Laura, F. Understanding the Role of AgNO3 Concentration and Seed Morphology to Achieve Tunable Shape Control in Gold Nanostars. (2018).
5. Behzadi, S. et al. Cellular uptake of nanoparticles: journey inside the cell. *Chemical Society reviews* **46**, 4218-4244 (2017).
6. Bhamidipati, M. & Fabris, L. Multiparametric Assessment of Gold Nanoparticle Cytotoxicity in Cancerous and Healthy Cells: The Role of Size, Shape, and Surface Chemistry. *Bioconjugate Chemistry* **28**, 449-460 (2017).
7. Yin, P.T. et al. Stem cell-based gene therapy activated using magnetic hyperthermia to enhance the treatment of cancer. *Biomaterials* **81**, 46-57 (2016).
8. Kyriazi, M.E. et al. Multiplexed mRNA Sensing and Combinatorial-Targeted Drug Delivery Using DNA-Gold Nanoparticle Dimers. *ACS nano* **12**, 3333-3340 (2018).
9. Hutchinson, E.C., von Kirchbach, J.C., Gog, J.R. & Digard, P. Genome packaging in influenza A virus. *The Journal of general virology* **91**, 313-328 (2010).
10. Cheng, Y. et al. Fluorescence Near Gold Nanoparticles for DNA Sensing. *Analytical Chemistry* **83**, 1307-1314 (2011).

Appendix: Enhancement of MALDI-TOF Mass Spectroscopy via Gold Nanoparticle Integration

A.1 ABSTRACT

Additional studies have been conducted towards this thesis towards the improvement of spectroscopic techniques for bioanalysis. Although this portion of the thesis does not directly relate to viral detection, it is relevant to the analysis of bioactive materials with the potential to become an analytical method for cellular and viral analysis. Gold nanoparticles were herein utilized for signal enhancement in matrix-assisted laser desorption/ionization –time of flight mass spectrometry (MALDI-TOF MS). Gold nanostars were integrated with various biological samples and analyzed using a MALDI-TOF MS. Unlike molecules with high absorption of laser radiation, molecules with low laser absorption require additional materials to assist with the desorption/ionization step of MS. Current methods utilize small organic molecules, or metallic coated surfaces, such as stainless steel or gold, onto which the analyte is drop casted. Despite these efforts, some molecules still do not absorb the laser radiation. Compared to current standards, we observed that the signals of the compounds examined were significantly enhanced when gold nanoparticles were integrated, especially compounds that contained polyunsaturated double bonds, such as fatty acids. We demonstrated that the gold nanoparticles led to high resolution, high selectivity, and low interference.

A.2 INTRODUCTION

Gold nanoparticles have become increasingly popular not only in biomedicine but also physical chemistry, materials science, and analytical chemistry.[1] Earlier in this thesis we discussed the advantages of gold nanoparticles in biomedical applications, such as viral RNA detection via surface enhanced Raman spectroscopy (SERS) and intracellular

tagging. In this section of the thesis we describe the advantages of gold nanoparticles in analytical techniques. Nanomaterials have significantly improved analytical methods such as SERS and Mass spectrometry (MS).[2, 3]

Current methods for enhancing MS signals utilize matrix-assisted laser desorption/ionization –time of flight mass spectrometry (MALDI-TOF MS). This is a highly sensitive analytical technique for analyzing biomolecules such as DNA, RNA, peptides, proteins, lipids and carbohydrates, and biological samples such as cells and tissue.[4, 5] This method is suited for molecules with low laser absorption cross sections. An additional molecule or material (i.e. the matrix) is used to assist with the desorption/ionization step of MS.[6, 7] Despite the success with these matrices, they require high concentrations, do not allow for the analysis of low molecular weight molecules, and are not compatible with certain classes of molecules such as polyunsaturated double bonds, small molecules, biomarkers, and protiens.[8] Researchers have developed new methods to overcome these obstacles including using nanomaterials for assisted laser desorption/ionization.[8]

The use of nanomaterials for assisted laser desorption/ionization was first demonstrated by Tanaka *et al.,* where cobalt nanoparticles were used for protein analysis and the technique was named surface-assisted laser desorption/ionization mass spectrometry (SALDI-MS).[9] This initiated the use of gold nanoparticles as a whole new class of materials used for MS. Herein, we describe a method for enhancement of matrix-assisted laser desorption/ionization –time of flight mass spectrometry (MALDI-TOF MS) signals

with gold nanoparticle assisted desorption/ionization. The laser radiation is efficiently absorbed by gold nanoparticles and the energy is transferred to the analyte. Gold nanoparticles can be used at low concentrations relative to the analyte due to their high surface area as compared to the organic molecules generally used as matrices, which need higher concentrations relative to the analyte. Gold nanostars were integrated with oils and compounds from dietary supplements as a proof of concept to determine their effects on MS signals.

A.3 MATERIALS AND METHODS

A.3.1 NANOPARTICLE SYNTHESIS

Gold nanospheres and surfactant free gold nanostars were synthesized using modifications of established protocols from the literature.[10, 11] Gold nanospheres, were synthesized according to a modified synthesis described by Turkevich.[10] Gold nanospheres were prepared by adding 8 mL of 0.025 M $HAuCl_4$ salt to 477 mL of milliQ water. The diluted gold salt was heated up to a boil under stirring to which 15 mL of 1% citric acid trisodium salt were added and left to boil for 5 minutes. After the 5 minutes, the solution turned a deep red and was allowed to cool to room temperature. The cooled product was purified by centrifugation at 6000 g for 30 to 45 minutes. The nanospheres settled at the bottom and the pellet was collected.

The gold nanostars were prepared via a seed mediated method described by Yuan *et al.*[11] Using the synthesized nanospheres, the gold nanostars were synthesized by adding 2 mL of 0.025 M $HAuCl_4$ salt solution, 200 µL of 1 N HCl, 48 mL of Milli-Q water, and 125 µL of 12 nm citrate capped spheres with an absorbance of 2.81 at a 1 mm path length

under gentle stirring. To the mixture, 2 mL of 3 mM $AgNO_3$ and 1 mL of 100 mM ascorbic acid were added simultaneously. The reaction was left to stir for 7 minutes, after which it turned a deep blue. The resulting product was purified by centrifugation at 3000 g for 15 minutes.

A.3.2 CHARACTERIZATION OF NANOPARTICLE

To optically characterize the nanoparticles, UV-Vis spectra were recorded using a Thermo Scientific Nanodrop 2000 and SI Photonics Model 440 CCD Array UV-Vis spectrophotometer.

Transmission electron microcopy (TEM) images were collected using a Philips CM12 transmission electron microscope. This was used to evaluate the morphology and size. The samples were drop casted onto carbon-coated TEM grids (Ted Pella).

The concertation of the particles were calculated using Beer Lambert's law.[12]

The hydrodynamic size and the charge were measured using DLS and zeta potential employing a Malvern Zetasizer Nano-S. The size was measured by diluting the samples in Milli-Q water in a disposable cuvette and was calculated by relating particle size to particle motion. The charge was measured by diluting the samples in Milli-Q water in a folded capillary zeta cell and calculated using Smoluchowski's theory.

Since gold nanostars employ $AgNO_3$ to enable anisotropic growth and increase stability, both X-ray fluorescence (XRF) and inductively coupled plasma optical emission spectrometry (ICP-OES) were measured to determine the starting concentration of silver and gold as means of calibrating the MS signals. Following standard protocols and to

calculate the concentrations via XRF, gold nanostars were tested against a 32.45 mM silver standard and a 25 mM gold standard. For ICP-OES, gold nanostars were tested both as whole unmodified nanoparticles and as digested nanoparticles using nitric acid and hydrochloric acid. The particles were tested both whole and digested to compare previously established protocols.[13] Briefly, 300 µL of nitric acid was added to 100 µL of nanostars. After an hour, 100 µL of hydrochloric acid were added and the mixture was diluted to 10 mL in Milli-Q water. To test the nanoparticles without digestion, 100 µL of nanostars were diluted to 10 mL in Milli-Q water. A 0.635 mM gold standard and a 0.927 mM silver standard were used to calculate the concentration.

A.3.3 PREPARATION OF BIOMATERIAL ANALYSIS

As a proof of concept, each nanoparticle batch was mixed 1:1 with easily accessible dietary supplements, macadamia oil, and fish oil. Dietary supplements are not regulated with same safety levels as prescription drugs, hence there is a need for a quick and efficient method to test the efficacy of active ingredients. The samples were each drop casted onto an ITO coated glass slide for analysis. Additionally, macadamia oil, and fish oil were drop casted onto a gold coated MS plate for analysis without the assistance of nanoparticles. The samples were analyzed using a Bruker Ultraflex III TOF/TOF Mass Spectrometer.

A.4 RESULTS AND DISCUSSION

The nanoparticles were each successfully synthesized and characterized to produce the correct morphology. Since mass spectrometry will ionize the particles, gold nanostars, which used silver salts during the synthesis to shape the spikes, were analyzed via XRF and ICP-OES to calculate the concentration of each. This provided a confirmation of the amount and presence of silver and gold ions that formed Au-Au, Au-Ag, and Ag-Ag clusters that are a means of calibrating the MS signals. The particles were analyzed in two trials for XRF. The results depicted in **Figure A.1** show clear overlap with the gold standard, with a significant peak at about 18 keV. However, the instrument was not sensitive enough to detect the low quantities of silver in gold nanostars. There is no overlap of the nanostar peaks with the silver peaks at 22 keV and 25 keV.

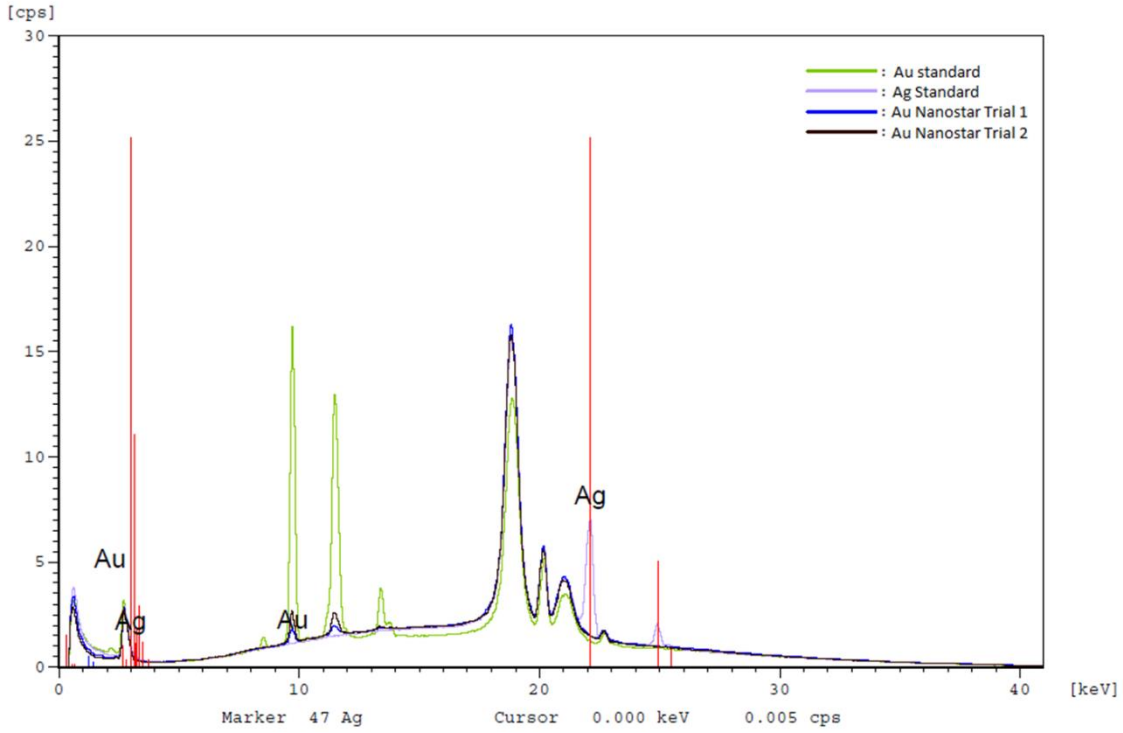

Figure A.1 XRF results of gold nanostars.

To detect silver, ICP-OES, which is a more sensitive analytical tool, was used. Gold nanostars were tested without digestion (whole) and digested using nitric acid and hydrochloric acid. The whole particle analysis showed that gold nanostars have a 0.062 mM concentration of gold and 0.008 mM of silver. The digested particles seemed to show a higher concentration of silver at 0.009 mM while the concentration of gold remained constant at 0.062 mM. **(Figure A.2)** This analysis helps to confirm that the sensitivity of MS is enough to detect silver clusters from the nanostars, thus eliminating any doubt about the origin of the silver signals.

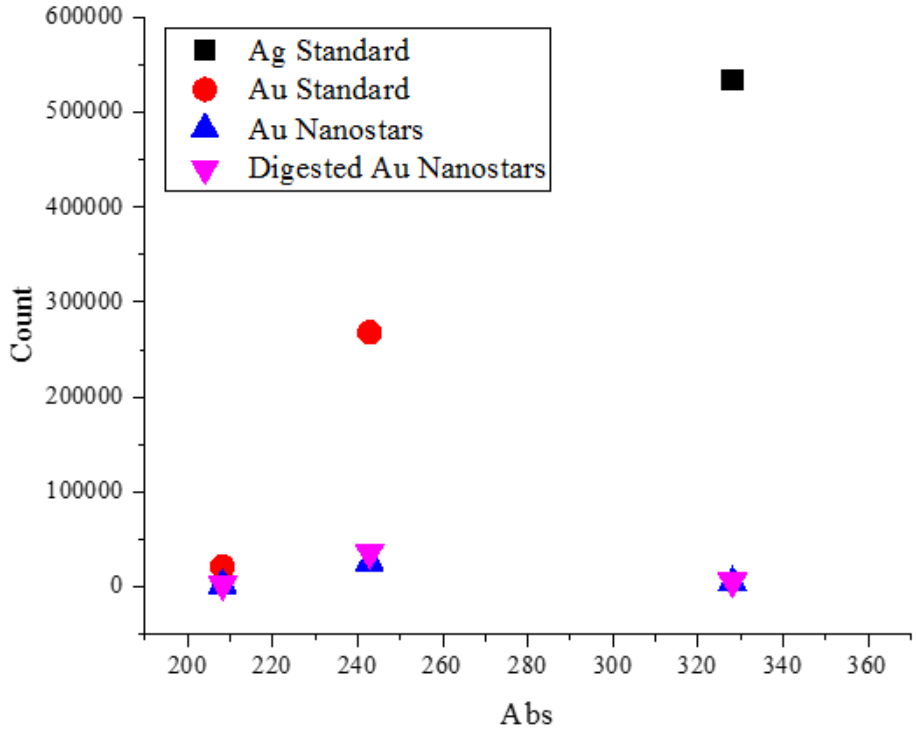

Figure A.2 ICP-OES results of whole and digested gold nanostars.

The nanoparticles were then each mixed in 1:1 ratio with macadamia oil and fish oil. Each mixture was drop casted onto an ITO-coated glass slide, which is a standard material for the MS instrument used. Macadamia oil and fish oil were tested without nanoparticles as a control. For each set of experiments we chose the highest signal depending on the plate type. **Figure A.3** shows a clear enhancement of the MS signals when nanostars are added to the macadamia oil and a significant enhancement of the polyunsaturated double bond, which was not detected without the addition of gold

nanostars. **Figure A.4** shows a clear enhancement of the MS signals when nanostars are added to the fish oil with an enhancement and detection of polyunsaturated double bonds.

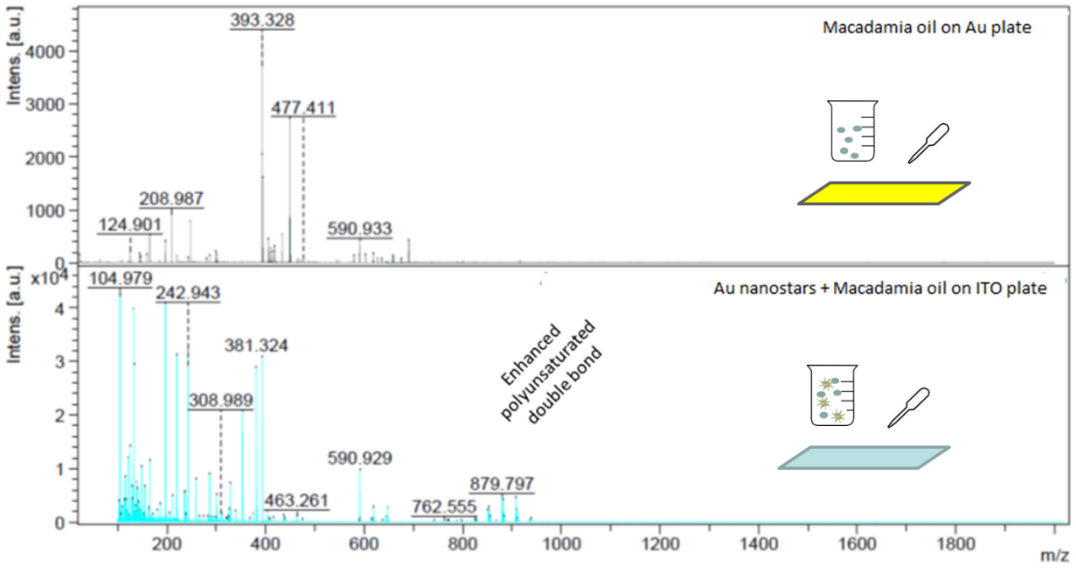

Figure A.3 MALD-TOF MS spectra of macadamia oil mixed with nanostars showed significant signal enhancement compared to macadamia oil analyzed without nanostars on a standard MS plate.

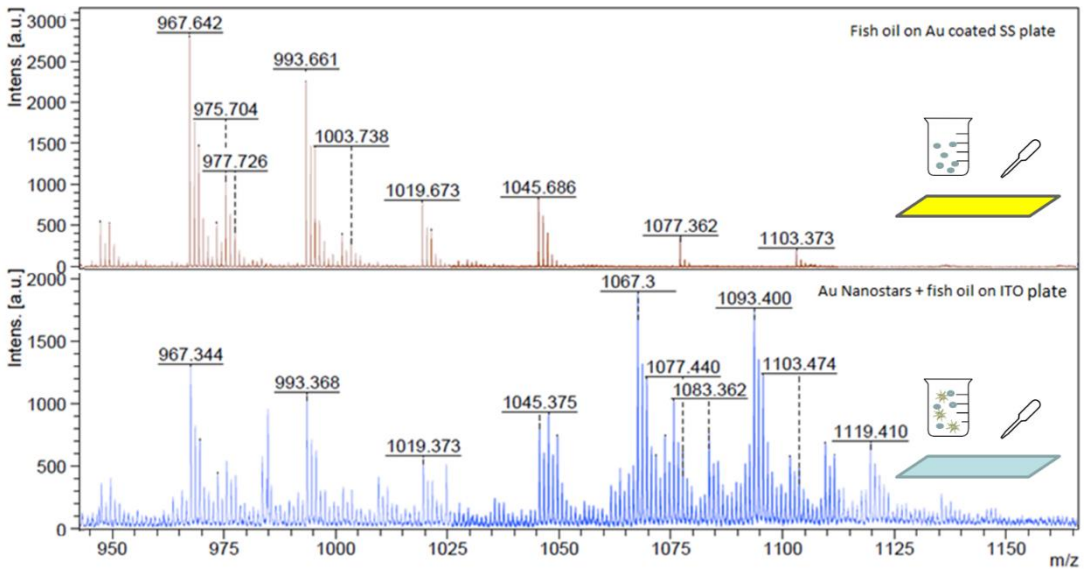

Figure A.4 MALD-TOF MS spectra of fish oil mixed with nanostars showed significant signal enhancement compared to fish oil analyzed without nanostars on a standard MS plate.

The results demonstrated the gold nanoparticle's ability to absorb the laser radiation and transfer the energy to the analyte for desorption/ionization process. The particles showed a great enhancement of the MALDI-TOF-MS signals specifically polyunsaturated double bonds that were previously not detected without the assistance of gold nanostars. Although this technique requires further development and research, it lays down a solid foundation and demonstration for future studies.

A.5 CONCLUSION

In conclusion, we demonstrated the effectiveness of gold nanostars as a tool for MALDI-TOF MS signal enhancement of molecules containing fatty moieties such as macadamia oil and fish oil. Gold nanostars were integrated in a 1:1 ratio with both macadamia oil and fish oil and drop casted onto an ITO plate. The results were compared to macadamia oil and fish oil drop casted onto a gold plate without the addition of gold nanostars. The samples integrated with gold nanostars showed significant enhancement of their signals for an improved analytical analysis.

A.6 ACKNOWLEDGMENTS

I would like to acknowledge Dr. Gene Hall for providing access and training on matrix-assisted laser desorption/ionization –time of flight mass spectrometry.

A.7 REFERENCES

1. Giljohann, D.A. et al. Gold nanoparticles for biology and medicine. *Angewandte Chemie (International ed. in English)* **49**, 3280-3294 (2010).
2. Qiao, L., Liu, B. & Girault, H.H. Nanomaterial-assisted laser desorption ionization for mass spectrometry-based biomedical analysis. *Nanomedicine (London, England)* **5**, 1641-1652 (2010).
3. Fabris, L. SERS Tags: The Next Promising Tool for Personalized Cancer Detection? *ChemNanoMat* **2**, 249-258 (2016).
4. Fenselau, C. & Demirev, P.A. Characterization of intact microorganisms by MALDI mass spectrometry. *Mass spectrometry reviews* **20**, 157-171 (2001).
5. Norris, J.L. & Caprioli, R.M. Analysis of tissue specimens by matrix-assisted laser desorption/ionization imaging mass spectrometry in biological and clinical research. *Chem Rev* **113**, 2309-2342 (2013).
6. Abdelhamid, H.N. & Wu, H.F. Furoic and mefenamic acids as new matrices for matrix assisted laser desorption/ionization-(MALDI)-mass spectrometry. *Talanta* **115**, 442-450 (2013).
7. Chen, S. et al. 2,3,4,5-Tetrakis(3',4'-dihydroxylphenyl)thiophene: a new matrix for the selective analysis of low molecular weight amines and direct determination of creatinine in urine by MALDI-TOF MS. *Anal Chem* **84**, 10291-10297 (2012).
8. Abdelhamid, H.N. & Wu, H.F. Gold nanoparticles assisted laser desorption/ionization mass spectrometry and applications: from simple molecules to intact cells. *Anal Bioanal Chem* **408**, 4485-4502 (2016).
9. Tanaka, K. et al. Protein and polymer analyses up to m/z 100 000 by laser ionization time-of-flight mass spectrometry. *Rapid Communications in Mass Spectrometry* **2**, 151-153 (1988).
10. Turkevich, J., Stevenson, P.C. & Hillier, J. A study of the nucleation and growth processes in the synthesis of colloidal gold. *Discussions of the Faraday Society* **11**, 55-75 (1951).
11. Yuan, H. et al. Gold nanostars: surfactant-free synthesis, 3D modelling, and two-photon photoluminescence imaging. *Nanotechnology* **23**, 075102 (2012).
12. Liu, X., Atwater, M., Wang, J. & Huo, Q. Extinction coefficient of gold nanoparticles with different sizes and different capping ligands. *Colloids and surfaces. B, Biointerfaces* **58**, 3-7 (2007).
13. Fabricius, A.-L., Duester, L., Meermann, B. & Ternes, T.A. ICP-MS-based characterization of inorganic nanoparticles--sample preparation and off-line fractionation strategies. *Analytical and bioanalytical chemistry* **406**, 467-479 (2014).